UNIVERSITÀ DI PISA

Facoltà di Ingegneria

Corso di Laurea Magistrale in Ingegneria Chimica

Dipartimento di Ingegneria Chimica e Industriale

TESI DI LAUREA MAGISTRALE

Integrated models approach for the prediction of aerosols in biomass power generation systems

Relatori

Dott. Ing Chiara Galletti

Prof. Ing. Leonardo Tognotti

Candidata

Laura Grassellino

Controrelatore

Prof. Ing. Vincenzo Tricoli

Anno accademico 2015/2016

To my sister Anna,
my best friends from ever

“Noi siamo quello che facciamo costantemente, l'eccellenza quindi non è un atto ma un abitudine.”

Aristotele

Summary

List of Figures

List of Tables

Abstract

The aerosol is constitued by fine particulates with characteristic dimension less than some micron, byproduct of combustion. The chemical composition of the aerosol coming from the combustion of the biomass is composed in large part of alkali sulphates and chlorides. These particles as well as being atmospheric pollutants, also lead to phenomena of slagging, fouling and corrosion.

All solid fuels contain a fraction of highly non-combustible minerals. The formation of deposits depends on the presence of these minerals. In recent years, it has increased the focus on renewable fuels that have a low cost, the possibilities of co-combustion of RDF with coal in the plants that already exist only for the coal.

The progress in recent years and the advent of new powerful computers have allowed experts to improve current CFD models for reactive turbulent flows and predict temperature and velocity fields with acceptable accuracy. However the prediction of minor species and pollutants, still demands for detailed kinetic schemes, with hundreds of chemical species and thousands of reactions; such complex schemes cannot be computed directly using the CFD grid (usually requiring a number of cells of about $10^5 – 10^6$) required for the modeling of industrial furnaces.

This has motivated the development of methods based on Chemical Reactor Networks, according to which the domain is divided into a series of interconnected pseudo-homogeneous macro-regions, that are hence treated as ideal reactors in which complex kinetic schemes may be solved.
Example of this approach are the Reactor Network Analysis (RNA) and the Kinetic Post Processor (KPP).

The RNA, used in the present work, defines the macro-homogeneous regions, characterized by average values of temperature, density and chemical compositions, on the basis of preliminary CFD simulation performeds with less accurate (and computationally demanding) models. The macro-regions are then represented as ideal 2D or 3D chemical reactors (with perfect mixing or plug-flow). Logically a prier mass flow exchange among the reactors should be considered to build a network model of relatively simple reactors (up to thousands of reactors).
Hence the detailed chemical kinetics that describes the formation/destruction of pollutants may be computes on such reactor network.

The present work is aimed for the prediction of inorganic aerosols from biomass-fired furnace with a CFD+RNA approach.

The first part of the work was dedicated to the analysis of experimental campaigns on aerosol formation conducted at IFRF on two different equipments: the Isothermal Plug Flow Reactor and 500 kW, both located at ENEL laboratories in Livorno. It was carried out an analysis of the experimental data with regard to the major pollutants and the production of particulate, with the purpose of being able to derive any tendency for the prediction of particulates by varying the experimental apparatus and the fuel.

The second part of the work was dedicated to the development of the CFD model of the 500 kW KVSA reactor, located at the University of Stuttgart. A special modeling strategy was adopted to decrease the number of computational cells required for the simulation of a multiphase reactive flow. The goal was to get the thermochemical fields in the furnace to define the reactor network.

The third part of the work was dedicated to the implementation of the RNA approach. This included the definition of proper kinetics and thermodynamic data. The influence of the number of reactors on the predictions was evaluated.

The last part of the work was dedicated to the formulation of detailed parametric models of depositions the convection zone of the combustion chambers for all examined experimental apparatus, such as IPFR, 500 kW and KVSA. The objective is to be able to study the deposition tendency of alkali on tube bank surfaces by applying a mechanism of condensation. The deposition models can quantify the deposition rate of alkali compounds in specific conditions of the convective pass and give an estimation of the most favourable factors to depositions.

Sommario

L'aerosol è costituito da particolato fine con dimensioni caratteristiche minori di qualche micron, sottoprodotti della combustione. La composizione chimica degli aerosol, che viene prodotto dalla combustione di biomassa, è composta in larga parte da solfati e cloruri di alcali. Queste particelle possono diventare inquinanti atmosferici, e possono portare anche a fenomeni queli slagging, fouling e corrosione.

Tutti i combustibili solidi contengono una frazione di minerali altamente non combustibile. La formazione di depositi dipende dalla presenza di questi minerali. Negli ultimi anni, è cresciuta l'attenzione sui combustibili rinnovabili e a basso costo, la possibilità di co-combustione di RDF con carbone in impianti già esistenti solo per carbone.

I progressi in questi ultimi anni e l'avvento di nuovi computer hanno permesso agli esperti di miglorare i correnti modelli di CFD per flussi turbolenti reattivi e prevedendo campi di temperatura e di velocità con una precisione accettabile. Tuttavia la previsione di specie minori e inquinanti, richiede ancora schemi cinetici dettagliati, con centinaia di specie chimiche e migliaia di reazioni; tali sistemi complessi non possono essere calcolati direttamente utilizzando la griglia di calcolo CFD (che di solito richiede un numero di celle di circa $10^5 – 10^6$) necessari per la modellazione di forni industriali.

Ciò ha indotto lo sviluppo di metodi basati sul Chemical Reactor Networks, secondo cui il dominio è diviso in una serie di pseudo-omogenee macro-regioni interconnesse, che vengono quindi trattati come reattori ideali in cui gli schemi cinetici complessi possono essere risolti. Esempio di questo approccio sono il Reactor Networks Analysis (RNA) e il Kinetic Post Processor (KPP).

L'RNA, utilizzato nel presente lavoro, definisce le regioni macro-omogenee, caratterizzate da valori medi di temperatura, densità e composizioni chimiche, sulla base di una precedente simulazione CFD con modelli meno precisi (e computazionalmente impegnativi). La macro-regione viene poi rappresentata come un reattore chimico (con perfetto miscelamento o plug-flow) in 2D o 3D.

Logicamente uno scambio di flusso di massa tra i reattori dovrebbe essere considerata per costruire un modello reletavimante semplice a rete di reattori (fino a migliaia di reattori). La cineticha chimica dettagliata che descrive la formazione/distruzione di sostanze inquinanti possono essere calcolate su tale rete di reattori.

Il presente lavoro è finalizzato alla predizione di aerosol inorganici da una fornace alimentata a biomassa con un approccio CFD+RNA.

La prima parte del lavoro è stata dedicata all'analisi di campagne sperimentali sulla formazione degli aerosol condotte dell'IFRF su due differenti apparati sperimentali: l'Isothermal Plug Flow Reactor e 500 kW, entrambi situati presso i laboratori dell'ENEL di Livorno. È stata effettuata un'analisi dei dati sperimentali per quanto riguarda i maggiori inquinanti e la produzione di particolato, con la finalità di riuscire a ricavare al variare dell'apparato sperimentale e del combustibile qualche tendenza sulla predizione del particolato.

La seconda parte del lavoro è stata dedicata alla sviluppo del modello CFD del reattore 500 kW KVSA, situato presso l'università di Stoccarda. Una strategia di modellazione speciale è stato adottato per diminuire il numero di celle computazionali per la simulazione di un flusso reattivo multifase. L'obiettivo è quello di ottenere campo termochimici nella fornace per definire la rete di reattori.

La terza parte del lavoro è stata dedicata all'implementazione dell'approccio RNA. Questo include la definizione delle proprietà cinetiche e dati termodinamici. È stata valutata l'influenza del numero di reattori sulla predizione di aerosol.

L'ultima parte del lavoro è stata dedicata alla realizzazione di un modello di deposizione del particolato nelle zone convettive delle camere di combustione per tutti gli apparati sperimentali esaminati, cioè IPFR, 500 kW e KVSA. L'obiettivo è quello di riuscire a studiare in modo analitico la deposizione su dei banchi (tubi), che rappresentano le sonde per il campionamento del particolato, degli aerosol inorganici che si sono condensati. Il modello di deposizione può quantificare la velocità di deposizione di composti alcalini nella zona convettiva e dare una stima dei fattori più favorevoli alla deposizione.

Chapter 1

Introduction

Solid biomass covers a wide range of materials: woods, straws, agricultural residues, processing wastes, algae and seaweeds. The early use of biomass was based on easy accessibility and availability, but the use decreased in many countries due to shortages in the 19th Century and by the emergence of fossil fuels. Biomass is still widely used in developing countries because it is cheap and easily available. Today, there is renewed interest in many indutrialised countries in biomass combustion, especially bio-heat, and, in Europe, co-firing. The biomass possesses the advantage of CO_2 neutrality, or nearly so, there are potential problems concerned with the enviromental pollution that it causes. A variety of methods of utilisation are possible for biomass that evolved from the technologies developed for the combustion of the solid fuels, coal and coke. In some cases, biomass is burned in equipment designed for coal firing, with only slight modification, and this influences the pollutants formed. All combustion applications have the potential to release airborne pollutants: methane and volatile organic compounds (VOC), nitrogen oxides, sulphur oxides, hydrogen chloride, polyaromatic hydrocarbons (PAH), furans and dioxins, as weel as organic and inorganic aerosol particulate. Biomass combustion consists of the steps: heating-up, drying, devolatilisation to produce char and volatiles, where the volatiles consist of tars and gases, combustion of the volatiles, combustion of the char. The nitrogen compounds are partially released with the volatiles, whilst some forms a C-N matrix in the char and is then released during the char combustion stage forming NOx and the NOx precursors, HCN and HCNO. Sulphur is released as SO_2 during both volatile and char combustion. Biomass cointains metals of which the most important is potassium, which varies from several thousand ppm in energy crops to a few wt% (dry basis) in certain agricultural residues.

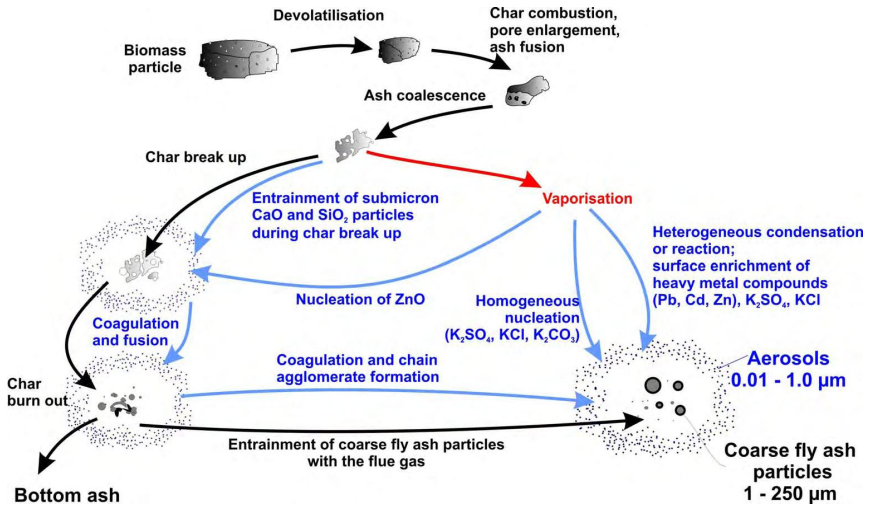

Fig. 1.1. Aerosol, deposits and pollutant formation pathways for K, Cl and S compounds

On combustion these are released, forming inorganic species that can condense and are deposited in the furnace causing slagging, fouling and corrosion, but a small quantity can be released into the atmosphere as aerosols, as illustrated in Fig. 1.1. The process of formation of the aerosol from the combustion of coal and/or biomass is characterized by three main phases:

- Volatilization of mineral matter;
- Formation of the precursors in the gas phase;
- Condensation and growth of aerosol particles.

When the fuel particles are heated in the combustion chamber, some compounds of mineral matter vaporize, species such as Na, K, S, Cl, Ca and Mg. This devolatilizing fraction depends on the characteristics of the fuel and the combustion chamber. Following volatilization of the gaseous species are involved in a series of gas phase chemical reactions leading to the formation of the main aerosol precursors. Because the low value of the vapour pressure, the chlorides and sulphates, produced by gas-phase reactions, condense in consequence to the cooling of the smoke and forming the first nucleus of condensation that will undergo further formation processes:

- Surface growth;
- Coagulation.

Studies on devolatilization of the species of interest (K, S, Cl) for the formation of aerosol from biomass combustion reveal that potassium is released in significant amount for combustion temperatures above 700°C and increase the volatilization with increasing temperatures. Other parameters that influence the devolatilization of potassium are the quantity of chlorine and silicon in the fuel, the release of potassium is favored in fuels with a higher content of chlorine and a lower silicon content. Similarly for biomass combustion, even in the case of coal volatilization of mineral matter deeply depends on the temperature and the chemical composition of the fuel, the extent of this phenomenon is reduced, usually vaporizes only 10% of inorganic matter. In any case it is seen that the volatilization is improved by the presence of a reducing enviroment. After evaluating the possibility of a heterogeous mechanism for the formation of sulfates and chlor-alkali (main precursors of aerosol) in the literature variuos authors agree consider the formation of precursor species only as a homogeneous process in the gas phase. The kinetic mechanism used is the Glaborg mechanism for describe the formation in the gas phase of sulfates, bisulfates and chlor-alkali (Na, K).

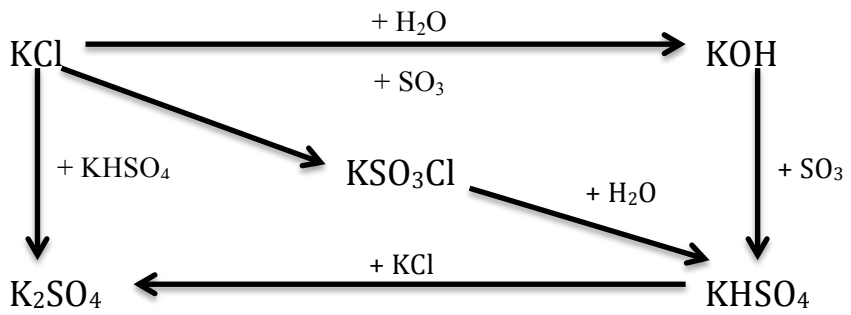

Fig. 1.2. Scheme of the formation mechanism in the gas phase of alkali metals

The Glaborg mechanism provides as a first step the conversion of SO_2 to SO_3, such as the slow stage and thus limiting the mechanism.

This passage occurs mainly through the following reactions:

$$SO_2 + OH\ (+M) = HOSO_2\ (+M)$$

$$HOSO_2 + O_2 = SO_3 + HO_2$$

A minor contribution also comes from direct oxidation reactions:

$$SO_2 + OH\ (+M) = SO_3\ (+M)$$

$$SO_2 + OH = SO_3 + H$$

$$SO_2 + O_2 = SO_3 + O$$

And from the sequence:

$$SO_2 + KO\ (+M) = KSO_3\ (+M)$$

$$KSO_3 + OH = SO_3 + KOH$$

The SO_3 formed is subsequently trasformed into K_2SO_4 by reaction with the chloride and hydroxide potassium, through the formation of stable intermediate species such as $KHSO_4$ and KSO_3Cl, as showns in Fig. 1.2. Aerosol formation is dependent on the thermodynamic equilibrium and also on the mechanism of transport. The major transport phenomena are nucleation, coagulation and surface growth, usually ignore processes such as: fragmentation, evaporation, thermophoresis, spread to surfaces and inertial impaction. By the term nucleation is ment a homogeneous condensation process that leads to formation of new particles that can later grow superficially, also working as condensation nucleus for other volatiles, or collide with each other and coagulate. The nucleation of new particles may compete with the surface growth process that usually prevails, however, in the case where the nucleus number of condensation is insufficient or the pressure of supersaturation is high enough you can have in any case the formation of new particles. Coagulation is the slowest process that occurs after the nucleation and surface growth.

Chapter 2

Formation of inorganic aerosols in pilot systems

2.1 Introduction

To correctly interpret the phenomenon of formation of aerosols (gas phase + condensation + particle grow) were studied two pilot systems located at the IFRF's headquarters site in Livorno. The experimental campaigns have been analyzed for both pilot systems to try to find trends by varying the fuel (so changing the elemental composition) and operating conditions. The two pilot systems are: IPFR and 500 kW.

2.2 IPFR

The Isothermal Plug Flow Reactor (IPFR) was designed and realized in 1994 in IJmuiden, the Netherlands, to characterize the combustion behavior of pulverized coal, substitute solid fuels and blends. It allows to run tests under conditions similar to industrial applications. After the transfer of the Foundation in Livorno (at ENEL Reaserch experimental area), the reactor was moved to next site. In this facility it is possible to investigate devolatilization and char burnout separately, under conditions that solid fuel particles experience in an industrial flame. The reactor is an example of advanced technique for pulverized fuel characterization. The IPFR is used to investigate combustion characteristics of pulverized coal and other solid fuels under a number of well-controlled specific environments. The reactor enables the coal to be evaluated at a wide variety of residence times under variable particle heating rates and combustion atmospheres. This flexibility enables the combustion performance of the coal to be studied under client/applications specified atmospheric conditions.
It is routinely used to investigate the following:

- Devolatilization characteristics of solid fuels and their blends;
- Burnout and combustion rates of various chars;
- Ignition properties of solid fuels and blends;
- Ash properties;
- Slagging;
- Nitrogen chemistry–fate of fuel nitrogen.

The reactor can be used to represent conditions found in full-scale combustion processes with heating rates in the order 104-105 K/s. Fuel is injected into a well-defined combustion environment and collected after a residence time in the reactor between 5 to 1500 ms.

The fuel conversion can be described with reaction kinetics on the basis of measurements made under these conditions. The application of kinetic data allows the prediction of the fuel behaviour under industrial conditions by means of mathematical modeling. The fuel characteristics can also provide a measure of the combustion performance relative to a reference fuel.

2.2.1 Description

Based on the IPFR 1994 model, several changes were made, mainly in heating elements, eletrical wiring, pneumatic connections, facility control and data acquisition system. The diagram of IPFR 2008 design is shown in Figure 2.1 and its characteristics are presented in Table 2.1.

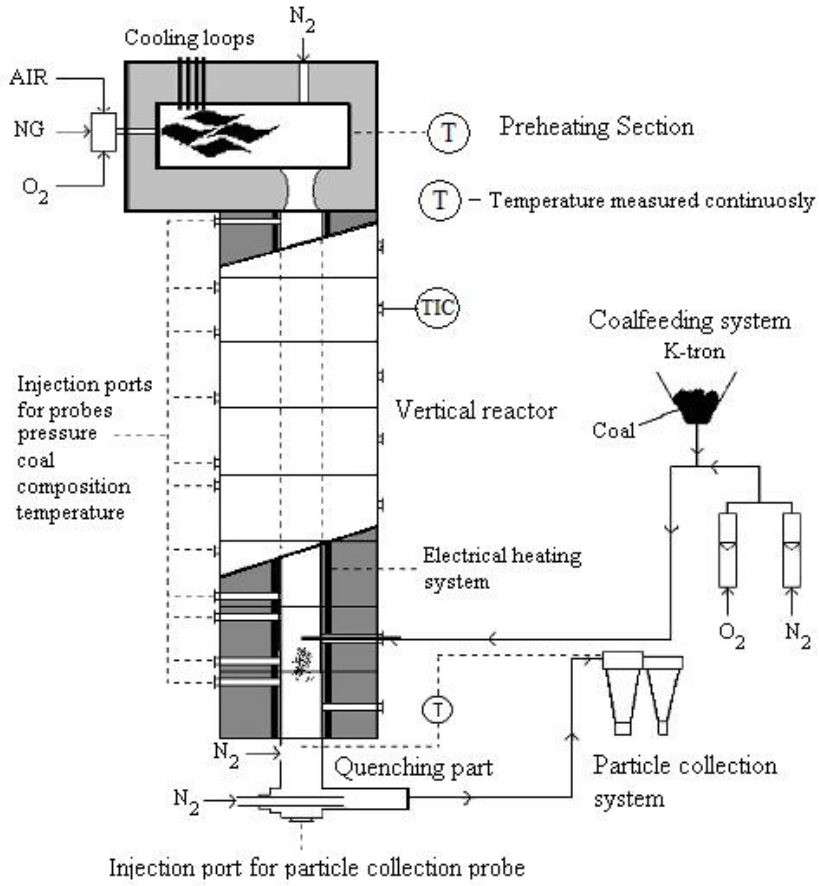

Fig. 2.1. IPFR scheme

The facility mainly consists of three sections:

- Gas pre-heating section;
- Vertical Isothermal Plug Flow Reactor;
- Exhaust with particle collection system.

In addition there are water-cooled probes that can be inserted into the reactor and a pulverized solid fuel feeding system.

CHARACTERISTIC	MEASURE
Reactor tube total length	4.5m
Reactor tube operating length	4.375m
Reactor tube inner diameter	150mm
Number of operatinf modules	8
Number of feeding ports	19
Max. Thermal input: Natural gas Electrical	 60 kW 54 kW
Operating temperature	700 – 1400°C
Residence time	5 – 1500 ms
Max. gas flow rate	75 Nm^3/h
Quenching gas (Air, N_2)	20 – 25 Nm^3/h
Carrier gas (Air, N_2, N_2/O_2 mixture)	1.8 – 2 Nm^3/h
Min. feeding rate of pulverized fuel	0.08 kg/h

Table 2.1: IPFR technical specification

The gas preheating section supplies the reactor with gases of a desired composition and temperature. This section consists in the pre-combusting chamber of one meter length with an internal diameter of 300 mm fired by a 50 kW aerodynamically air staged natural gas burner (AASB). The pre-combustor provides hot primary gas in the temperature range from 700 to 1400 ºC. Flue gases can be mixed with additional gases like nitrogen and carbon dioxide in order to adjust the desired gas composition flow going though the reactor tube. The additional gases were injected with an injection probe. It is not possible at present to feed pure oxygen. The reactor tube (Figure 2.2) consists of eight 500 mm height modules which can be independently controlled and heated electrically with silicon carbide U-type heating elements. In this way isothermal conditions within a margin of 10 ºC can be obtained along the reactor tube in the temperature range of 700 to 1400 ºC (nominal operative range). The moduled refractory tube is made of 90V High Alumina which is relatively inert and may be used under both oxidizing and reducing conditions to a maximum temperature of 1400ºC. The tube has an operating length of 4 m with an internal diameter of 150 mm.

Fig. 2.2. Vertical isothermal plug-flow reactor

There are two 250 mm height modules at the top and at the bottom without electrically heating system. A K-tron mass flow controller provides a continuous mass flow of pulverized coal. This system consists of a control unit and a device which exist of a reservoir with an electric driven screw on a balance. At the outlet of the K-tron the pulverized coal is mixed with gasses in order to transport the particles to the furnace. This transport gas has the same oxygen concentration as the gas mixture in the tube reactor. The coal feeder sprays the coal-gas mixture into the tube-reactor. Coal can be fed with automatic or manual system. To introduce the pulverized fuel in the reactor, a water-cooled fuel-feeding probe is used. The pulverized fuel coming from the coal feeding system is transported by air, nitrogen or nitrogen-oxygen mixtures at ambient temperature to reproduce flue gases oxygen concentration in the flue gases. The feeding flow can be adjusted to have the same velocity at the nozzle exit of the probe as the assumed mean reactor velocity in order to inject the fuel isokinetically. An axial and a radial feeding probe are available.

The axial probe is inserted from the precombustion-chamber in the reactor. It is used at present to feed additional nitrogen to the reactor. Figure 2.3 shows a schematic drawing of the axial feeding probe.

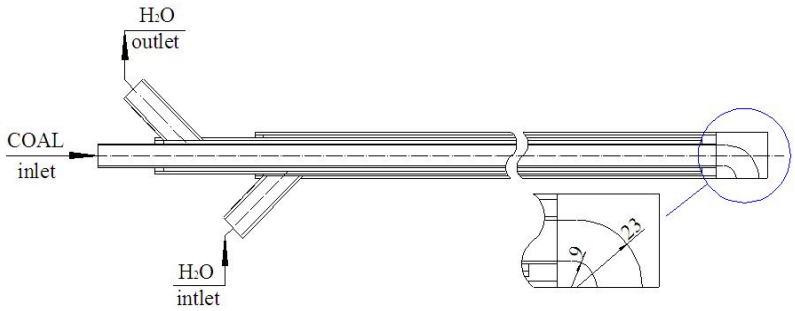

Fig. 2.3. Axial feeding probe

The radial feeding probe is inserted in the reactor by making use of the various ports in the tube. The probes are inserted the injector nozzle is placed exactly on the central line of the reactor tube. Figure 2.4 shows a schematic drawing of the radial feeding probe.

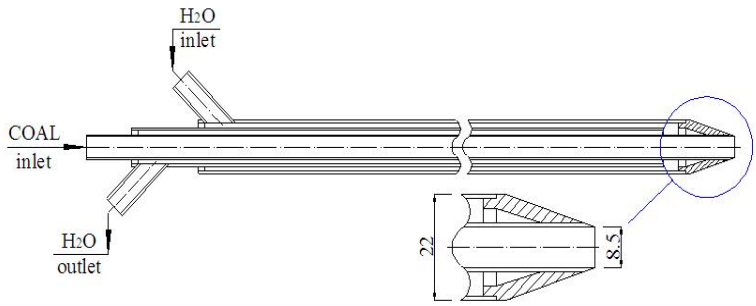

Fig. 2.4. Radial feeding probe

The sampling probe is inserted in the reactor in order to collect part of the gas-solid mixture out of the reactor. The water cooled jacked preserves sample probe steel walls and maintains the cooling gas at ambient temperature. Sampling probe characteristics are shown in Figure 2.5. Samples of different residence times are collected by inserting the feeding probe at different heights in the reactor tube.

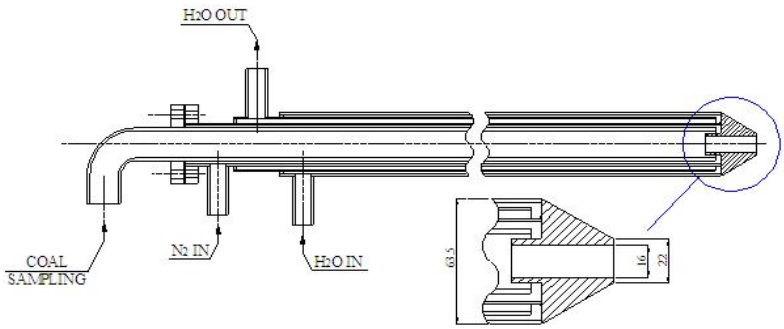

Fig. 2.5. Sampling probe draw

The sampled particles are nitrogen quenched to temperatures below 200ºC to allow no further reaction and they are separated from the flue gas by a cyclone separator. This allows the observation of processes such as particle heating, devolatilization, gasification, combustion (oxidation), reduction and defragmentation of solids. The mixture which is not sampled is air quenched; particles are collected in a separation system, which consists of two cyclones and a bag filter. The mixture which is not sampled is indicated as exhaust and the corresponding line is named exhaust line.

2.2.2 Setup for aerosol test

In the experimental system that is used for the production and the measurament of the aerosol it is reproduced in controlled enviroment conditions close to those characteristics of the actual combustion processes. The system consists of: a IPFR reactor, already previously described, a flue gas cooling stack, a sampling system and dilution of the aerosol product, a system of measurament of the aerosol in terms of mass, chemical composition and grain size distribution of particles. The scheme of the experimental apparatus is shown in Figure 2.6.

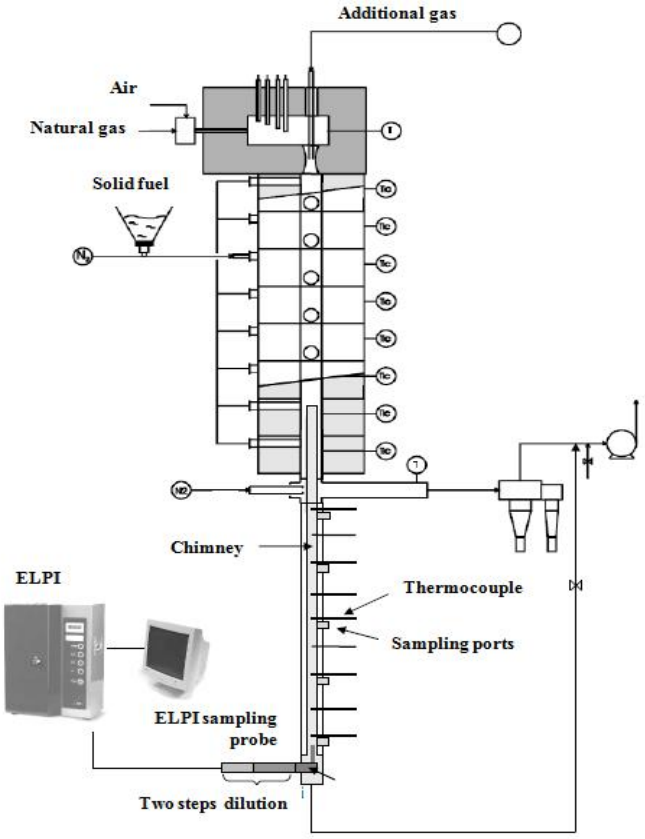

Fig. 2.6. The IPFR setting for aerosol formation test

The production of aerosol precursors in the gas phase takes place inside the IPFR, then, in the cooling chimney are produced the first condensation nucleus which occur coagulation phenomena and surface growth. In order to follow the process of formation and growth of the aerosol, has been carries out a sampling isokinetic three access doors along the chimney profile, using an appropriate dilution system so as to avoid, after sampling, further modifications of the particles. The sampled aerosol has been sent to the measuring instrument ELPI (Eletrical Low Pressure Impactor) made available by ENEL laboratories, through which are obtained measurament of grain size distribution of particles and sampled aerosol mass. The samples collected on the impactor plates can be analyzed with the SEM (Scanning Electron Microscope) equipped with one X-ray spectrometer (EDX), which provides the quantitative elemental chemical composition of the sampling.

The chimney is made of stainless steel and is 2.5 meters lenght, have six sampling ports and nine thermocouples to check the flue gas temperature. An additional 1.1 meters length ceramic tube was fixed inside the IPFR to keep the separation between the quenching air and the flue gas. The dimensions chosen for the chimney grant a temperature at the end of it in the range 200-300°C. The flue gas velocity at the inlet was regulated to grant an isokinetically sampling. The sampling and diluting apparatus used was the Dekati FPS. A raw sample is extracted from the source (i.e. exhaust or flue gas) by using a stainless steel probe. The sample is subsequently diluted in two stages employing perforated tube and ejector dilution, respectively. Dilution temperatures and pressures are measured in real-time by a control unit enabling second-by-second dilution ratio calculation, which takes changes in raw sample properties directly into account. The dilution ratio calculation result is saved in real-time along with temperature and pressure data in an easily accessible form for post-processing of the data. As mentioned earlier, the impactor multistage ELPI (Figure 2.7) of Dekati company is an instrument that measures the patricle size distribution and the mass in real time of the particulates. The ELPI operates in the size range of the particles between 7 nm and 10 microns.

Fig. 2.7. The ELPI

The operating principle of ELPI can be divided into three parts: charge of the particles in a unipolar corona charger, classification of the particles according to the dimensions in a cascade impactor, electrical detection with electrometers. The particles are first charged to a known level in the charger; after being loaded the particles enter into a low pressure cascade impactor with collection step electrically isolated. The collection of the particles at each stage of a collision depends on the aerodynamic size of the particles.

The electrical charge carried by the particles in each impact is measured in real-time by multichannel electrometers. This measured current is directly proportional to the concentration of the number of particles and the size.
The processing of data has been uniformly carried out by imposing the following terms:

- Diluition ratio read in the FPS instrument;
- Density 2 g/cm^3;
- Stokes diameter;
- Considered diameter of 10 channels (from #2 to #11), with the exclusion of the diameter of channels extremes (the finer #12 and the coarser #1).

With these conditions the sampled particulate is belong to the category PM2.5. It is important to emphasize that the ELPI tool does not provide a direct measure of the particulate concentration in the sampled gas.

2.2.3 Combustion conditions

The solid fuels used are: South African coal and sunflower expeller ground (biomass). These two fuels were fed individually and in a mixture of 50% of thermal input. In addition to facilitate the interpretation of the measures it was also fueled a "source" of aerosol chemically pure, a mixture of KCl and graphite. The title of KCl of this mixture and the flow rate fed have been determined so as to match the potassium such as that of coal-biomass mixture. In this case KCl assumes the role of the source of alkaline aerosols, the graphite takes the role of inert powder suitable for transport KCl powder, having the same specific weight. The panel of sunflower is the main byproduct of the pressing (mechanical and/or chemical) of the seeds of sunflower for biodiesel production. The chemical analysis of the biomass and composition of ash (further elements expressed as oxides) are reported in Table 2.2.

Proximate Analysis	**Mass fraction (%dry)**
Volatiles	72.6
Fixed carbon	19.2
Ash	8.2
Moisture	9.1
Ultimate Analysis	**Mass fraction (%w/w, daf)**
C	46.5
H	5.7
N	6.1
S	0.5
Cl	0.143
F	0.007
O	41.05
HHV (cal/g)	4104
LHV (cal/g)	3785
Ash Analysis	**Mass fraction (%)**
Al_2O_3	0.2
CaO	12.9
Fe_2O_3	0.6
K_2O	26.7
MgO	14.5
MnO_2	0.08
Na_2O	0.4
P_2O_5	28.3
SiO_2	1.7
TiO_2	0.01

Table 2.2. Chemical analysis of panel of sunflower and ash made in laboratory

This biomass is from plant origin, so is rich of K, P and Ca, this element promotes the formation of fine particles and the deposition phenomenon on convective surfaces (fouling). Potassium is an alkali metal that, vaporizes at flame temperature, can condense on the exchange surfaces thermal radiation, also it give low-melting ash. Also S is not trascurable (0.5% dry), characteristic not comune in biomass adoperate as fuel, and a medium presence of Cl (0.14% dry). Chlorine can give problems of corrosion on the tube of the vapour and can promote the formation of dioxine.
The coal used is South African coal, the chemical analysis of it and composition of ash (further elements expressed as oxides) are reported in Table 2.3.

Proximate Analysis	**Mass fraction (%dry)**
Volatiles	26.9
Fixed carbon	57.1
Ash	16.0
Moisture	2.8
Ultimate Analysis	**Mass fraction (%w/w, daf)**
C	72.2
H	3.9
N	1.8
S	0.6
Cl	0.04
F	0.224
O	21.236
HHV (cal/g)	6478
LHV (cal/g)	6265
Ash Analysis	**Mass fraction (%)**
Al_2O_3	25.3
CaO	8.3
Fe_2O_3	3.4
K_2O	0.6
MgO	1.7
MnO_2	0.04
Na_2O	0.1
P_2O_5	1.7
SiO_2	45.2
TiO_2	1.5

Table 2.3. Chemical analysis of coal and ash made in laboratory

This coal is richer than biomass in carbon and fluorine, meanwhile is poorer in chlorine and nitrogen. The fraction of volatiles present in coal is about 60% less than biomass, meanwhile the ash is higher in the coal case. In Figure 2.8 is shown the analysis of ash in comparison.

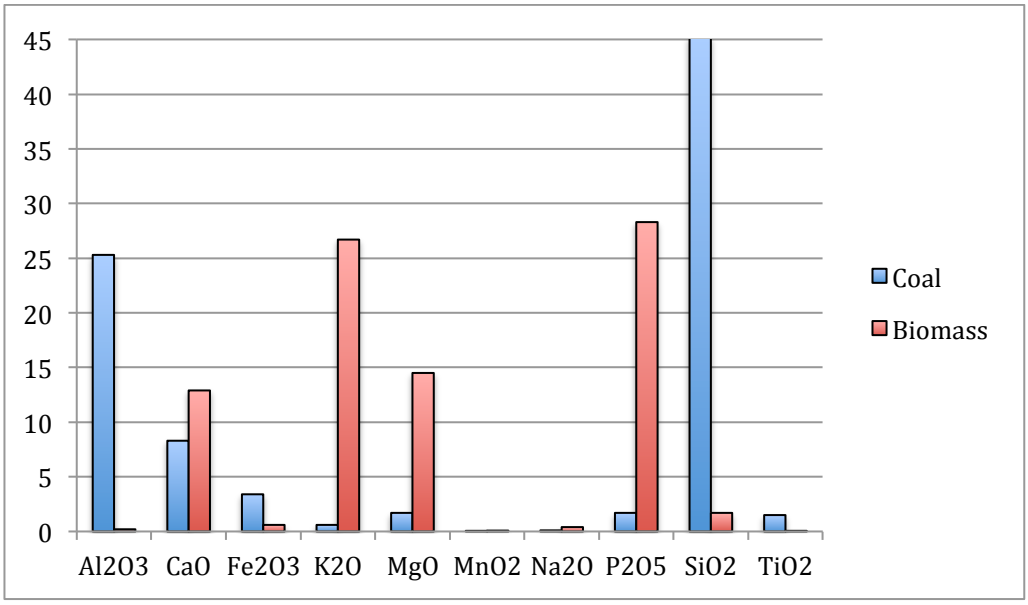

Fig. 2.8. Comparison of the ash analysis

Based on the characteristics of the dispenser that feed the powder to the IPFR reactor and analysis of chemical fuels, it has been eleborated the matrix of operating conditions of the power supplies. All measuraments were acquired IPFR maintaining the reactor at a temperature of 1300°C and with 25 Nm^3/h of flue gas. The sampling was acquired for three doors at different levels of temperature (315 to 680 °C). The matrix of the measurements is shown in the Table 2.4.

Sampling ports	Type of fuel	Flow IPFR (Nm^3/h)	Additional gas (ppmv)	T IPFR (°C)	Excess % O_2	Type of Measurament
P_1, P_3, P_4	KCl + graphite	25	SO_2 0,250,500,1000	1300	0.5%, 2%	ELPI (number)
P_1, P_3, P_4	Biomass coal	25	SO_2 0,250,500,1000	1300	0.5%, 2%	ELPI (number)
P_1, P_3, P_4	Biomass	25	SO_2 0,250,500,1000	1300	0.5%, 2%	ELPI (number)
P_1, P_3, P_4	Coal	25	SO_2 0,250,500,1000	1300	0.5%, 2%	ELPI (number)

Table 2.4. Matrix of experimental tests

In all these measures the ELPI was used for sampling in number. The acquired data were processed with the instrument software. The particulate sampled results belong to the category $PM_{2.5}$. It is important to emphasize that the ELPI instrument does not provide a direct measurement of particulate concentration in gases sampled. So the amount of patriculate is a relative value, that indicate the variation of the production of the particulates while change the combustion conditions.

2.2.4 Results

The data have been implemented to try to find the trends to vary the process parameters, such as quantity % of O_2 and SO_2 present. The figures belowe (Figure 2.9, 2.10, 2.11, 2.12, 2.13, 2.14) report the tendency of the particles size distributions in biomass and co-firing conditions. The data were normalized to the maximum value for each measurement.

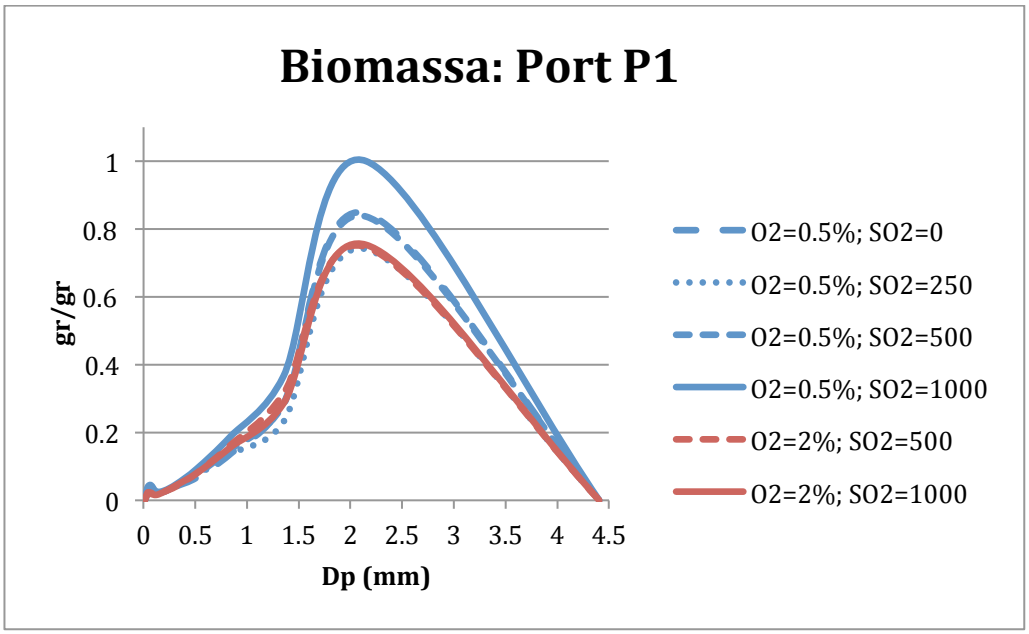

Fig. 2.9. Biomass trand port P1

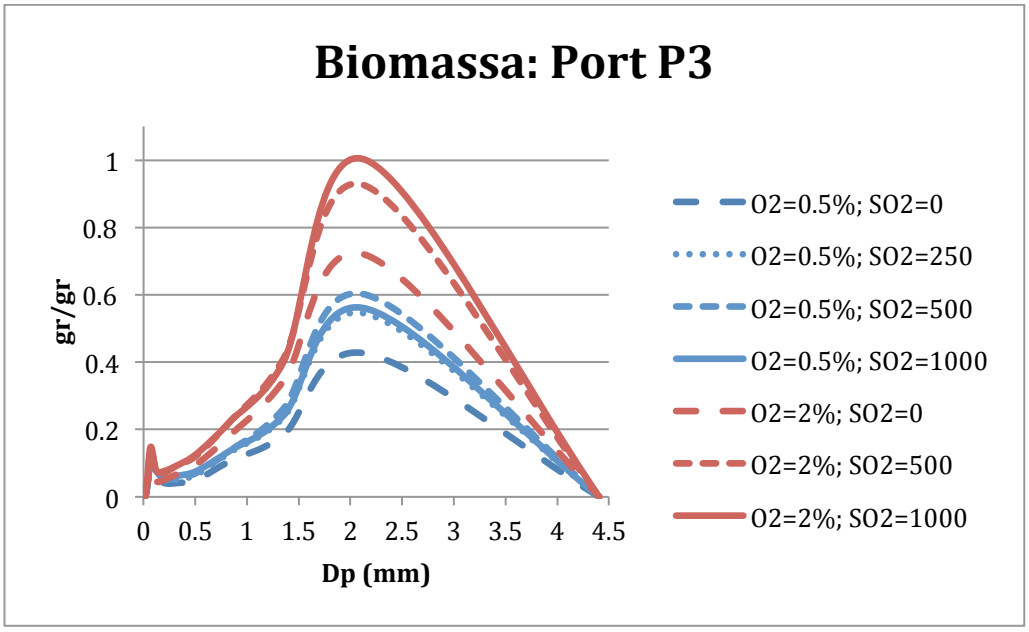

Fig. 2.10. Biomass trend port P3

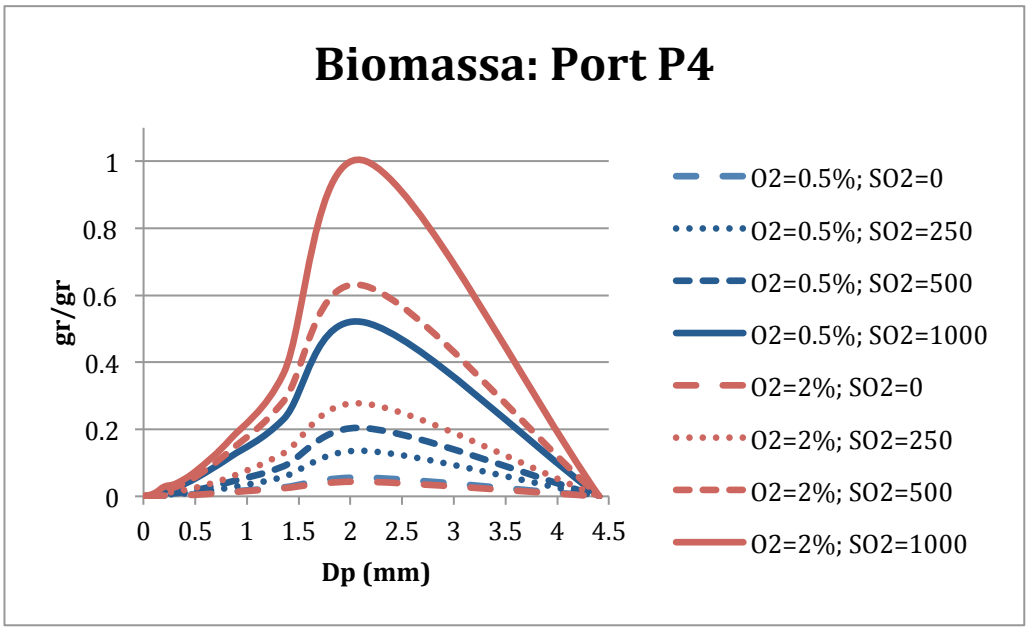

Fig. 2.11. Biomass trend port P4

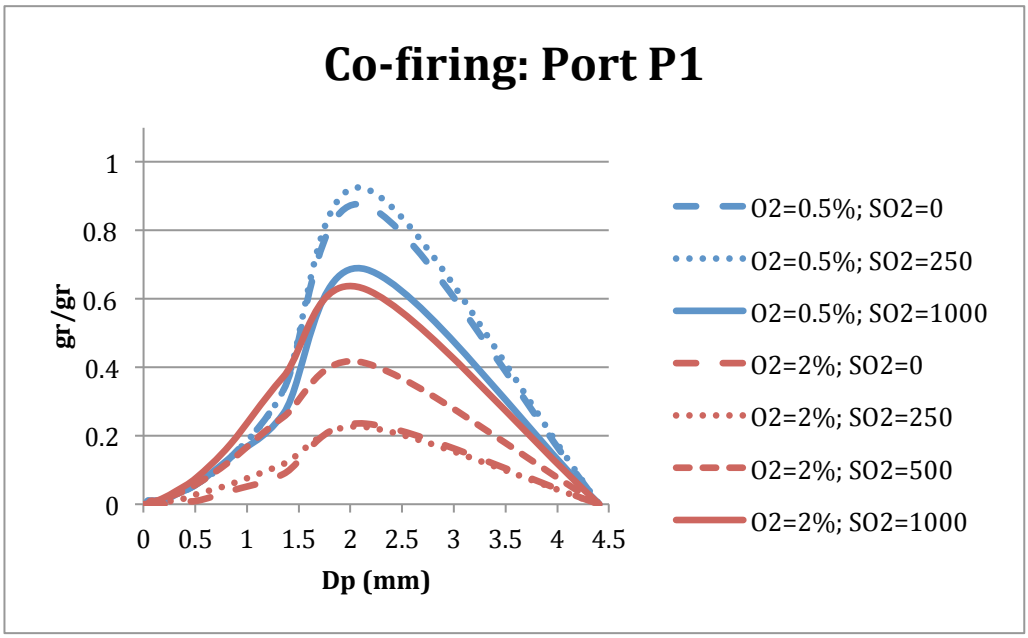

Fig. 2.12. Co-firing trend port P1

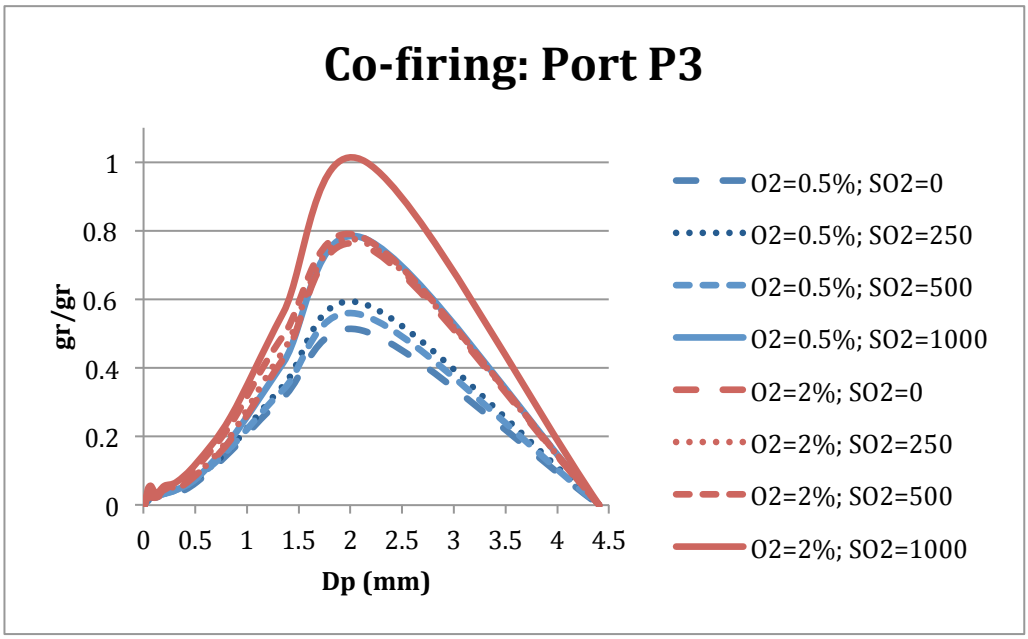

Fig. 2.13. Co-firing trend port P3

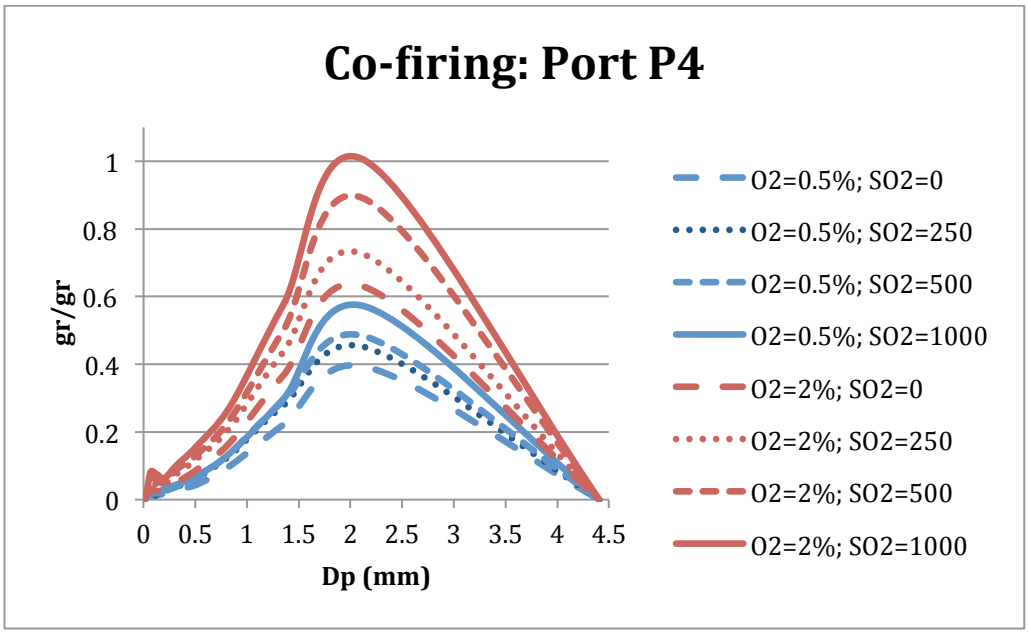

Fig. 2.14. Co-firing trend port P4

The following figures (Fig. 2.15, 2.16, 2.17, 2.18) shows the $PM_{2.5}$ concentration in mass by varying the sampling ports, oxygen and SO_2 in the flue gas.

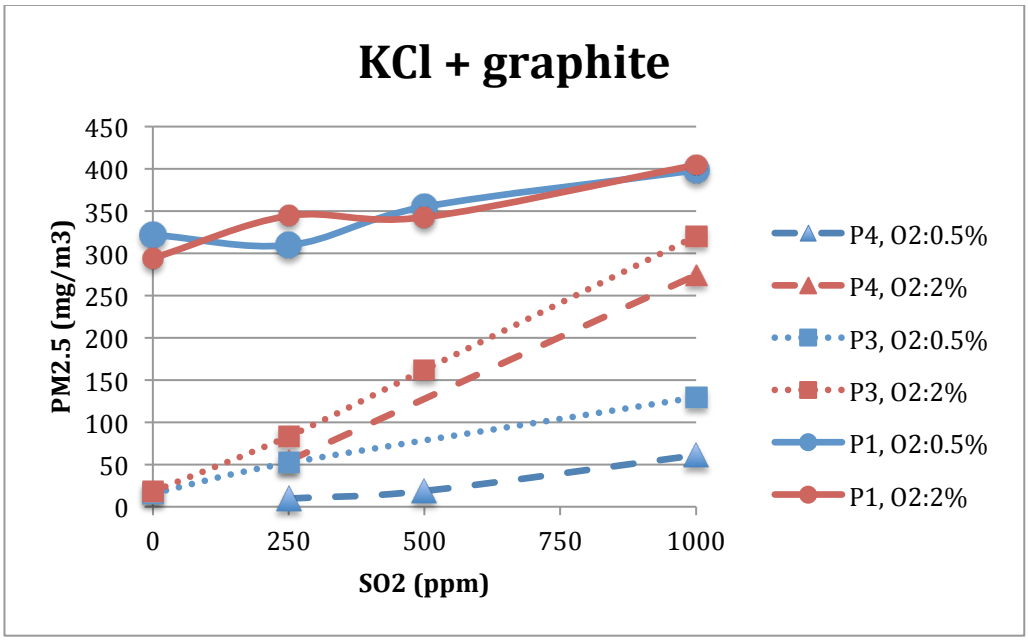

Fig. 2.15. Fuel supply KCl

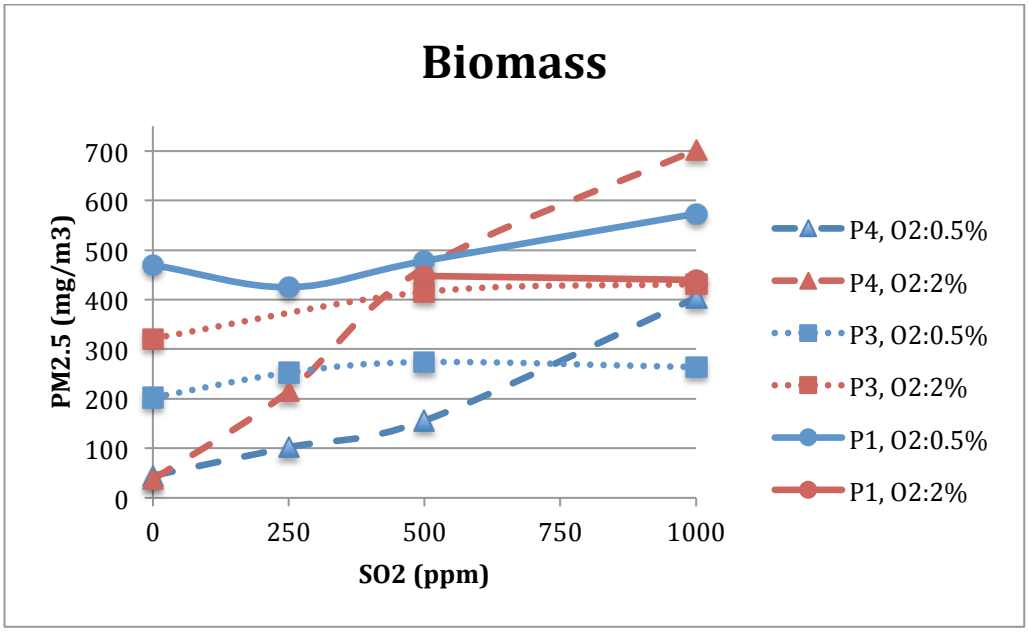

Fig. 2.16. Fuel supply Biomass

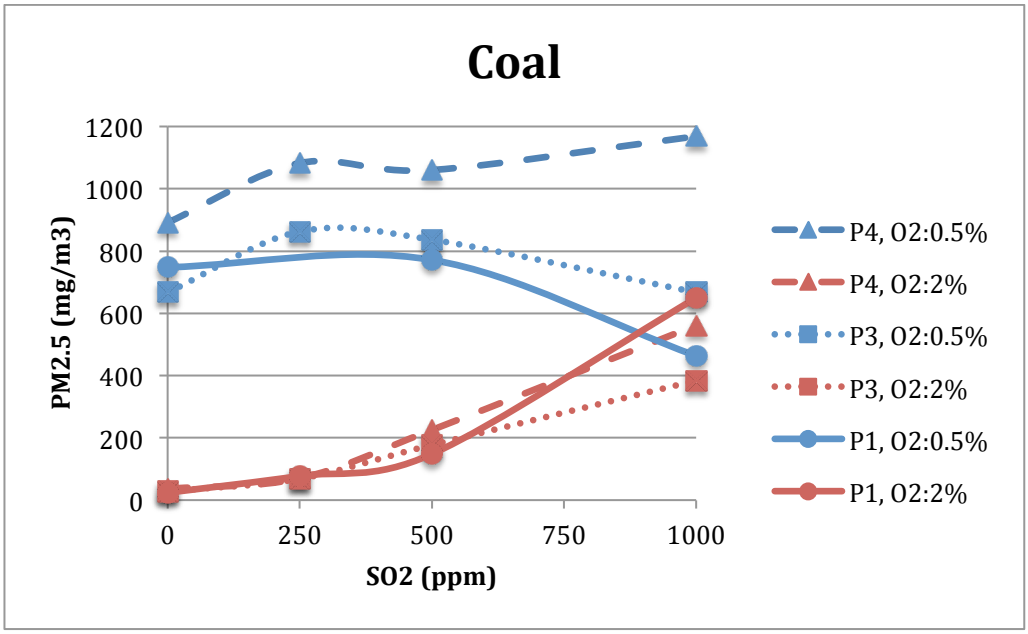

Fig. 2.17. Fuel supply Coal

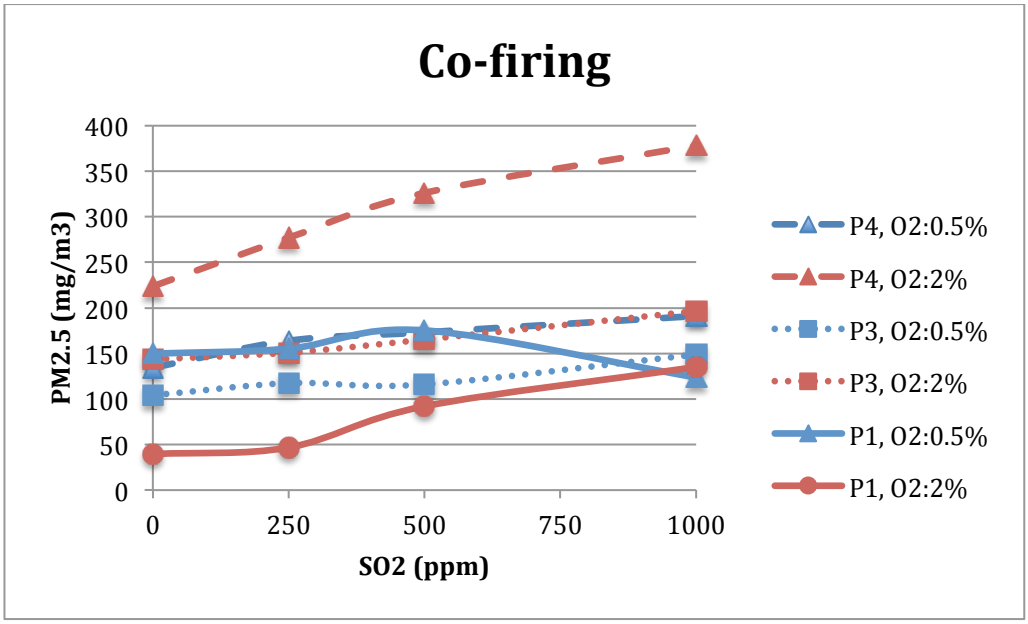

Fig. 2.18. Fuel supply Co-firing

2.2.5 Comments

In case the fuel feeding is **KCl** with graphite, the main phenomenon of formation of $PM_{2.5}$ is suppose that both the chlorination and sulfation of potassium hydroxide, promoted by SO_3 gaseos, which is formed by oxidation of SO_2, through a chain of "slow" reactions at the temperatures of the passage in the chimney flue. An interpretation of the measure shown in figures is propose. The sampled particulate from the port P1 (the hottest being the closest to the entrance of the fumes in the chimney) shows a trend costant to vary the oxygen and SO_2, in agreement with the fact that at high temperatures and short residence times there wasn't appreciable conversion of SO_2 into SO_3 able to activate the sulfation of hydroxides. The level differences between the concentration ports may be because moving to the lower temperatures and longer residence times, alkaline vapors undergo heterogeneous condensation processes. In this case, this type of condensation is favored that in the following structure, because the level of coarser powders due to the inert graphite is roughly 6 times by mass of that of fly ash present in other feeds. The trend of the concentration for the measures related to the doors P3 and P4 show the same trend with respect to oxygen and SO_2, suggesting that in the fumes to those temperature and residence time of sulfation reactions are promoted by SO_3 contributing to the formation of aerosols.

In the case of **Biomass/Coal** co-firing figures show a consistent trend for all the sampling ports and a moderate dependence of the concentration of the $PM_{2.5}$ by varying oxygen, and poor SO_2 influence, with the exception of the measures to 2% oxygen recorded at P4 sampling ports. Furthermore the particulate concentration levels are lower overall subsequent supplies only biomass and coal only, to equal heat input. The low SO_2 influence may be due to the fact that potassium and other elements that generate aerosols are present in panel of sunflower already form sulphates and phosphates, given the high proportion of these two elements. Also a part of the alkali vapors can be adsorbed by the coal ash in the first seconds of flight in the reactor. So, overall production would take place in $PM_{2.5}$ first seconds of permanence in the reactor and IPFR not invest, if not secondarily, the permanence of the smoke in the chimney. Note also, as in all ports, the concentration of $PM_{2.5}$ grow with the excess oxygen, confirming the hypothesis that the aerosol is produced "in combustion" and suggesting a low level of soot. Finally, the highest concentration of $PM_{2.5}$, with increasing SO_2, recorded at port P4 to 2% of excess oxygen it could be due to the formation of acid mists.

In the case fed with one **Biomass** the figures show concentration levels overall higer then the previous case. This is a consequence of the fact that the quantity alkali and alkaline earth metals fed with biomass is approximately double compared to the co-firing. There may be a little less clear dependence of from the concentration of SO_2 level and for low oxygen values, with the exception of the port P4, and a more pronounced dependence to 2% of oxygen excess. So in the formation of $PM_{2.5}$ are intervening both phenomena which develop in the combustion, both phenomena promoted by sulfation reactions during the stay of the smoke in the chimney.

If fed only **Coal** figures show a clear distinction between the particulate concentration in the measurements performed at the 0.5% excess oxygen and that to 2% of oxygen. The level clearly higher $PM_{2.5}$ concentration in measures to 0.5% of oxygen is due to the soot that is formed in this severe atmosphere for the combustion of coal. The $PM_{2.5}$ level drops drastically at higher oxygen concentrations. In these cases, in the absence of SO_2, the concentration of $PM_{2.5}$ not vary much by varying the sampling ports and is maintained at minimum values, confirming both the lesser susceptibility of coal to produce $PM_{2.5}$ inorganic compared to biomass, that formation take place in combustion and not in the cooling chimney. Instead the upward trend of the concentration values with increasing SO_2 they are to be attributed to the formation of acid mists.

2.3 500 kW

In January, 2012, when the control room and fuel lines were adapted to the new safety legislation, the 500 kW experimental furnace became again available. The facility can operate using natural gas or coal as a fuel, but a dedicated feeder was adapted to feed also biomass thus performing co-firing tests.

2.3.1 Description

The furnace develops around a vertical combustion chamber, covered with refractory material. The burner is located vertically (as shown in Figure 2.19) and the flame develops from the top to the bottom. The exhausts flow from the combustion chamber to two convective heat exchangers after which a bag filter is located to remove dusts in the exhausts. The bag filter can also be by-passed. The exhausts composition is monitored online with a gas analysis system, which allows to determine the CO, CO_2, O_2, NO_x, SO_2 concentration. As stated above, the maximum thermal input for the furnace is of 500 kW, whereas the time required to heat the furnace to the operating temperature is of about 60 hours.

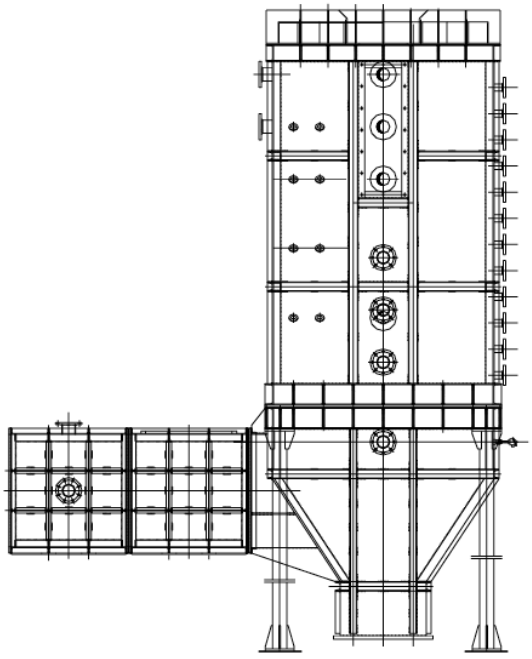

Fig. 2.19. Combustion chamber and horizontal duct

The combustion chamber is provided with several ports, which are located at different heights and allow to access the chamber itself (as shown in Figure 2.20). From the ports it is possible to perform temperature and heat flux measurements, or to sample gases and solid particles directly from the flame. Some other ports are located along the horizontal duct that links the combustion chamber with the first convective section.

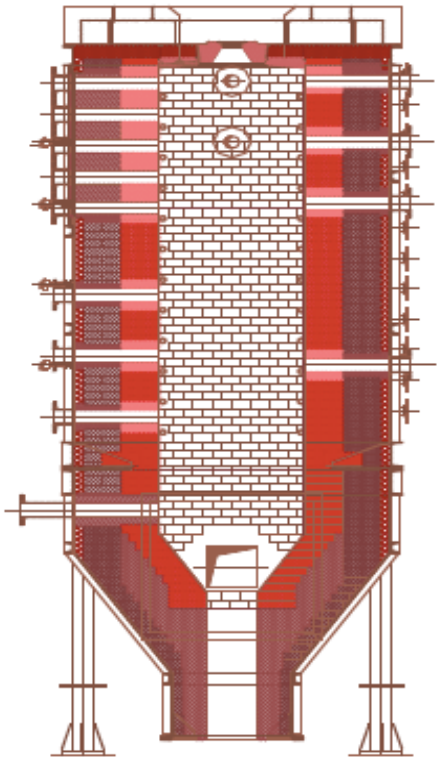

Fig. 2.20. Combustion chamber scheme

The combustion chamber is 4 m long and has a square section of 84 cm. The refractory wall of the furnace has a width of 50 cm. The facility is provided with an automatic system to acquire all the parameters concerning its operation, which are useful to analyze the results at the end of the experimental campaign. In particular, four thermocouples allow to monitor the temperature inside the combustion chamber's refractory, whereas other three ones measure temperature along the horizontal duct. Finally, the gases' temperature is measured by three additional thermocouples inside the combustion chamber, and by another one inside the horizontal duct.

The furnace is provided with a poli-fuel low-NO_x burner (shown in figure 2.21), with a gas injection probe on the center. The burner also has primary, secondary and tertiary air feeding tubes, as well as coal feeding ones. On the external side of the burner, the swirlers and secondary/tertiary air dampers control levers are located.

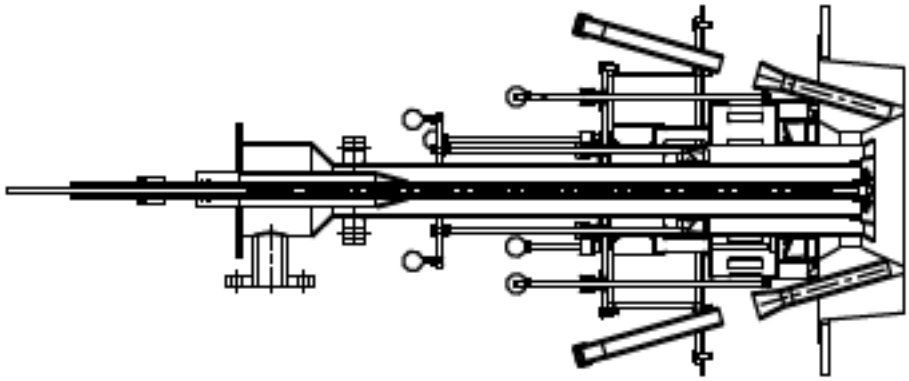

Fig. 2.21. Poli-fuel low-NO_x burner

The facility is provided with two natural gas lines. The former one has a fixed flow, and it feeds the pilot torch, which is used only to switch on the furnace; the latter has a variable flow, and it is used to fire the furnace with natural gas. The coal is stored into two silos, which are located near to the facility. From the silos, coal is carried to the burner by a pneumatic system; the mass flow regulation is carried out by a rotatory cell. The biomass used during co-firing tests was carried to the furnace through a dedicated system designed by IFRF to operate under the new safety standards. This system consists of a storage from which the biomass is fed, through a screw, to a cut mill. The milled biomass is carried through an ejector to the coal feeding line, where mixing between the fuels is guaranteed.

2.3.2 Measurements

The temperature measurements were performed with the IFRF pyrometer, shown in figure 2.22. The measurements were performed through port number 2 and number 5. Moreover, also the port of horizontal duct was used to measure the temperature of the gas in the point where fouling was sampled. For each port, seven measurements were performed, at a distance of 10 cm between each point. The first measurement point was at 10 cm from the wall of ports, and the last point was at 10 cm from the opposite wall. Before taking the measurement value, it was waited 2-3 minutes to achieve a stable temperature. The estimated error is of about 10°C for each point. As expected, during the experimental campaign several ceramic shields had to be substituted, due to occlusions caused by the melted ashes.

Fig. 2.22. The IFRF pyrometer inseted in port number 2

The fouling sampling was performed in the horizontal duct located after the combustion chamber. The dedicated probe is made of two air-cooled concentric tubes, with two thermocouples to control temperature in the two points, shown in Figure 2.23. After the insertion of the probe in the horizontal duct, it was waited for the thermocouple TC0 to reach 650°C. Then, temperature was kept around this value for 15 minutes using the cooling air. At the end of the sampling, the probe was extracted and cooled before sampling the material.

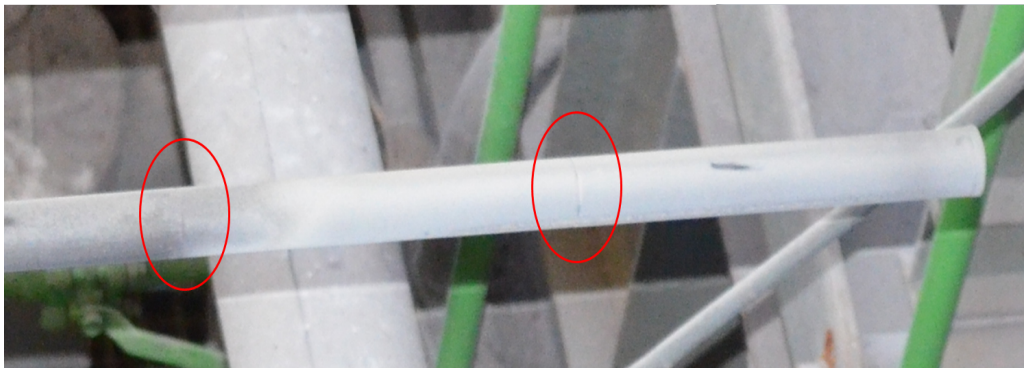

Fig. 2.23. Fouling sampling probe, with the TC0 (right) and TC1 (left) thermocouples

As stated above, the sampling was performed after the probe had cooled down. In particular, using a clean funnel, a small brush and 100 ml of demineralized water, the fouling was sampled. After the collection, a small amount of sample was separated to be sent to SEM analysis. The same sampling operations were repeated twice for each operating condition.

2.3.3 Combustion conditions

The solid fuels used are: coal from Venezuela and a torrefied biomass, named E-coal. The results of the standard analyses perfomed on both fuels are shown in Table 2.5 and 2.6. The planned tests to characterize different coal-biomass blends are shown in Table 2.7, where the fractions of coal and biomass are calculated on the thermal input.

Proximate Analysis	**Mass fraction (%dry)**
Volatiles	39.7
Fixed carbon	53.2
Ash	7.1
Moisture	5.5
Ultimate Analysis	**Mass fraction (%w/w, daf)**
C	76.3
H	5.4
N	1.5
S	1.4
O	8.3
LHV (MJ/kg)	30.46

Table 2.5. Chemical analysis of coal

Proximate Analysis	**Mass fraction (%dry)**
Volatiles	19.2
Fixed carbon	73
Ash	7.2
Moisture	4.2
Ultimate Analysis	**Mass fraction (%w/w, daf)**
C	79
H	1.9
N	0.5
S	0.1
O	18.4
LHV (MJ/kg)	27.59

Table 2.6. Chemical analysis of torrefied biomass

	Coal	**Biomass**	**Oxygen**
Run 1	100%	0%	
Run 2	88%	12%	4.5%
Run 3	73%	27%	2.5%
Run 4	93%	7%	2%

Table 2.7. Composition of the blends tested

The 500 kW furnace configuration allowed to sample, after testing the combustion of a coal-biomass blend, ashes collected in the box located at the bottom of the convective heat exchangers. The composition of those ashes was determined through standard laboratory analyses both for major and minor substances. The Table 2.8 shows the composition of ashes collected at the bottom of the convective heat exchangers for each tested coal-biomass. That are shown in figure 2.24.

Coal-biomass blend composition	**73-27 (%)**	**88-12 (%)**	**93-7 (%)**	**100-0 (%)**
Al_2O_3	20.13	21.36	22.26	24.43
CaO	9.97	6.2	5.59	3.54
Fe_2O_3	4.43	8.57	4.47	4.51
K_2O	2.95	1.33	1.26	0.63
MgO	1.94	1.49	1.44	1.23
MnO_2	0.7	0.29	0.25	0.06
Na_2O	0.51	0.45	0.47	0.47
P_2O_5	0.84	0.58	0.6	0.52
SiO_2	48.69	52.6	57.69	59.09
TiO_2	1.69	1.78	1.89	2.09

Table 2.8. Composition of the convective ashes for different run

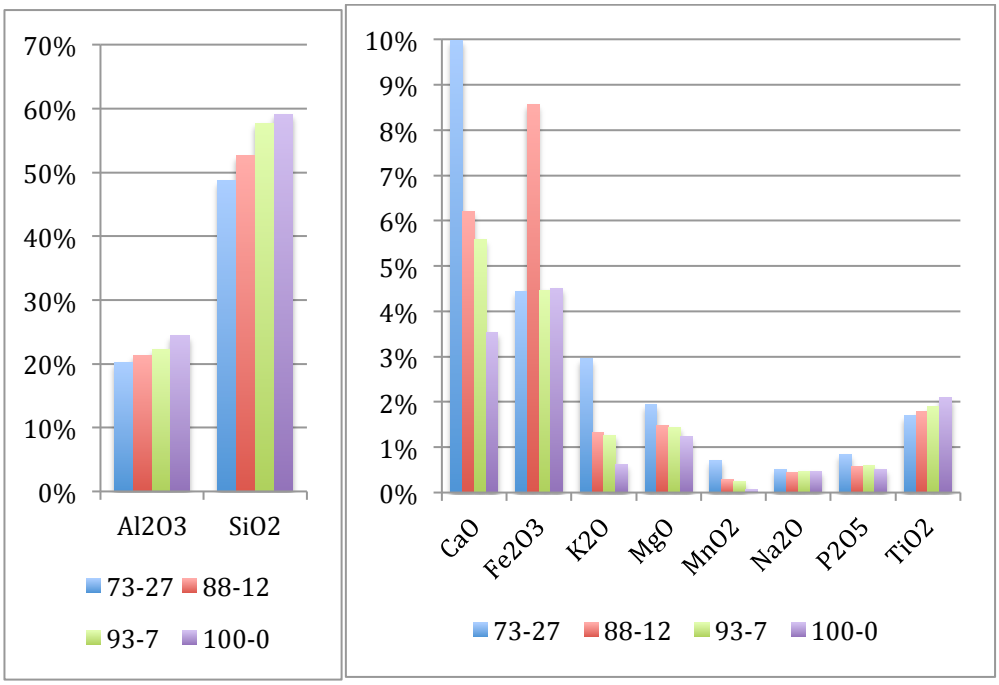

Fig. 2.24. Convective ashes composition for different run

From the fouling compositions shown in the above figure 2.24, it is possible to determine a fouling index, defined as the ratio between the concentration of basic and acid species (B/A ratio). The applied correlation is the following one: usually a fuel is considered having a low fouling tendency if the B/A ratio is lower than 0.6.

$$\frac{B}{A} = \frac{Fe_2O_3 + CaO + MgO + Na_2O + K_2O}{SiO_2 + Al_2O_3 + TiO_2}$$

Figure 2.25 shows the values of the B/A index calculated for each tested coal-biomass blend. Although it is not clear the relation between the fouling tendency and the amount of biomass in the blend, it can be noted that the fouling tendency is higher for the material sampled during combustion of a blend with a higher biomass fraction.

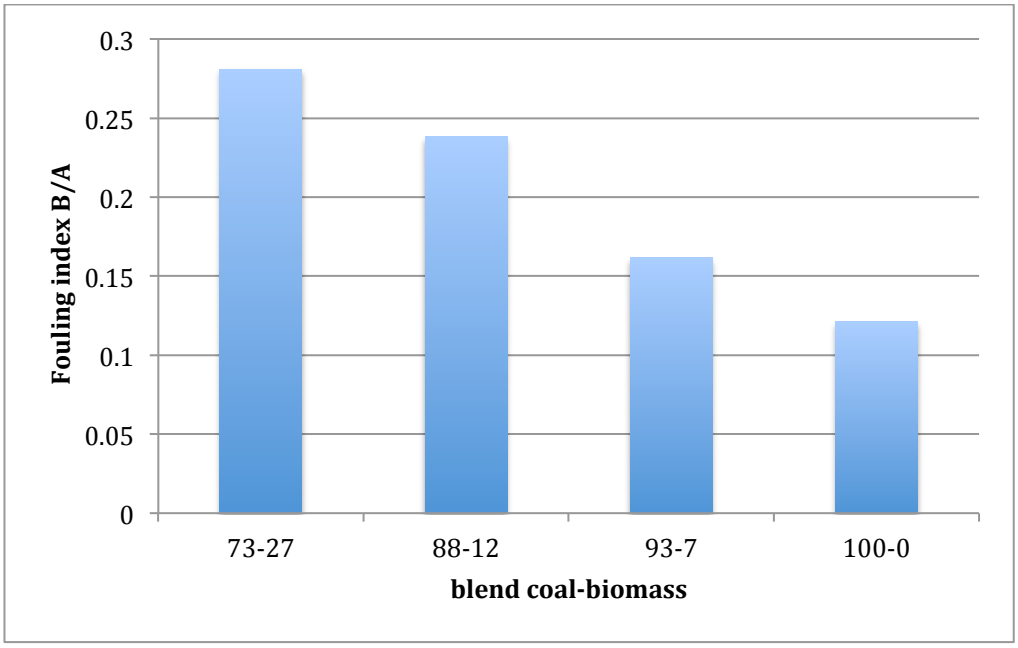

Fig. 2.25. Fouling index

2.3.4 Results

The pyrometry measuraments are shown in figures 2.26 and 2.27. For the port 2 the tendency are similar by varying the run, that is the fraction of biomass. For the port 5, the tendency are a little bit strange, also here is not clear the relation between the measure and the different run.

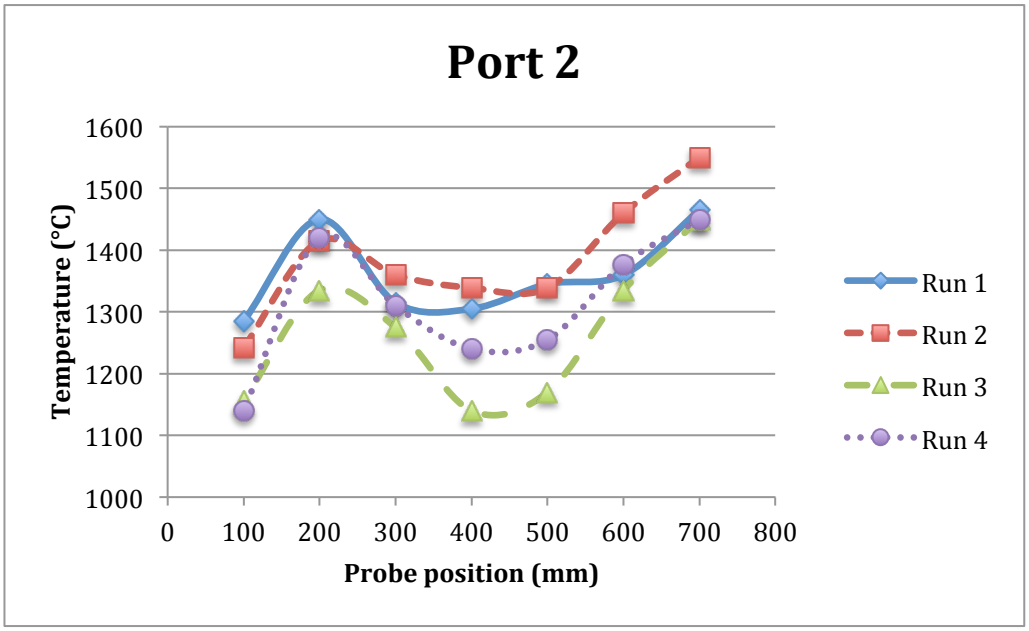

Fig. 2.26. Pyrometry measurament at port 2

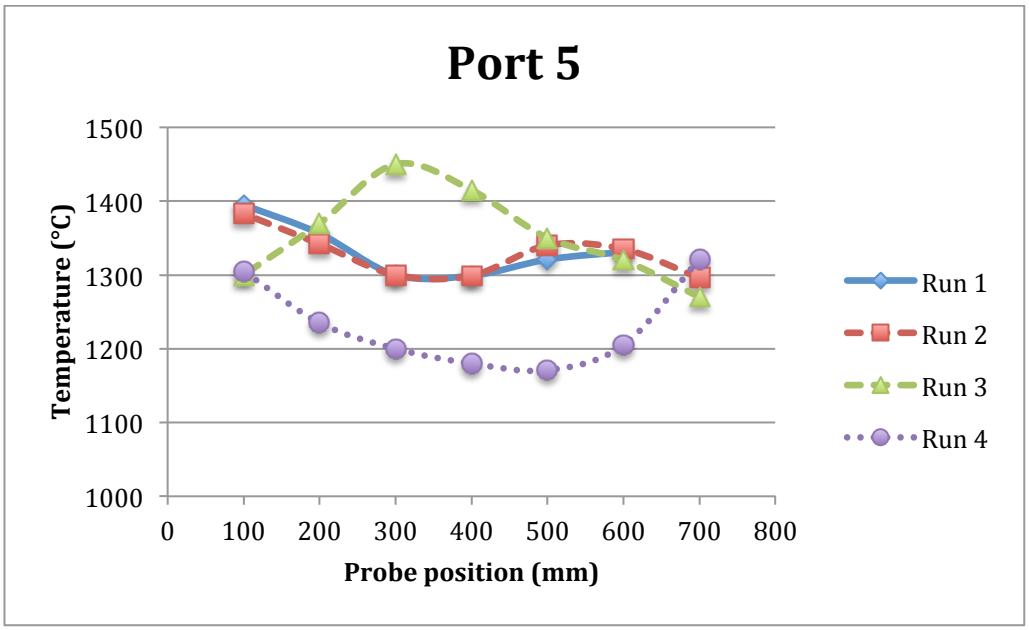

Fig. 2.27. Pyrometry measurament at port 5

The facility is provided with an online measurement system for the NO_x, CO, SO_2 and CO_2 concentration in the exhausts during the tests. Thus, it is possible to determine their trend as a function of the oxygen concentration for each tested blend. In particular, figure 2.28, 2.29, 2.30, 2.31 show respectively the trend of the NO_x, CO, SO_2 and CO_2 concentrations measured at the chimney as a function of the oxygen concentration and of the composition of the blend.

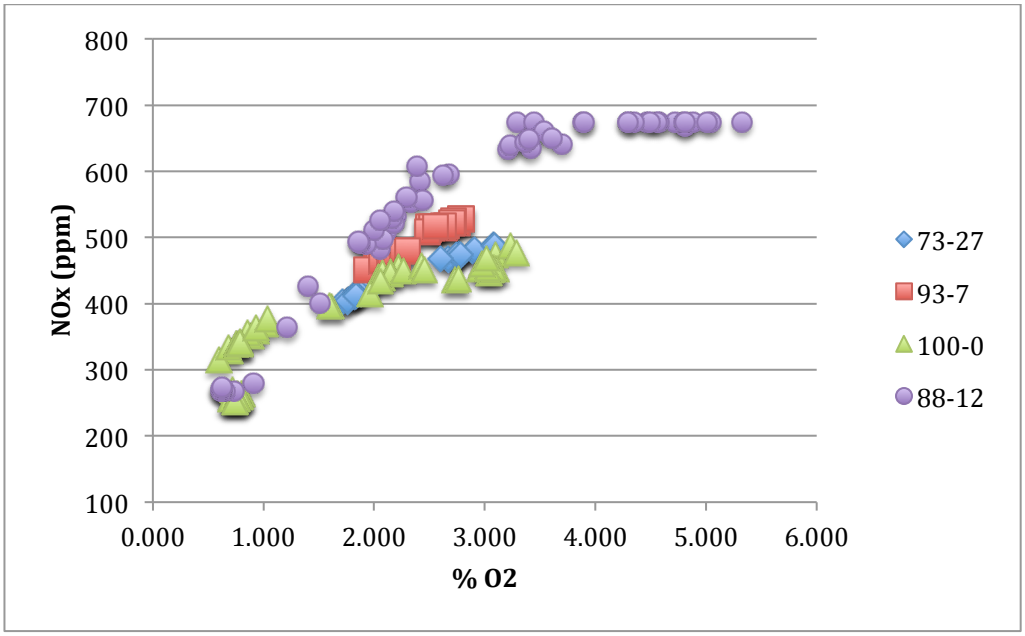

Fig. 2.28. NO_x emission trend

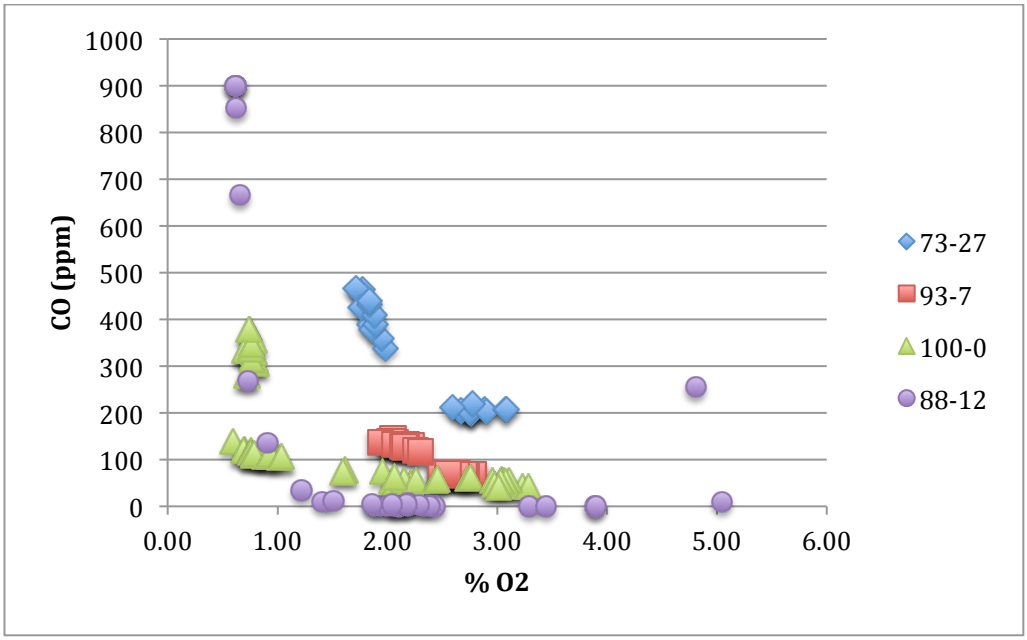

Fig. 2.29. CO emission trend

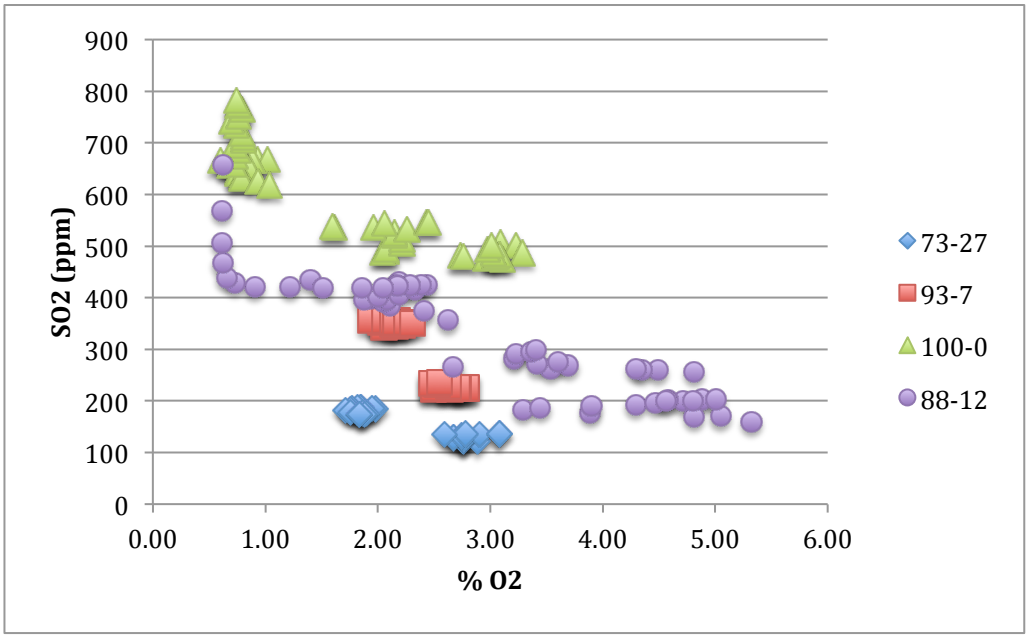

Fig. 2.30. SO_2 emission trend

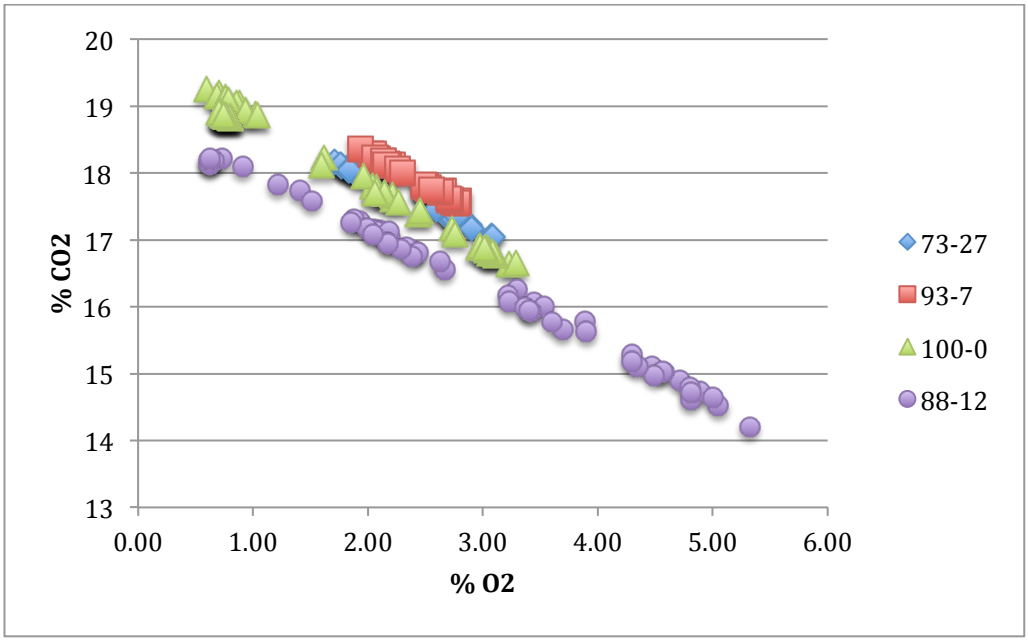

Fig. 2.31. CO_2 emission trend

2.3.5 Comments

The NO_x concentration increases with the oxygen concentration in the exhausts, as expected, whereas there is no clear relation with the biomass fraction in the blend. The NO_x emissions are not simply proportional to the decrease in the nitrogen input in the blend, but they also strongly depend on the combustion temperature, which is influenced by the biomass fraction. The CO and SO_2 trends show a relation with the biomass fraction in the blend. In fact, the CO concentration increases with the biomass fraction, which indicates a less efficient combustion, whereas the SO_2 one decreases with the biomass fraction, due to the lower sulfur content in the biomass compared to coal, and to the enhanced retention of sulfur in ashes. The CO_2 emissions were very similar for all the tested blends, probably due to the similar characteristics of the tested coal and biomass.

2.4 Comparison between the pilot systems

The results are compared in common between the two pilots systems, which are more related to the coal data, in particular the amount of SO_2 (figure 2.32), the composition of the ash (figure 2.33) and the fouling index (figure 2.34).

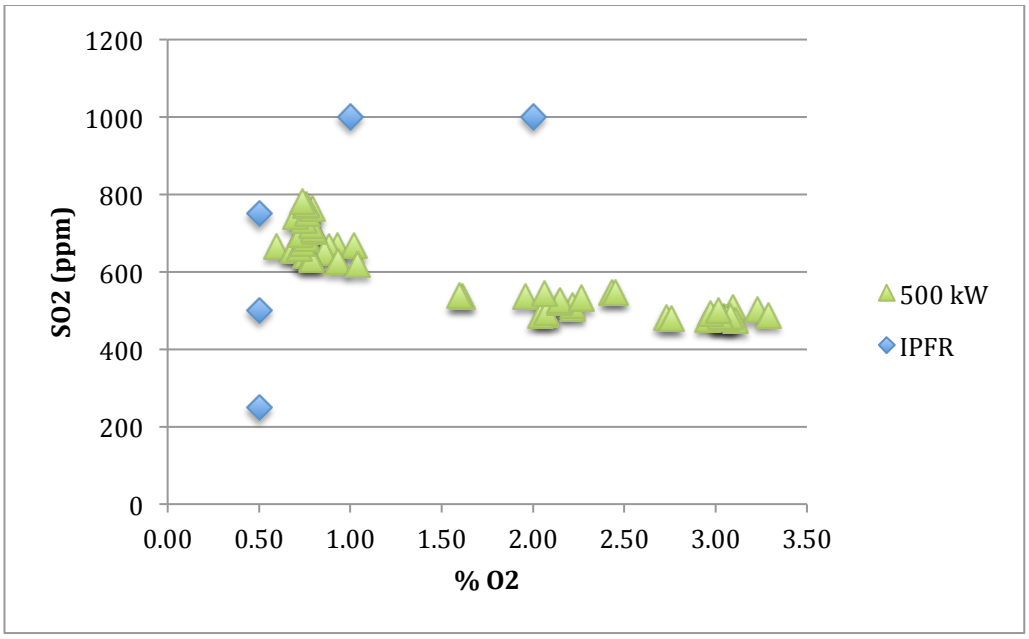

Fig. 2.32. SO_2 concentration comparison

Between the two pilots systems two different procedures were perfomed, in IPFR it was entered an exact amount of SO_2 while in the 500 kW is calculated by the online system, described before.

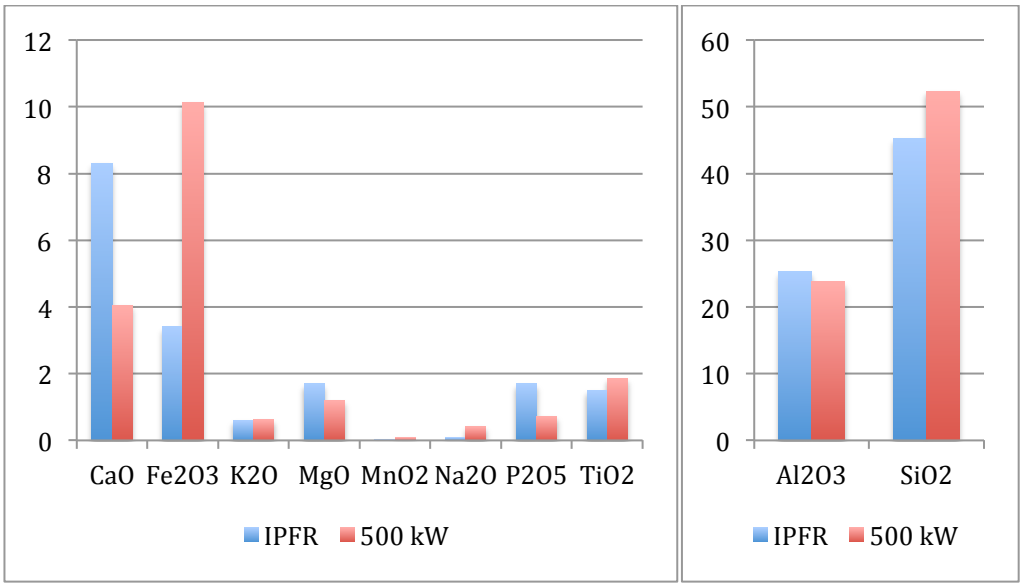

Fig. 2.33. Ash comparison for coal fuel

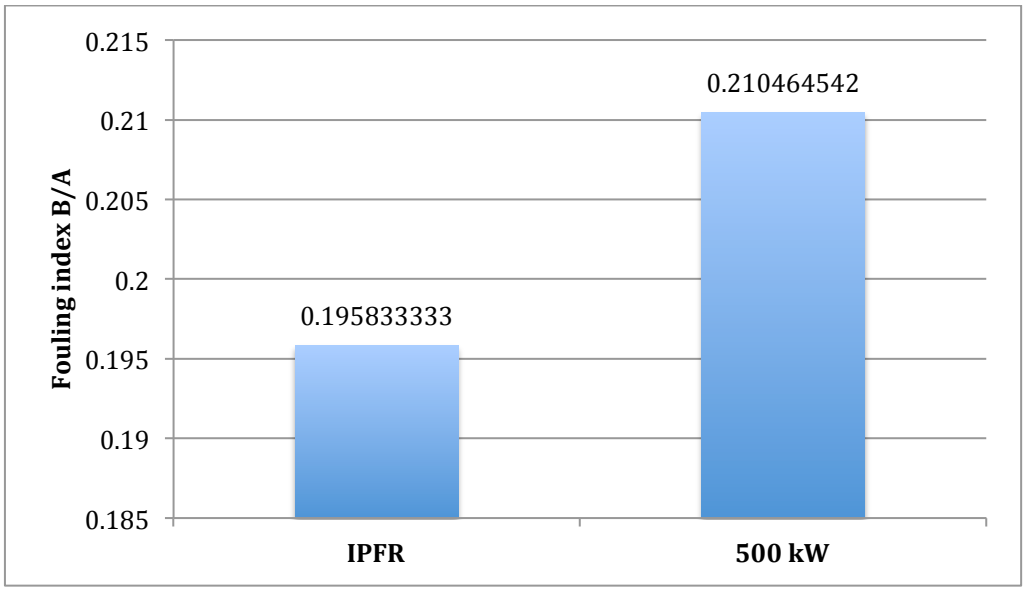

Fig. 2.34. Comparison between ash composition

Comparing the two systems, there is strong dependence to the fuel element composition. For our research, we focus more on biomass and co-firing, which have been already widely discussed in the preceding paragraphs.

Chapter 3

Model for aerosol forming compounds in Entrained Flow Reactor

3.1 Introduction

In the EU-project OnCord the use of biomass and its inorganic constituents such as sulphur and alumina-silicates as a protective agent to prevent the formation of alkali metal chlorides, and consequently avoid chlorine-rich deposits, will be investigated at both small and mid scale test rigs and in the large scale. The basic chemical mechanisms are reasonably well understood but further research and demonstration at plant scale is needed. The present chapter illustrates the pilot-scale KVSA reactor that will be used in the Oncord project. Aimed for the thesis was to develop a modeling tool to predict aerosol formation from the KVSA experiments that are planned in the project.

3.2 KVSA

The pilot scale 500 kWth combustion facility is a top fired, vertical combustion chamber constructed for pulverized fuels such as coals, biomass fuels and other pre-treated solid combustibles. The test facility is optimized for the investigation of pulverized fuel combustion processes and allows the characterization of different kinds of fuels at staged and un-staged combustion conditions.

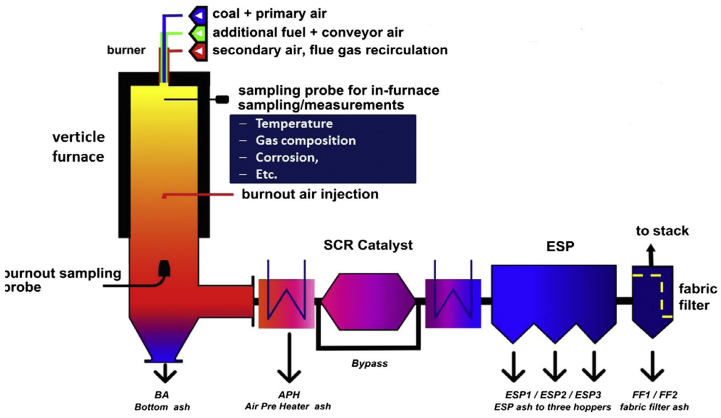

Fig. 3.1. KVSA test facility schematic

It can also simulate the flue gas side of a power plant including flue-gas cleaning with a high-dust SCR catalyst, an electrostatic precipitator (ESP) and a bag-house filter. The flue gas cleaning devices can be by-passed or brought on-stream depending on the test requirements and focus of the investigations.

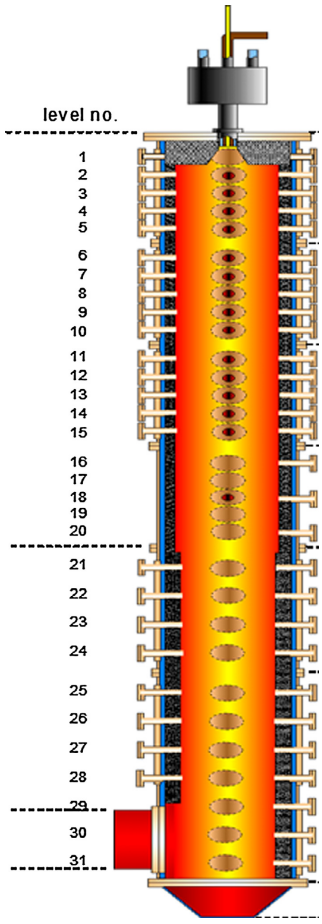

Fig. 3.2. Test case

The combustion chamber (figure 3.2) consists of six cylindrical segments with a total length of 7000 mm and an inner diameter of 800 mm. Refractory lining covers the inner surface of the upper four segments of the combustion chamber to a distance of 4000 mm from the burner.

A water jacket is inserted into the double-wall of the reactor. Numerous measurement openings are integrated into the reactor wall with distances between each level of 150 to 170 mm. Flame detectors are installed with inclined view to the combustion flame core. Either air or CO_2 is used for cooling of the detectors depending on the applied combustion modes: conventional or oxy-fuel combustion. All tests performed were conventional air combustion tests. The combustion chamber is covered with a burner plate of 1400 mm in diameter and the burner is installed directly at the middle. A single flexible coal/biomass swirled burner is used for all experiments. The different fuels were injected in separate streams (how shown in figure 3.3) and blended along a pipe length on the burner for combustion.

Coal was pulverized online during the combustion tests while biomass was first pulverised in a hammer mill and then fed pneumatically via a double screw conveyor to the burner inlet.

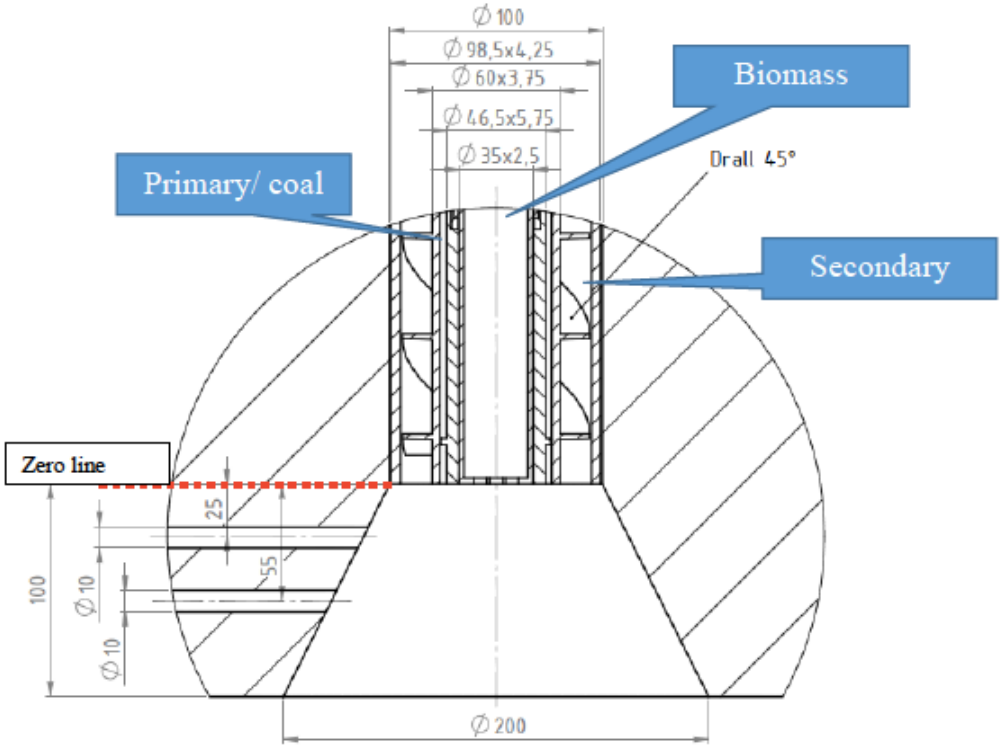

Fig. 3.3. Detailed geometry of the burner

The flue-gas path shown in figure 3.1 consists of an air pre-heater (APH), a selective catalytic reduction chamber (SCR) and an electro-static precipitator (ESP). The bag-house filter is used as backup filter in case of maintenance or by-pass operation of the ESP. These were connected or by-passed depending on the demands of the investigation. Gas species (CO, CO_2, O_2, SO_2, NO_x), in-flame temperatures and gas composition were continuously monitored and recorded. Ash samples are collected at several locations representing ashes of different particle sizes and investigated for burnout and ash composition. Slag and deposit samples from probes in the furnace and ash samples at the sample locations can be taken and analyzed. The flue gas is extracted at the final section of the reaction tube (port level 26 shown in figure 3.2). This is transported to a filter (to remove ash) and to a sample gas chiller (to remove moisture) before it enters the gas analyzers as dry gas. The experimental campaign for this pilot system has not yet been made, but is scheduled for the month of August.

3.3 Numerical model

3.3.1 Methodology

In this chapter we are given a description of the computational domain and the physical model used for the system examined in this work of thesis. The computer code used is Fluent 16.1 Ansys Inc.
In recent years the development of computing resources has allowes to use computers to conduct computational fluid dynamics simulations ever more detailed, until arriving to consider the numerical simulation means for the design of engineering interest systems. It was performed a CFD simulation of a biomass found in the literature. The CFD simulation provides distribution of temperature, density and chemical species. These parameters will constitute the input data to the Reactor Network Analysis (RNA), that divides the domain in the macro-homogeneous region to allow calculation of detailed kinetics, including about 200 species and 3000 chemical reactions. Fluent is expected to predict gas-phase chemical species and hence a subsequent tool is needed to emulate the condensation of aerosol during measuring campaigns.

3.3.2 CFD modeling

The simulations involved the KVSA furnace operated with biomass fueled burner. The whole geometry is very big, so a particular strategy is adopted to reduce the computational cost. The geometry was divided in two parts, i.e. the burner and the furnace.

3.3.2.1 Burner

- **Domain and computational grid**

The burner computational domain included the secondary air with swirl. The idea is to run a non reactive simulation, saving the calculation time which is instead necessary for a reactive simulation. Hence velocity and turbulence characteristics efforts were made to achieve a good grid for the burner. The burner was treated in this way, that is, creating the geometry on Desing Modeler of Ansys Workbench of Ansys Inc. and later were imported to Ansys ICEM with which the structured grids in both cases were generated.

Initially, an unstructured mesh was employed, which however, gave convergence problems during simulations, so it was decided to create a structured grid for the burner and to have non convergence problems during the simulations in Fluent. For the structured grid has been carried out the independence of the grid which is reported in the Appendix A. The following figures shows the unstructured (figure 3.4) and the structured (figure 3.5) grids.

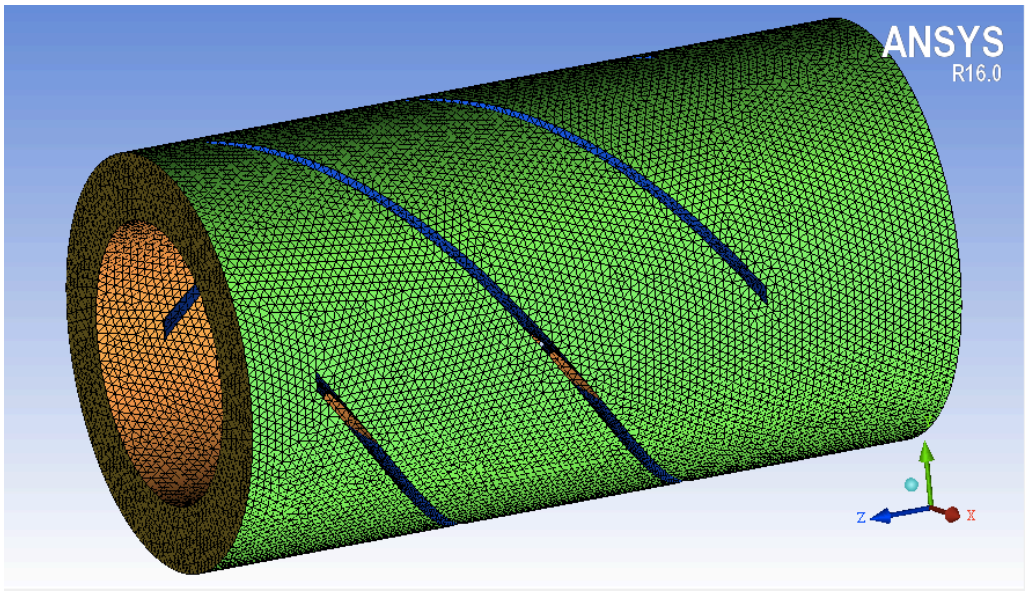

Fig. 3.4. Unstructured grid burner

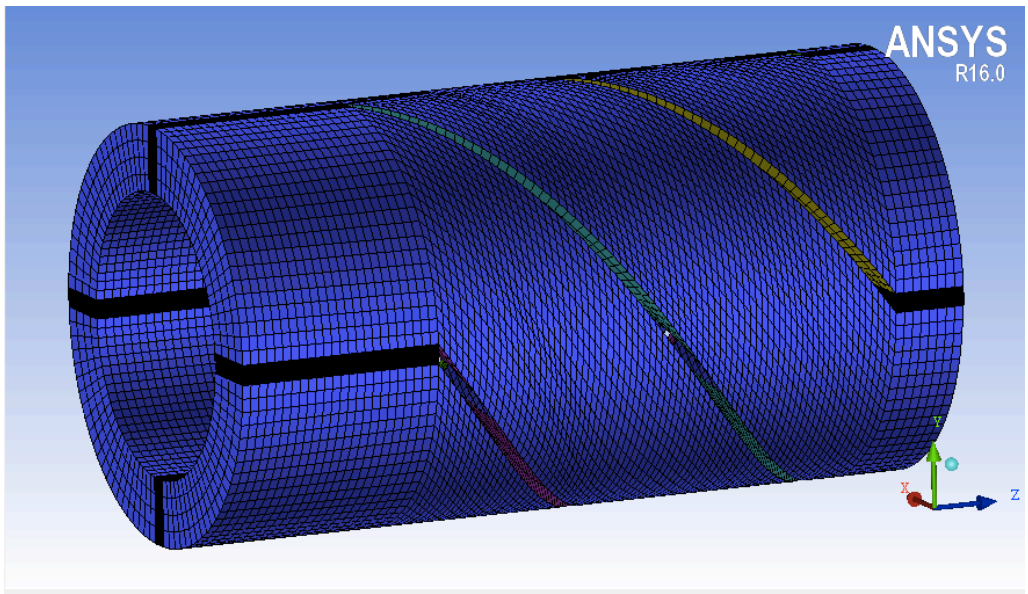

Fig. 3.5. Structured grid burner

- **Physical model**

As stated before on the burner it is only conducted the simulation with only air, without combustion, to save the computing time. The simulation was carried out with a RANS (Reynolds-Averaged Navier-Stokes), the one used for non-reactive system. The turbulence model chosen is the SST k-ω model, as in the previous thesis works it is seen that is the one that best approximates the phenomenon. For the turbulence models, please refer to the turbulence models explained in the section on the physical model of the furnace (paragraph 3.3.2.2). The model in gas phase resolves the equation of motion quantity and the total mass, since they are not present reagent species, but only air.

- **Boundary conditions**

The boundary conditions are summarized in the following tables (3.1, 3.2, 3.3). For the **secondary air inlet** has been selected *velocity inlet* condition, the velocity has been chosen by typical values that are used in this type of situations.

Velocity inlet	
Velocity specification method	Magnitude, Normal to Boundary
Velocity magnitude	7 m/s (constant)
Supersonic/Initial Gauge Pressure	0 Pascal
Turbulent intensity	5%
Hydraulic Diameter	0.028 m

Table 3.1. Boundary condition for inlet

For the **outlet** have been selected *pressure-outlet* condition, with a zero relative pressure condition given that the burner operates at atmospheric pressure.

Pressure outlet	
Gauge Pressure (Pascal)	0
Backflow direction specification method	Normal to Boundary
Backflow turbulent intensity	5%
Backflow Hydraulic diameter	0.028 m

Table 3.2. Boundary condition for outlet

For the **wall-in** and **wall-ext** have been selected *wall* condition, being only a non reactive simulation no particular parameter has been changed from the default.

Wall	
Wall motion	Stationary wall
Shear condition	No slip
Wall roughness	
Roughness height	0 m
Roughness constant	0.5

Table 3.3. Boundary conditons for the walls

- **Numerical parameters of the simulator**

As regards the choice of the solver parameters, it is adopted a segregated *pressure-based* algorithm with the second order resolution scheme, due to the low number of cells and the simple model adopted, not reactive. The simulation was conducted assuming steady flow. As convergence criterion was set a limit of 10^{-5} for the square root of the average of residuals (Residual RMS), this value ensures a good level of convergence, sufficient for engineering applications.
A summary of the solver parameters is shown in Table 3.4.

Time model	Steady
Solver	Pressure-based
Formulation	Implied
Convergence scheme	Second order
Convergence criterion	RMS < 10^{-5}
Pressure-velocity coupling	SIMPLE

Table 3.4. Solver parameters for the burner

- **Results**

The result of the simulation is shown in figure 3.6, about the axial velocity, where we see a higher speed at the inlet of the swirler. Also the velocity field in the outlet is shown in figure 3.7.

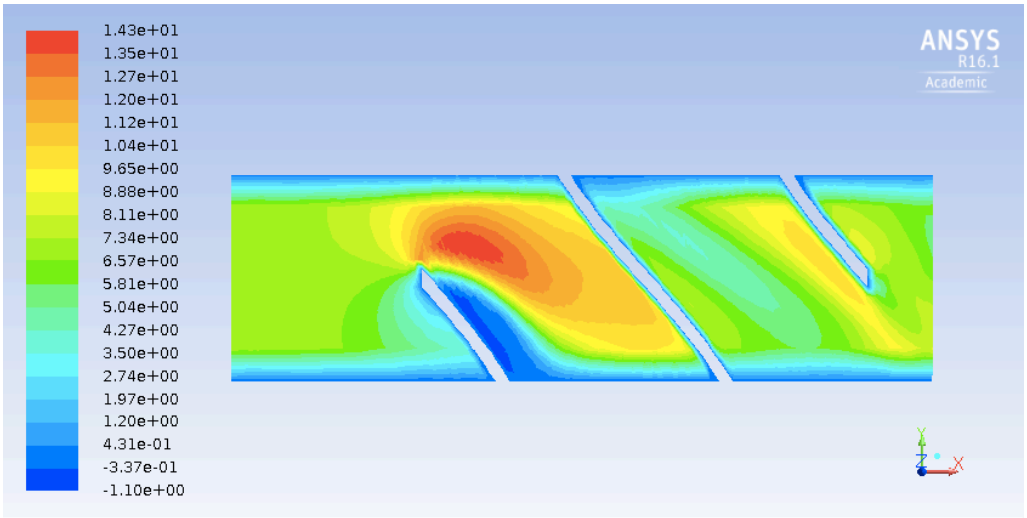

Fig. 3.6. Contours of axial velocity in the burner

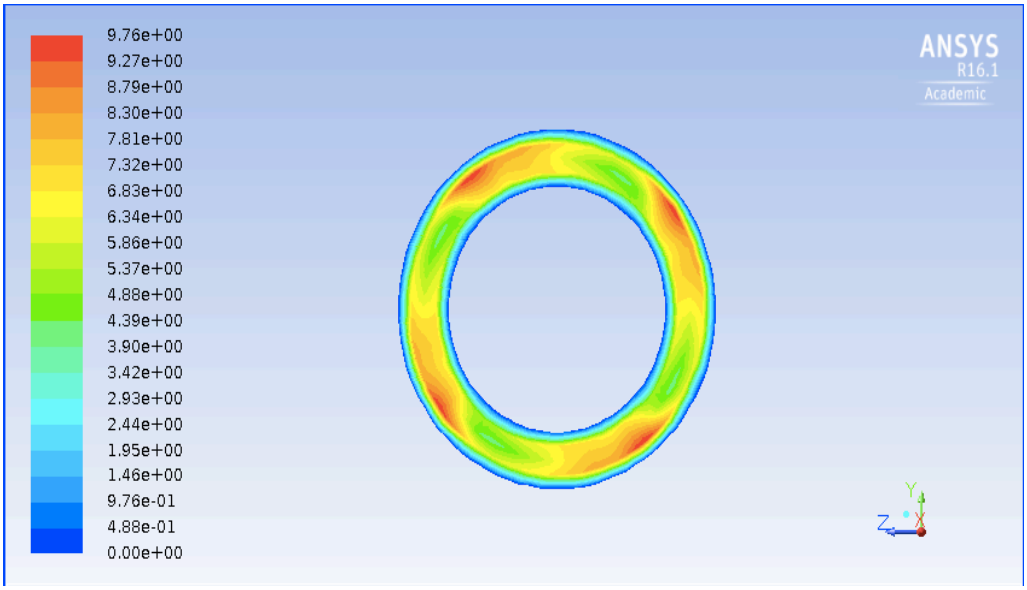

Fig. 3.7. Contours of axial velocity at the outlet of the burner

3.3.2.2 Furnace

- **Domain and computational grid**

The geometry of the furnace is very large, then for reduce the time required for the CPU has been decided to simulate only a quarter of the furnace by exploiting the symmetries of the system. One of the efforts pursued in this work has been to achieve a good grid in such a way as to simulate the combustion of biomass. The furnace geometry was created in Design Modeler of Ansys Workbench of Ansys Inc., then was imported to Ansys ICEM with which the grid was generated. To reduce the numer of cells without compromising the quality of the grid was decided to created a structured grid, to do this it is used in particular the O-grid function. An O-grid will have lines of points where the last point wraps around and meets the first point. Thus, you'll have some grid lines that look like the letter 'O'. In our case the O-grid will be divided into four because the cut made by simmetry. For the structured grid has been carried out the independence of the grid, which is reported in the Appendix A. The following figures show the computational grid for the furnace, first all furnace (figure 3.8) and then the particular of the O-grid at the inlet and quarl (figure 3.9 and 3.10).

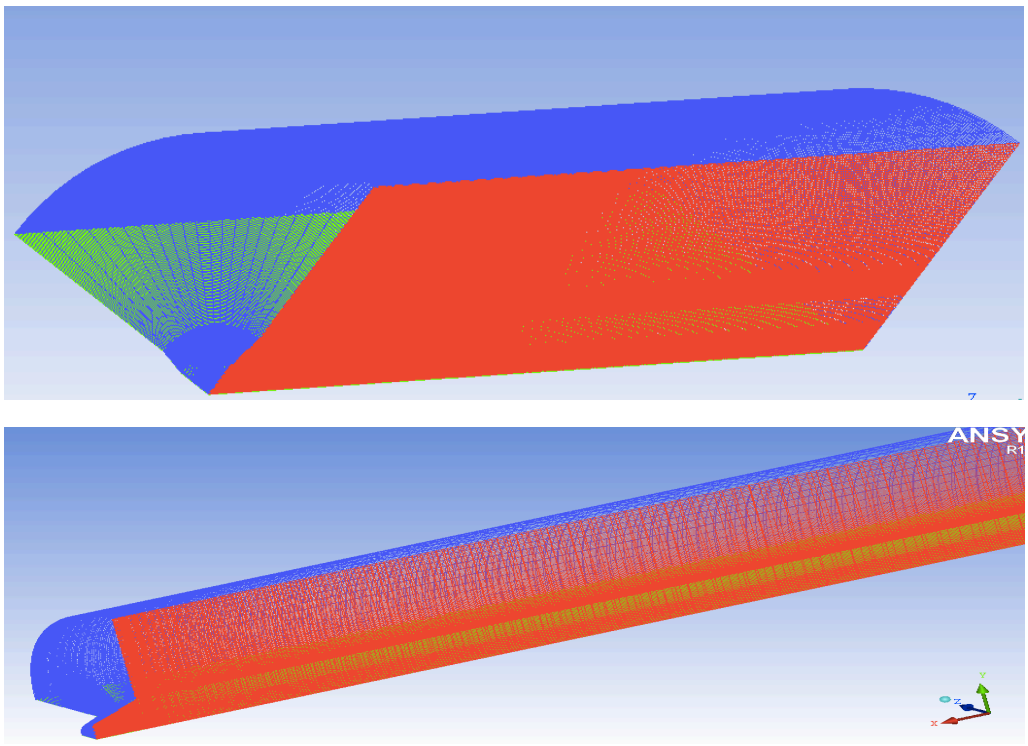

Fig. 3.8. Structured grid for the furnace

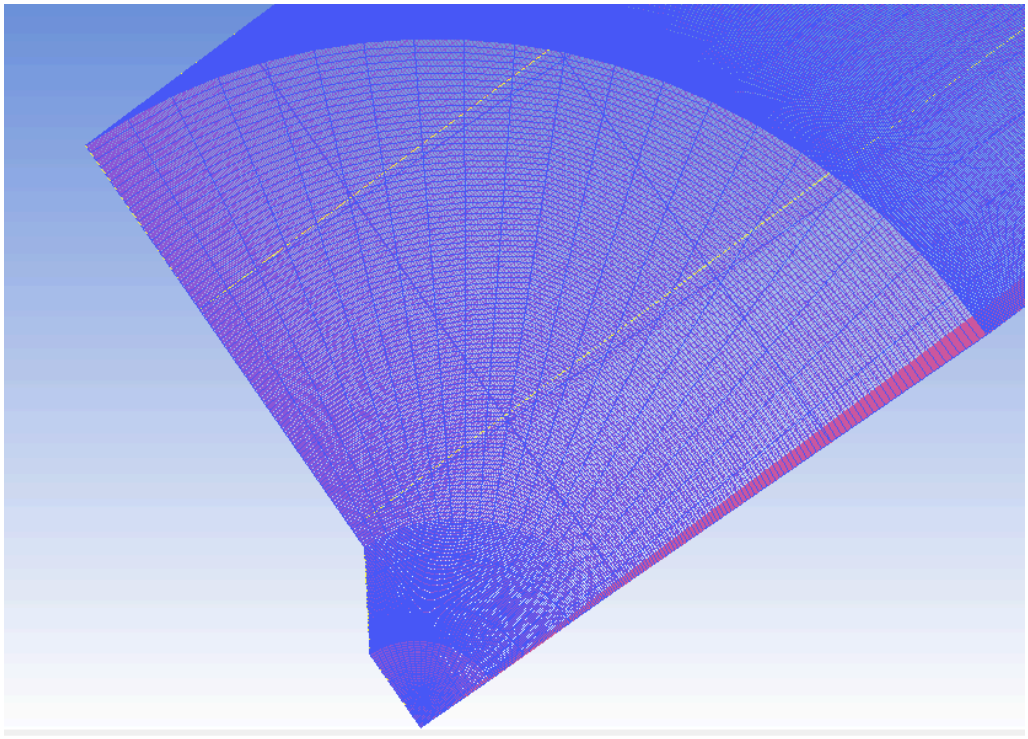

Fig. 3.9. O-grid in the quarl and wall-top

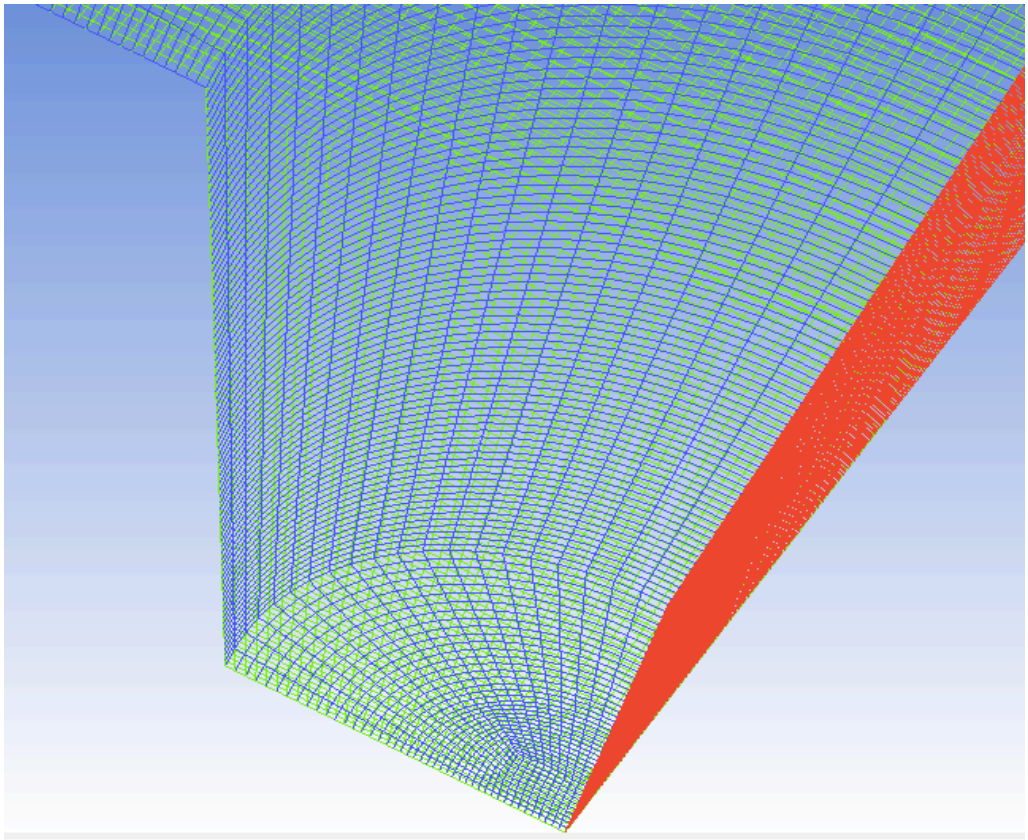

Fig. 3.10. O-grid in the inlet

- **Physical model**

In this case, the system studied is costitued of a gaseous continuous phase and a dispersed phase (the biomass particles) that interact with each other for exchange of matter, energy and momentum. For this reason we have chosen to use an Eulerian – Lagrangian approach, in which the gas phase is resolved by reference Eulerian while the motion of groups of particles is described by a Lagrangian track. The Eulerian – Lagrangian approach is generally used to describe phase dispersed diluted, such as the droplets or particles of gas or bubbles in a liquid. In that approach the **dispersed phase** is modeled by a set of ordinary differential equations describing the change in its properties along the path travelled by the droplets, bubbles or particles. So in this way is possible to describe in grater detail the elementary physical processes on particle scale. Generally it is not possible to follow all the particles and make a balance on them, for which the behaviour of the dispersed phase is determined by following the track of one or more samples of particles (particle tracking or Lagrangian tracking) through the flow. The results obtained on these samples are then used to describe the average behaviour of the dispersed phase. The basic assumption for the application of this model is that the discrete phase is sufficiently diluted namely that its volume fraction is negligible compared to that of the fluid (< 10-12%). Also the phenomena of exchange of energy and matter between phases require a resolution of two-way type coupling. The numerical analysis of the discrete phase allows to follow the track of particle samples from their injection point until it comes out from the domain. Each injected sample represents the average behaviour of a group of particles and generates source terms that interact with the balance equations of matter, energy and momentum of the fluid.

A simplified scheme of the calculation procedure is shown in figure 3.11.

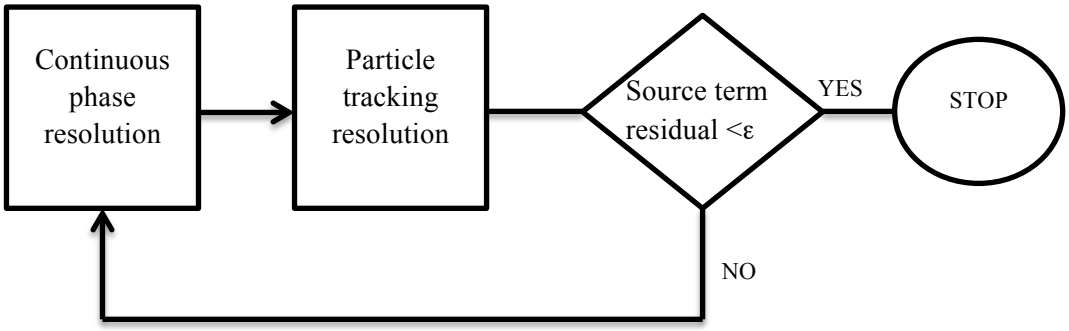

Fig. 3.11. Calculation procedure for the two-way coupling

The dispersed phase is formed by particles of biomass that is assumed to be spherical and of constant size. Their characterization was carried out through the input conditions supplied to the resolver for the physical properties of the biomass and for the modeling of the injection system. The discrete phase setting allows to define the area of injection of the particles, their diametrical distribution and the data relating to the input conditions (velocity, flow rate and temperature). The physical and numerical parameters entered as input to the program are reported in Table 3.5.

Physical parameters	
Inject using face normal direction	Yes
Velocity magnitude	30 m/s
Diameter distribution	Uniform
Diameter	100 μm
Temperature	300 K
Total flow rate	0.0278 Kg/s
Injection type	Surface
Release from surface	Biomass
	Coal
Numerical parameters	
Tracking parameters:	
Max number of steps	60000
Step lenght factor	5
Number of continuous phase iterations for DPM iteration	100 → 50

Table 3.5. Inputs related to the biomass particles injected into the combustion chamber

As regards the size of the particles, since the size distribution is not know, it was chosen to use a constant diameter equal to 100 μm in accordance with the average diameters found in the literature. The number of continuous phase iterations for DPM iteration, in the amount of 100 in the early stages of the iterative process, has been reduced to 50 when made stable the numerical calculation.

For the **continuous phase**, given the phenomena of interaction between phases, in addition to the equation of conservation of momentum and the total mass, it was necessary also to solve transport equations of single species and energy. The direct resolution (DNS) of the conservation equations is possible only in the case of flow with low Reynolds number, the condition that rarely occurs in the case studies. The DNS requires a very fine spatial and temporal discretization, such as to completely solve even the smallest scale of the phenomena concerned. The level of detail obtained is maximum and there is no substantial loss of information. However with increasing Reynolds number (Re) decreases the size of the smallest vortical structures and the computational cost of the simulations it is, therefore, prohibitive. In particular it can be shown how the computational cost of a DNS is proportional to $Re^{11/4}$. Furthermore, even if the resolution of the equations were possible, the high degree of spatial and temporal detail obtainable would have little practical interest, given that in the field of engineering applications, the focus is on the average values of the magnitudes involved, such example the average speed of the fuel consumption or the average rate of formation of pollutant species. The conservation equations are then averaged on the basis of a statistical description of turbulent flow using the RANS (Reynolds-Averaged Navier-Stokes) approaches, for non-reactive systems, or FANS for reactive flows. There is a third approach to the resolution of the conservation equations, the Large Eddy Simulation (LES) in which are resolved directly the biggest energy scales while the smaller ones are modeled. The LES approach is able to provide better accuracy of RANS as the direct modeling of the vortical structures more able to capture various phenomena of instability which may be present. To be considered, at the end, that the computational cost of a simulation LES of a turbulent and reactive flow is significantly higher than the RANS (or FANS) but obviously lower than that necessary for a DNS. For the furnace the approach used for the numerical simulation is FANS approach.
The **turbulence models** allow to express tensor of Reynolds stresses as a fuction of variables averaged over time. They are divided into two main classes:

- Diffusion models for gradient;
- Direct models.

The diffusion models for gradient (Eddy viscosity models) are based on the Boussinesq assumption, which allows to describe the Reynolds stress as a function of the average fluid velocity gradient. The hypothesis of the gradient transport and Boussinesq moving the closure problem of the conservation equations for the determination of turbulent viscosity μ_t. The disadvantage of these models is that it assumes μ_t as a isotropic scale quantity, which is not always verified. The various turbulence models based on the assumption of Boussinesq are classified on the number of equations used to evaluate μ_t:

- zero-equation models;
- one-equation models;
- two-equation models.

The direct models achieve the closure of the Navier-Stokes averaged through the resolution of transport equations for the individual components of the stress tensor of Reynolds stress. The direct models have a higer computational cost than the diffusion models for gradient, but allow a more accurate prediction of the turbulent phenomena not having to consider the approximation of the implicit isotropy of Boussinesq assumption.
In the present work were used 2 turbulence models of a diffusion gradient for two equations: mainly the k- ω SST (Shear Stress Transport), while it was initially used the k – ε which is seen to be not suitable to our case study, such as swirling flows.

Standard k – ε turbulence model

The model is a semi-empirical model. The turbulent viscosity is defined by the following relationship:

$$\mu_t = \rho C_\mu \frac{k^2}{\varepsilon}$$

where $C_\mu = 0.09$ is one of the 5 costants of the model, which requires the resolution of the two additional transport equations for the turbulent kinetic energy k and its dissipation ε. The k – ε standard model is numerically very stable but has some limitations, in particular:

- The equations are derived for high Reynolds numbers and not much indicated to the simulation of the flows near solid walls, at low Reynolds number, where the treatment of the flow is achieved by algebraic expressions;
- Limited accuracy in the case of flows with strong vorticity or anisotropy of turbulence.

SST (Shear Stress Transport) k – ω turbulence model

The model is an empirical model based on the turbulent transport equations of the kinetic energy k and the specific dissipation rate ω calculated as the ratio of ε and k. The model differs from k – ω standard for the definition of the turbulent viscosity which in this case is modified to take count of the contribution of the transport. In addition to this is combined the model k – ω with model k – ε so to exploit the accuracy of this last for the high Reynolds numbers and k – ω for the low Reynolds numbers, and to control the passage between the two models it uses two interpolating functions (blending functions). Then there must be a transformation of the equation on k – ε so as to express it as a function of ω.

The **modeling of the combustion process** provides heterogeneous and homogeneous reactions where: there is a first stage heating and devolatilization of biomass particles, followed by oxidation of the volatiles and char residue. A simplified scheme of these reactions is shown in figure 3.12.

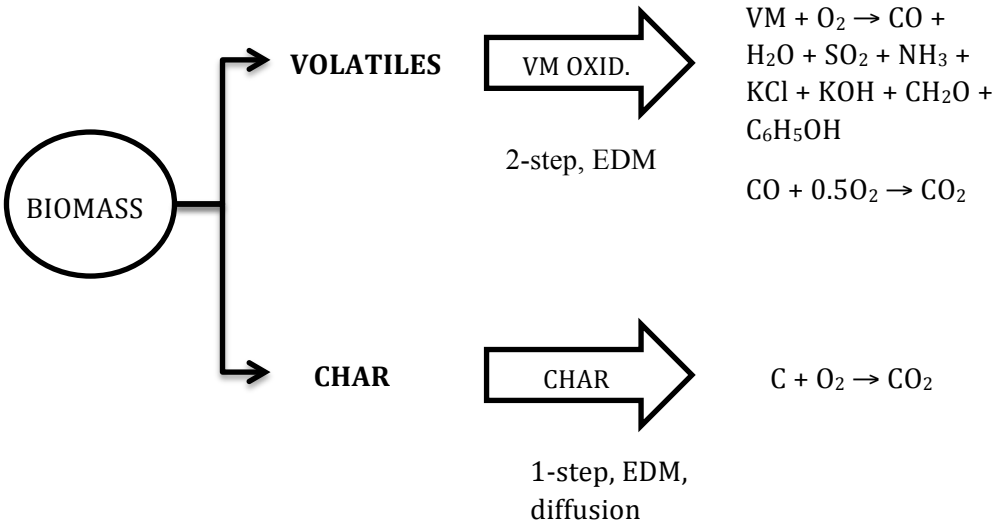

Fig. 3.12. Reaction scheme for the combustion modeling for pulvirized biomass

The exchange of matter and energy of the biomass particles are analyzed with the models implemented in Fluent code relating to heating phases, devolatilization and combustion of char. The heat balance equation resolution, that is reported below, allows to determine the exchange of the heat during the heating stage before the devolatilization and the heat transfer of the ash.

$$m_p c_p \frac{dT_p}{dt} = hA_p \left(T_\infty - T_p\right)$$

where:

- m_p is the mass of the particle;
- c_p is the specific heat of the particle;
- A_p is the surface of the particle;
- T_∞ is the local temperature of the continuous phase;
- h is the convective heat transfer coefficient;

It is assumed that the internal resistance to heat transfer is negligible and therefore the temperature of the particle is uniform. This equation applies when the temperature of the particle is lower than the temperature of vaporization, T_{vap}, and after which the initial presence of volatile fraction, $f_{v,0}$, has been consumed.

These conditions can be expressed by the following relations:

$$T_p < T_{vap}$$

$$m_p \leq (1 - f_{v,0}) m_{p,0}$$

where $m_{p,0}$ is the initial mass of the particle.
In the conditions just defined, there is no mass exchange between the phases and the fuel is not affected by chemical reactions. The heat released or absorbed by the particle crossing of each calculation cell appears as a source/disappearance term of the heat in the subsequent resolution of the balance equation of energy for the continuous phase. The key problem in the modeling of reacting flows is the term that the mass of the individual chemical species appears in the equation of conservation, the reaction rate of the chemical species $\dot{w}_k$. In general, the combustion reactions can be described in terms of M elementary reactions involving N_C components:

$$\sum_{k=1}^{N_C} \nu'_{k\,j} \cdot R_k \Leftrightarrow \sum_{k=1}^{N_C} \nu''_{k\,j} \cdot R_k \qquad \text{per j} = 1,2,\ldots,\text{M}$$

where $\nu_{k\,j}$ is the stoichiometric coefficient of the component R_k in the elementary reaction j, defined as:

$$\nu_{k\,j} = \nu''_{k\,j} - \nu'_{k\,j}$$

For each component that participates in the reaction, this source term that is in the equation of chemical species conservation can be evaluated as:

$$\dot{w}_k = W_k \sum_{j=1}^{M} \nu_{k\,j}\, Q_j$$

where W_k is the molecular weight of the species k. The term Q_j represents the degree of advancement of reaction j, expressed as:

$$Q_j = k_{f\,j} \prod_{k=1}^{N_C} \left(\frac{\rho Y_k}{W_k}\right)^{\nu'_{k\,j}} - k_{r\,j} \prod_{k=1}^{N_C} \left(\frac{\rho Y_k}{W_k}\right)^{\nu''_{k\,j}}$$

where $k_{f\,j}$ and $k_{r\,j}$ represent, respectively, the constants direct and inverse of kinetic reaction j, while $\left(\frac{\rho Y_k}{W_k}\right)$ is the molar concentration of species k.

The kinetic constants are usually expressed using the Arrhenius relationship and the equilibrium constant, K_{eq}:

$$k_{f\,j} = A_{f\,j}\, T^{\beta\,j} exp\left(-\frac{E_{a\,j}}{RT}\right)$$

$$k_{r\,j} = \frac{k_{f\,j}}{K_{eq}}$$

where $A_{f\,j}$ is the pre-exponential factor, $\beta\,j$ is the exponent of the temperature and $E_{a\,j}$ is the activation energy. From the expressions given for the calculation of the reaction rate is apparent that the term $\overline{\dot{w}_k}$ is strongly non-linear and can not be simply expressed as a function of the mass medium fractions, $\langle Y_k \rangle$, the average density, $\bar{\rho}$ and the average temperature, $\langle T \rangle$. For the clousure of the term $\overline{\dot{w}_k}$ is necessary to resort to models derived from physical analysis. The degree of progress of a reaction depends on two aspects: the efficiency of mixing of the reactants and the real kinetics reaction. The relative importance of these two factors can be evaluated by the number of Damkhöler:

$$Da = \frac{\tau_{turb}}{\tau_{chem}}$$

where τ_{turb} and τ_{chem} are respectively the turbulent mixing and chemical kinetics. The *Da* provides a measure of the degree of interaction between chemistry and turbulence:

- High number of *Da* (*Da*>>1) correspond to very fast chemical reactions than the other processes;
- Low number of *Da* (*Da*<<1) lead to consider a global reaction rate controlled by the chemistry of oxidation reactions, while the reactants are well mixed due to the turbulent motion.

On the basis of these considerations, some of the models that can be used for the assessment of $\overline{\dot{w}_k}$ are:

- *Finite Rate Chemistry* (FR) model, that consider as the controlling parameter the chemical kinetic (*Da*<1);
- *Eddy Dissipation Model* (EDM), applied to the study of non-premixed flames in which the phenomenon that have control is the mixing of the reactive flows;
- *Combined model Eddy Dissipation/ Finite Rate Chemistry* which allows to take into account the chemical kinetics and the turbulent mixing in the evaluation of the reaction rate.

In the present work it used the model Eddy Dissipation which will be shortly described below.

Eddy Dissipation Model (EDM)

The EDM created as an extension of the *Eddy Break-up model* in non-premixed flames. The turbulence causes the mixing of cold reagents, fuel and comburent between them and with the hot products inside the reactor, where the combustion occurs rapidly. In these cases result controlling for the system, the mixing degree (slow) compared with velocity of reaction (fast), and the kinetic reaction rate, often unknown, can be neglected. The EDM model therefore assumes that the velocity can be directly connected to the time requires for reagent mixing on the molecular level. According to this scheme, the average degree of reaction progress of the j-th elementary reaction is evaluated by the average molar fraction of the reactants or the products:

$$\langle Q_j \rangle_{MIX} = A \frac{\varepsilon}{k} min \left(min \frac{\langle [R_k] \rangle_R}{v'_{kj}}, B \frac{\sum_p \langle [R_k] \rangle_P W_k}{\sum_P v''_{kj} W_k} \right)$$

with A and B constants of the model. The degree of reaction progress, is therefore limited by the chemical species present in a defect within the system. This model is only inidicated for the description of the simplified reactions.

The **devolatilizing model** is the *constant rate devolatization model* available in Fluent 16.1. This model assumes that the volatiles are released at a constant rate, according to the law:

$$-\frac{1}{f_{v,0}\,(1-f_{w,0})m_{p,0}} \frac{dm_p}{dt} = A_0$$

where:

- m_p is the mass particle [kg];
- $f_{v,0}$ is the fraction of the volatiles present initally in the particulate;
- $f_{w,0}$ is the fraction of the evaporated material;
- $m_{p,0}$ is the initial mass of the particulate [kg];
- A_0 is the constant rate [s^{-1}].

It was chosen this model because for the work of this thesis focuses more to get a thermochemical field and study deeply the formation of aerosols (pollutants), so mainly on post-processing.

After the volatile component of the particulate is fully evolved begins the oxidation of the solid part of the biomass, this continues until it remains only the inert part defined as char. The laws of the **char oxidation** are:

$$m_p < (1 - f_{v,0})(1 - f_{w,0})m_{p,0}$$

$$m_p > (1 - f_{v,0} - f_{comb})(1 - f_{w,0})m_{p,0}$$

The law considers the char oxidation stochiometric coefficients as shown in the following formula:

$$char\ (s) + \ S_b OX(g) \rightarrow products\ (g)$$

where S_b is defined in terms of oxidant mass per mass of char.

Fluent allows to choose between 4 different heterogeneous surface model of combustion of the soot: *diffusion-limited rate model, kinetics/diffusion-limited rate model, intrinsic model, multiple surface reactions model.* The model chosen for the case study is the *diffusion-limited rate model*. This model assumes that the surface reactions take place with a rate determined by the diffusion of the oxidant gas on the particulate surface:

$$\frac{dm_p}{dt} = \ -4\pi d_p D_{i,m} \frac{Y_{OX} T_\infty \rho}{S_b (T_p + T_\infty)}$$

where:

- $D_{i,m}$ is the diffusion coefficient of the oxidant [m^2/s];
- Y_{OX} is the local mass fraction of the oxidant in gas;
- ρ is the density of the gas [kg/m^3].

In this equation is ignored kinetic contribution of the surface reaction rate. The diffusion-limited rate mechanism is also assumed that the diameter of the particle does not change, since the mass of the char decreases this means that the particulate becomes more porous.

It is reasonable to assume that the introduced biomass goes encounter to a rapid pyrolysis whose products are made up of an aromatic component and a carbonyl component with minor species such as those alkaline (aerosols). In the literature has been found that species belonging to the most appropriate detailed kinetic mechanism to represent the component aromatic and carbonyl are respectively the phenol and formaldehyde. For what concerns the alkaline species, assuming 80% of the potassium present in the fuel vaporize, from the elementary composition of the biomass (Proximate and ultimate analysis are shown in Table 3.6) is calculated a constant concentration of K and a constant concentration of chlorine Cl assuming a constant complete devolatilinzg for the Cl. The Cl was then introduced into the kinetic mechanism on the form of KCl and K in excess of the Cl in the form of KOH. As regards instead the S and N, were introduced respectively as SO_2 and NH_3 (representing the amino groups present in the organic component of the biomass). The organic component (C, O, H) has been inserted as mentioned above through a combination of C_6H_5OH and CH_2O and the mass balance was closed by the CO.

Proximate Analysis	Mass fraction (%dry)
Volatiles	86.7
Fixed Carbon	7.3
Ash	5.9
Ultimate Analysis	**Mass fraction (%w/w, daf)**
Carbon	46.2
Hydrogen	5.9
Nitrogen	1.5
Sulfur	0.04
Oxygen	45.34
Chlorine	0.17
Potassium	0.85

Table 3.6. Proximate and ultimate analysis of biomass

The combustion of volatiles occurs in two stages: in the first one has the oxidation of volatile with production of aerosol precurors, sulfur dioxide, water vapor and carbon monoxide which in the next stage is oxidized to carbon dioxide.

The first step is as follows:

$$Volatiles + O_2 \rightarrow C_6H_5OH + CH_2O + KCl + KOH + H_2O + CO + SO_2 + NH_3$$

The volatile species involved in the reaction has been obtained from analysis of the biomass, the detailed calculation is reported in Appendix B, getting:

$$\boldsymbol{Volatiles = C_{1.04}H_{1.92}O_{0.92}S_{0.0004}K_{0.007}N_{0.034}Cl_{0.0015}}$$

So the reaction balanced will be:

$$C_{1.04}H_{1.92}O_{0.92}S_{0.0004}K_{0.007}N_{0.034}Cl_{0.0015} + 0.1\ O_2 \rightarrow 0.092C_6H_5OH + 0.092CH_2O + 0.0015KCl + 0.005KOH + 0.54H_2O + 0.4CO + 0.0004SO_2 + 0.034NH_3$$

The second step of oxidation, instead, is the following:

$$CO + 0.5O_2 \rightarrow CO_2$$

- **Boundary conditions**

To reduce the computational cost, as already said, the simulation were conducted on ¼ of the domain, by the symmetry. The boundary condition of major interest is on the symmetry wall, a periodic boundary condition was built. First, the symmetry of the walls have been set with an interface condition, then with mesh interface was created a periodicity condition specifying the periodic zone, shadow zone and type of periodicity. In our case we have been chosen rotational and then have to specify the offset of angle in deg, such as 90°. At this point Fluent created a virtual wall in correspondence of the real wall, in which a condition of symmetry to the contour has been set.

Another strategy endeavoured to reduce the computational cost has been to use a coupling burner – furnace, so do not resolve in the burner the reactive simulation. Using the function of Fluent export/import profile, the profiles of X velocity, Y velocity, Z velocity, turbulent kinetic energy k and specific dissipation rate ω have been exported and imported at the inlet at the secondary air of the furnace. The boundary conditions are summarized in the following tables (3.7, 3.8, 3.9).

For the inlet of biomass, there are two entrances of fuel that have the same boundary conditions that are *velocity inlet* because a carrier air is injected for transport the particle of fuel. The velocity chosen is a typical velocity for a carrier gas.

Velocity inlet	
Velocity specification method	Magnitude, normal to boundary
Velocity magnitude	30 m/s (constant)
Turbulence	
Specification method	Instensity and Hydraulic diameter
Turbulent intensity	5%
Hydraulic diameter (biomass)	0.0465 m
Hydraulic diameter (Coal)	0.006 m
O_2	0.232
Discrete phase BC type	Escape
Thermal	300 K (constant)

Table 3.7. Boundary conditions for the biomass inlet

For the **outlet** have been selected *pressure-outlet* condition, with a zero relative pressure condition given that the furnace operates at atmospheric pressure.

Pressure outlet	
Gauge Pressure (Pascal)	0
Backflow direction specification method	Normal to Boundaty
Turbulence	
Specification method	Intensity and Hydraulic diameter
Backflow turbulent intensity	5%
Backflow Hydraulic diameter	0.75 m

Table 3.8. Boundary condition for outlet

For all the wall have been selected *wall* condition, it has been imposed a heat flux on the external wall, while all other wall were considered adiabatic thermal conditions.

Wall	
Wall motion	Stationary wall
Shear condition	No slip
Wall roughness	
Roughness height	0 m (constant)
Roughness constant	0.5 (constant)
Thermal	
Heat Flux – Wall	1200 W/m^2 (constant)
Heat Flux – Other wall	0 W/m^2 (constant)
Discrete phase model conditions	
Boundary conditions type	Reflect
Discrete phase reflection coefficients	
Normal	0.3 (constant)
Tangent	0.3 (constant)

Table 3.9. Boundary conditons for the walls

- **Numerical parameters of the simulator**

As regards the choice of the solver parameters, it is adopted a segregated *pressure-based* algorithm with the first order resolution scheme, so as not to weight down the already high computational cost for the numerous models and submodels used. The simulation was conducted assuming steady flow. As convergence criterion was set a limit of 10^{-5} for the square root of the average of residues (Residual RMS), this value ensures a good level of convergence, sufficient for engineering applications. Also it has monitored the outlet temperature of the fumes, considering the convergence achieved once it had settled on a constant value. A summary of the solver parameters is shown in Table 3.10.

Time model	Steady
Solver	Pressure-based
Formulation	Implied
Convergence scheme	Second order
Convergence criterion	RMS < 10^{-5}
Pressure-velocity coupling	SIMPLE

Table 3.10. Solver parameters for the furnace

- **Final consideration**

The development of a CFD model on KVSA furnace described in some reports has posed some problems and driven to choices that can interfere the solution. The dearth of operational data and boundary conditions has not allowed a validation of the physical submodels. Other missing data are the fuel used, the elemental composition and size distribution, which have been hypothesized using a biomass found in literatures. All the choices that are made may introduce errors on the prediction of thermo-chemical field inside the furnace. Given the different points that require more detailed information, therefore, it is desirable to a schedule of experimental tests also based on modeling requirements. In table 3.11 summarizes the characteristics and the models used in the simulation carried out for the furnace.

Fuel	Turbulence model	Combustion model	Devolatilization model	Char oxidation
Biomass	k-ω SST	EDM	Constant rate	Diffusion limited rate

Table 3.11. Summarize simulation for the furnace

3.3.2 Reactor Network Analysis

New combustion methods can be categorized into pre-treatment, modern combustion mechanisms and post-treatment. Catalytic treatment and fuel switching are some of the pre and post-treatment methods currently in place. The complexity of design and manufacturing of combustion chambers requires a through computational analysis of the flow before producing the combustor for further experiments. In order to meet the demand at reasonable costs, they are obliged to take advantage of modern fluid dynamic simulations to reduce the number of rig tests required. Computational Fluid Dynamics (CFD) has been used extensively for the reasons mentioned above, however, the complexity of long reaction mechanisms pose severe time penalties for detail combustion simulations. The coupling of CFD-combustion interaction often takes advantage of simplified models, which can predict temperature, velocity and fast species in higher concentration with reasonable accuracy while failing to predict the production of slower species such as minor pollutants. The complex nature of combustion processes and their comprising intermediate reactions render detail CFD turbulent combustion simulations impractical. One method to compute the detailed chemical kinetics is via a simplified Reactor Network Analysis (RNA). RNAs allow the user to investigate the concentration, of slower species such as aerosol. A typical RNA comprises of a series of theoretical reactors (e.g. perfectly stirred reactor PSR, plug flow reactor PFR), which resemble unique parts of the CFD flow field. Due to the stiff nature of the equations and the complexity of the flow field, it is highly challenging to obtain convergence with reasonable accuracy. This requires several iterations in producing a reactor network and numerical adjustments in the settings of the solver. There are variuos models for the reactor network analysis, which are briefly presented in Appendix C. In this thesis, it used the Fluent code, which recently implemented this feature in it.

3.3.2.1 RNA model with Fluent

The reactor network model is used to simulate species and temperature fields in a combust or using a detailed chemical kinetic mechanism. The reactor network is constructed from a converged ANSYS Fluent simulation modeled with a fast chemistry combustion model, such as the Non-Premixed, Partially Premixed, or Eddy-Dissipation model. A full chemical mechanism in CHEMKIN format can be imported into Fluent and solved on the reactor network. The combustor volume is automatically subdivided into a small number of connected perfectly stirred reactors. The mass fluxes through the network are determined from the CFD solution, and the species and temperatures in the reactor network are solved together. Hence, the reactor network model is used to simulate finite-rate chemistry effects with detailed kinetic mechanisms, in particular pollutant emissions such as NO_x, CO, and unburnt hydrocarbons. Since the specified number of stirred reactors is much smaller than the number of CFD cells, the reactor network model allows much faster simulations of the

species and temperature fields than solving for detailed chemistry in every cell, as in the Laminar, EDC, and PDF Transport models. Typically, the reactor network model is executed on a converged steady-state RANS solution or a time-averaged unsteady solution. The model can also be run on an unsteady flow representing a "snap-shot" in time. Since there is no backward coupling of the reactor-network solution to the flow, the model is useful for predictions where the detailed chemistry has little impact on the flow, such as pollutant formation. The model is inappropriate for highly unsteady flows such as flame ignition or global extinction and also for flows that are strongly influenced by the chemistry, such as soot with significant soot-radiation interaction. The first step in a reactor network simulation involves agglomerating the CFD cells into the specified number of reactors, $N_{reactor}$. Since each reactor is a perfectly mixed representation of a region of the combustor, ideally cells that are closest in composition space should be grouped together. In other words, for optimal performance, the CFD cells grouped together in each reactor should have temperatures and species mass fractions that are as similar as possible. By default, for Non-Premixed and Partially-Premixed cases, Fluent groups cells that have similar temperatures and mixture fractions, and for Species Transport cases, Fluent groups cells that have similar temperatures and mass fractions of N_2 and H_2O. These defaults should provide good cell clustering in most cases. However, Fluent allows user controlled clustering through custom-field functions when these defaults are not sufficient. After similar cells have been clustered, Fluent splits non-contiguous groups, then agglomerates clusters with the smallest number of cells to their closest neighbors until the specified number of reactors, $N_{reactor}$, is obtained. The second step in a reactor network simulation involves the solution of the reactor network, which proceeds as follows. The mass flux matrix, $\dot{m}$, is calculated from the cell fluxes in the CFD solution, where each matrix component $\dot{m}_{ij}$ is the mass flux from reactor i to reactor j. The k^{th} species mass fraction in reactor i, Y_k^i, is governed by the algebraic equation:

$$\sum_{j=1,j\neq i}^{N_{reactor}} \dot{m}_{ij} Y_k^j - \dot{m}_i Y_k^i = V_i \dot{\omega}_k^i + S_k^i$$

where V_i is the volume of reactor i, $\dot{\omega}_k^i$ is the k^{th} species reaction rate in the ith reactor, and S_k^i is a mass source term. $\dot{m}_i$ is the net mass flux into reactor i and is calculated as:

$$\dot{m}_i = \sum_{j=1,j\neq i}^{N_{reactor}} \dot{m}_{ij}$$

The mass source term, S_k^i, accounts for contributions from the CFD inlet species mass fluxes through the CFD boundaries and from volume sources, such as the Discrete Phase Model (DPM). The system of equations for Y_k^i, has the dimension of $N_{reactor}$ x $N_{species}$, where $N_{reactor}$ is the user-specified number of reactors, and $N_{species}$ is the number of species in the chemical mechanism. ANSYS Fluent solves this system with a segregated alghoritm by default, although the option to use a fully coupled algorithm is available.

An energy equation is not solved in the reactor network. Instead, by default, the temperature in each reactor is calculated from the equation of state. The reactor pressure is fixed and determined as the mass-averaged pressure of the CFD cells in the reactor. Note that the density of each reactor is fixed since both the reactor volume and the reactor mass are constant. This approach ensures that heat loss (or gain) in the CFD simulation is appropriately accounted for in the reactor network. Fluent also provides an option to not solve for temperature, in which case the temperature is fixed as the mass-average temperature of the CFD cells in the reactor.

In summary, the input parameters for the reactor network model are:

- Thermodynamic data;
- Detailed chemical kinetics, which comprises:
  - Aerosols mechanism;
  - Hydrocarbons mechanism;
  - Formation of NO_x.
- Number of reactors.

The overall kinetic model used to describe the entire combustion process, and thus the formation of aerosol precursors in the gas phase was obtained from the union of the modules including the reactions of NO_x and hydrocarbons to which is added the model of Glaborg for the compound of Cl and S and the production of aerosols. In particular the mechanism of the gaseous phase consist of a core prepared from Ranzi, et al, constitued by the pyrolysis and the oxidation of hydrocarbons with up to 6 carbon atoms to which is added another block that described separately the nitrogenous species. The mechanism of the hydrocarbons was obtained using a kinetic mechanism of hydrocarbons up to 8 carbon atoms and eliminating the species of no interest since the last precursor of the organic phase present in the reaction of devolatilization is C_6H_5OH. The thermodynamic data and kinetic data are reported respectively in the Appendix D and E. It has examined the variation of species taking part in the kinetic mechanism to vary the number of reactors to see the influence of the agglomeration of the reactors on the results. The cases examined are: 100, 150 and 200 reactors.

3.3.3.2 Numerical parameters of the simulator

The parameters used in the Reactor Network Analysis are listed in Table 3.12.

Parameters	
Detailed mechanism material name	Chemkin – mechanism
Number of reactors	100 – 150 – 200
Solve Temperature	NO
Expert options	YES
Reactor net convergence tolerance	1e-06
Solver	Segregated
Number of iterations	1000 – 2000 – 3000

Table 3.12. Solver parameters for reactor network model

The output that Fluent provides for the graphical plots are:

- Reactor Net Zone ID;
- Reactor Net Temperature;
- Reactor Net Mass fraction of species-n.

Chapter 4

Results on aerosol forming compounds in Entrained Flow Reactor

This chapter shows the results of numerical simulations obtained with the Fluent code 16.1 conducted on the combustion system KVSA.

4.1 CFD simulations results

4.1.1 Temperature field

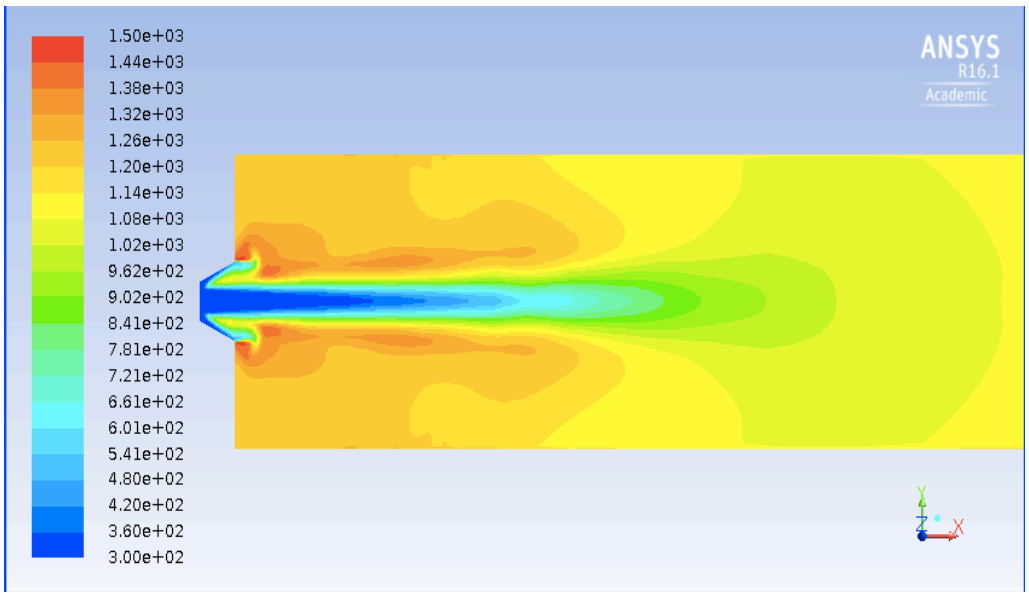

Fig. 4.1. Temperature field

For the temperature field can be noted the recirculation zones created by the swirler present on the burner for the secondary air. There are three hot points in the flame to support the thesis of the highly swirling flame. The temperature range is absolutely agree with those that expected, unfortunately, the experimental data is not available so is not possible to have a real confrontation necessary for the validation.

4.1.2 CO_2 field

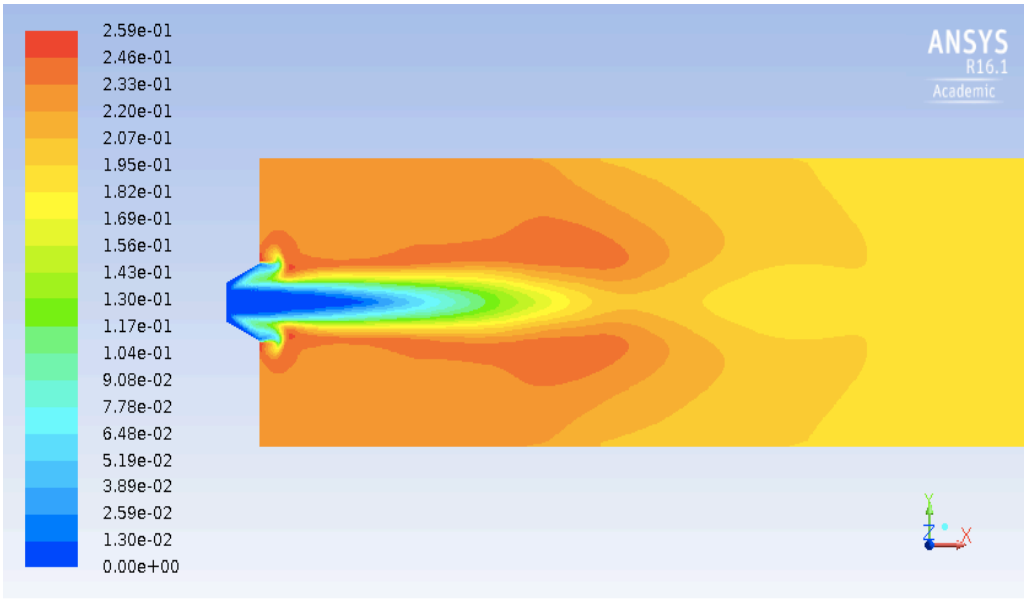

Fig. 4.2. Field of mass fraction of CO_2

4.1.3 O_2 field

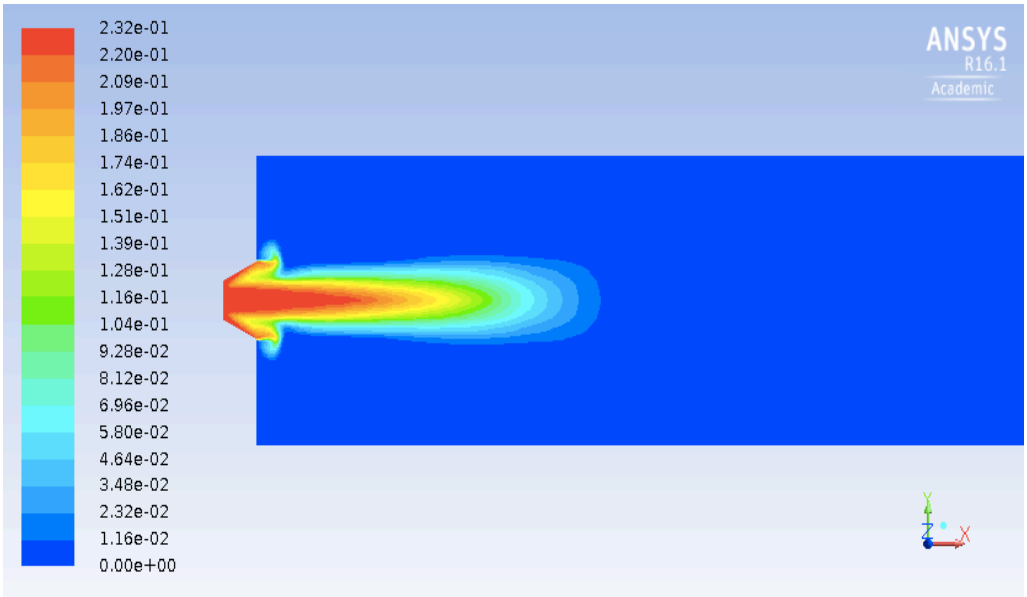

Fig. 4.3. Field of mass fraction of O_2

4.2 RNA simulations results

4.2.1 Clustering

This paragraph shows the results of the clustering of the previously thermochemical field. The clustering method was explained in paragraph 3.3.2.1. The cases studied are three: 100, 150 and 200 reactors. The graphs plotted by Fluent are related to the position, but our interest is not to position, but on the mixture fraction. The mixture fraction was calculated by the following equation:

$$Z = \left[\frac{sY_F - Y_O + Y_{O,0}}{sY_{F,0} + Y_{O,0}}\right]$$

where

$$s = AFR_{stoich} = \frac{W_O * \upsilon_O}{W_F * \upsilon_F}$$

$Y_{F,0}$ and $Y_{O,0}$ represent the fuel oxidizer mass fractions at the inlet, W_F and W_O are the species molecular weights, and υ_F and υ_O are the fuel and oxygen stoichiometric coefficients, respectively. A big mistake that commits Fluent during the export of the results of clustering zones is an interpolation, which gives the false results of some zones of the Reactor Network. The procedure carried out to solve the problem was to export the zone data and the homogeneous temperature in the reactors, then these quantities have been put in relation with the mixture fraction, previously calculated. At this point all the data of the interpolated zones were removed; the Table 4.1 shows the error that commits this interpolation.

Reactor Network n°	Temperature RN	Mixture fraction Z
50	903.807	0.551016808
50.0375	1159.37	0.673531435
50.0384	1159.38	0.664025182
50.1196	1121.03	0.644752874
50.2364	643.715	0.494492033

Table 4.1. Error on the reactor network zones

The results of this procedure are shown in the following figures (4.4, 4.6, 4.8). In the figures 4.5, 4.7 and 4.9 are shown the fields obtained through Fluent code.

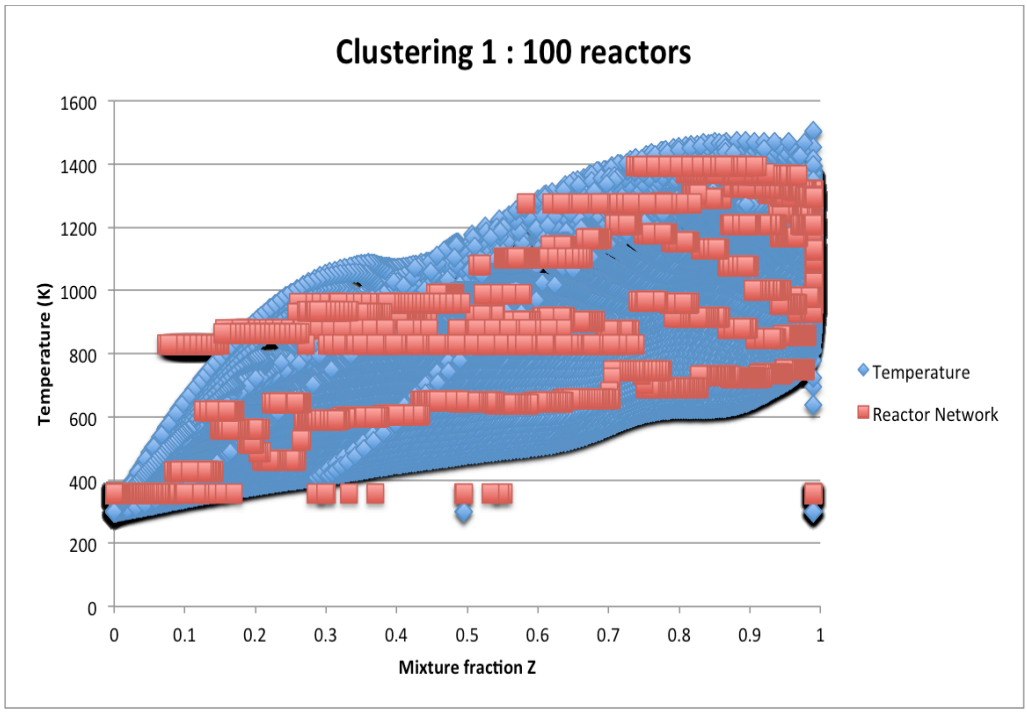

Fig. 4.4. Clustering 100 reactors

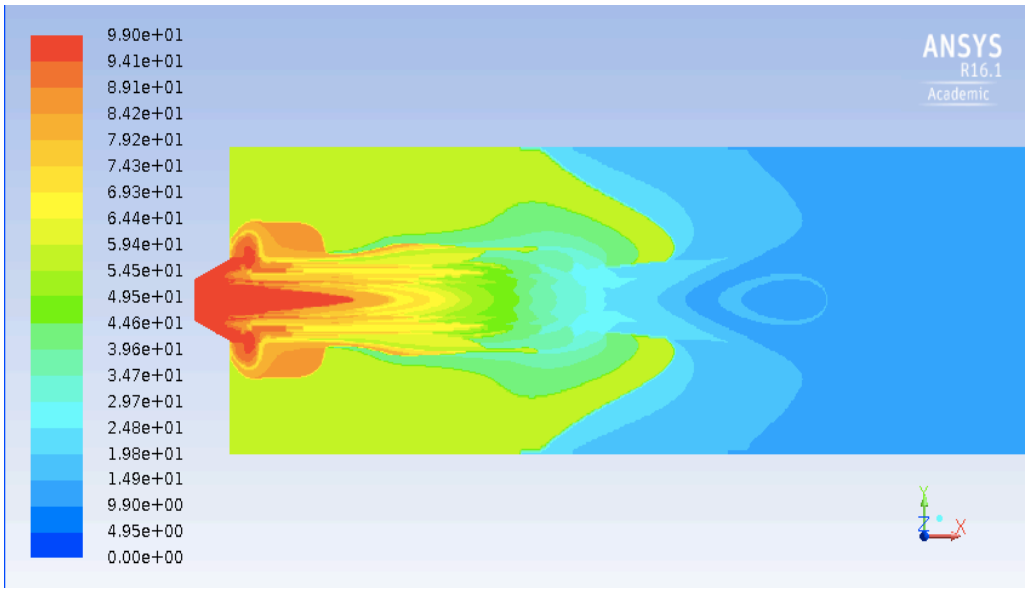

Fig. 4.5. Field of 100 reactors zone

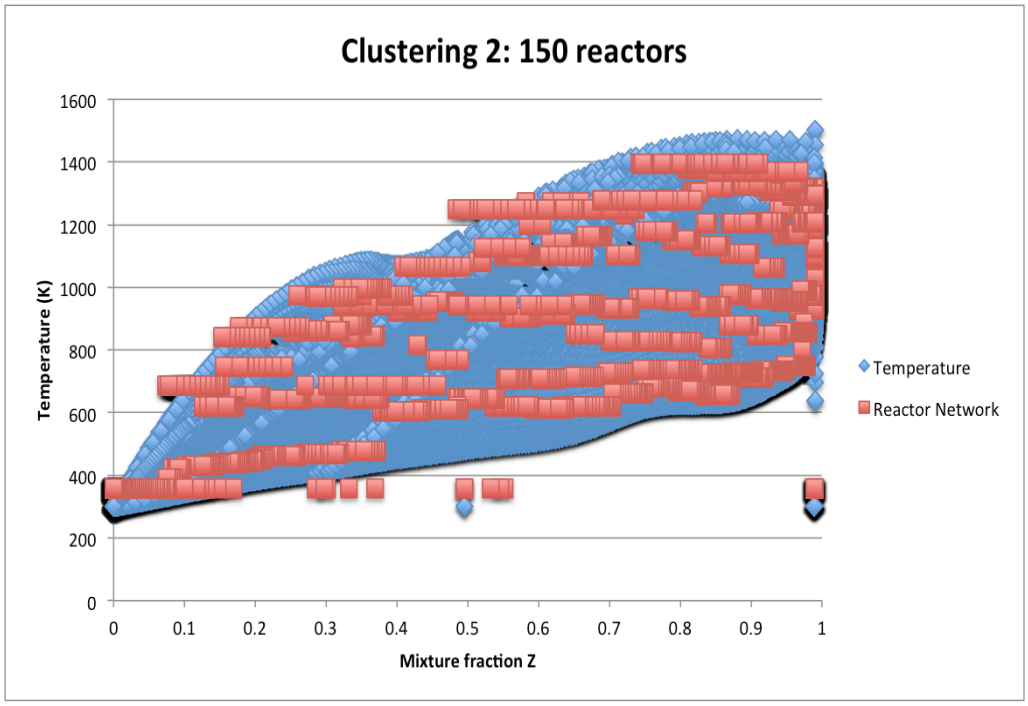

Fig. 4.6. Clustering 150 reactors

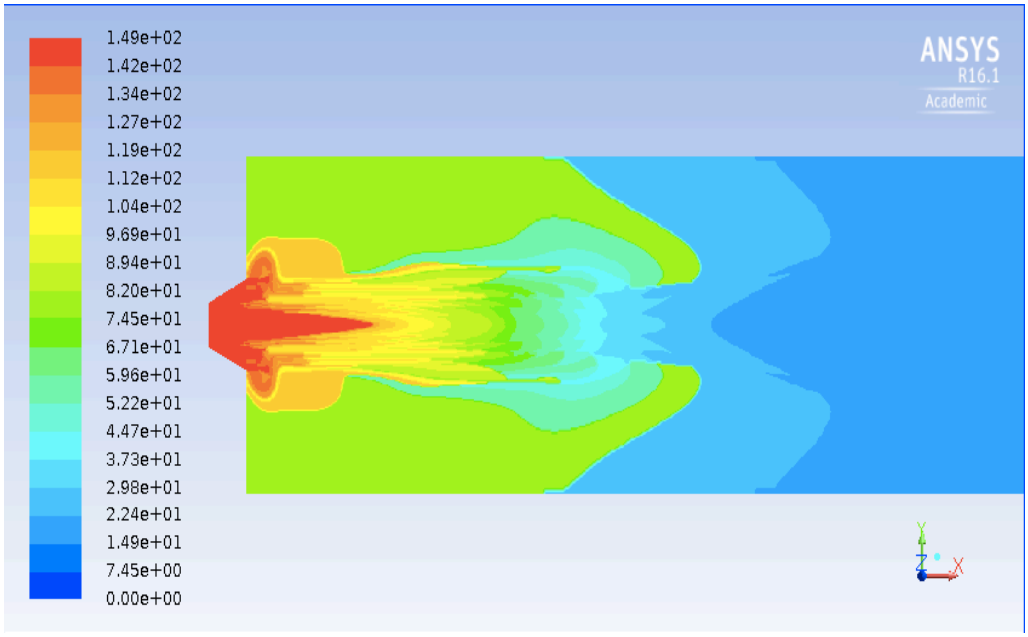

Fig. 4.7. Field of 150 reactors zone

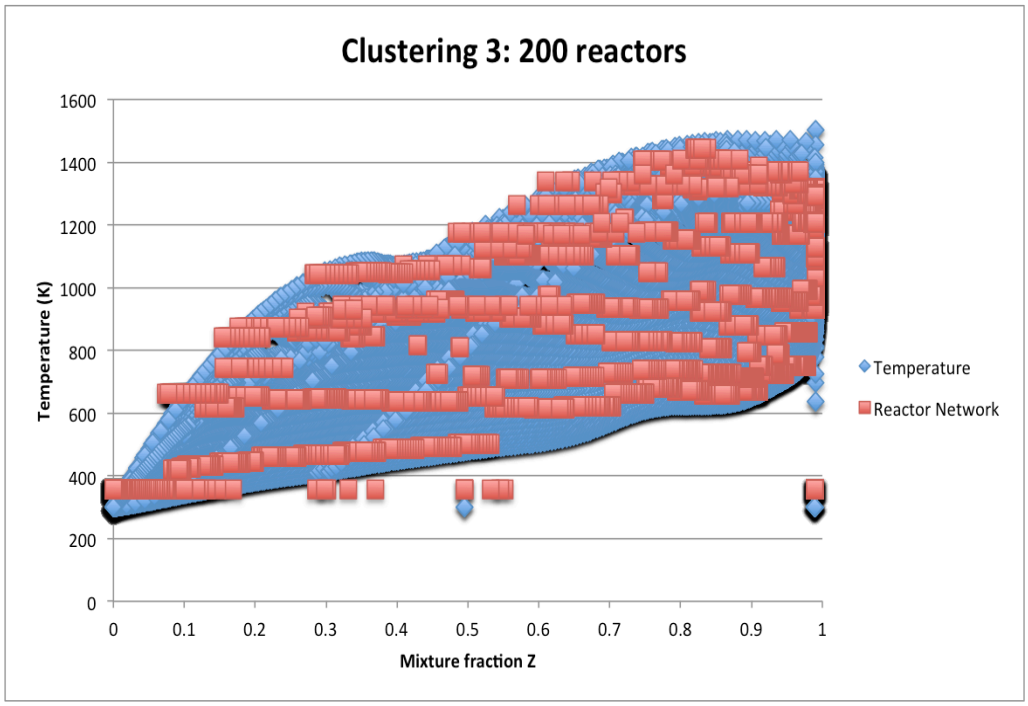

Fig. 4.8. Clustering 200 reactors

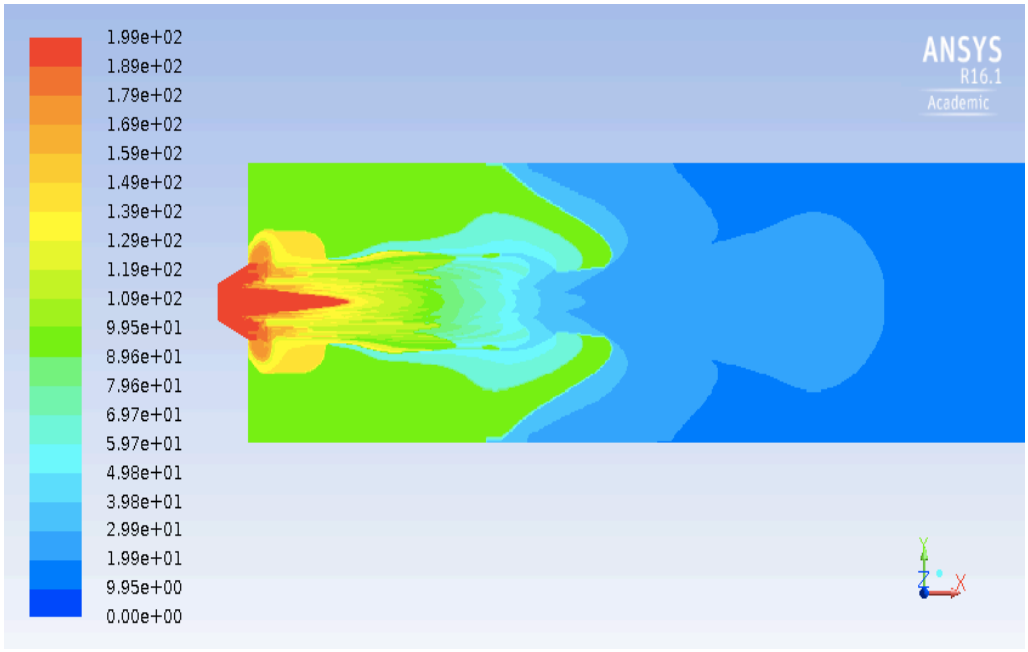

Fig. 4.9. Field of 200 reactors zone

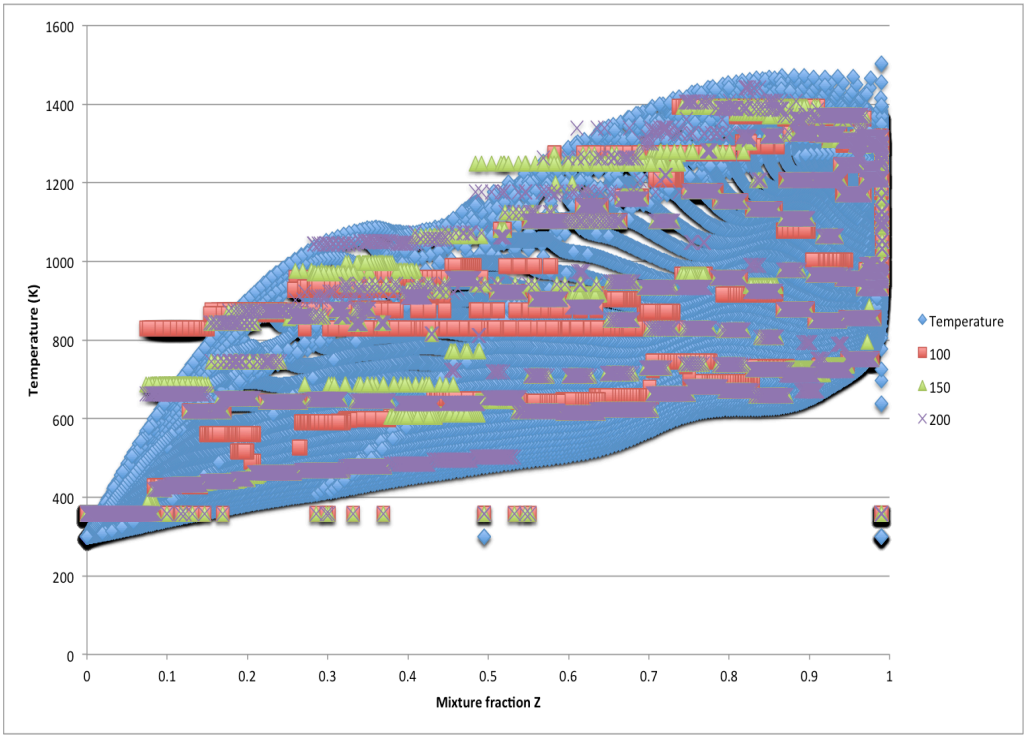

Fig. 4. 10. Comparison between the different reactor networks

In figure 4.10 is shows the comparison between the various reactor network obtained. The figure shows that the increase in the number of reactors the temperature range is homogenized better, in fact as can be seen in the figure for the case with 100 reactors at about 800 K and for the case with 150 reactors at about 1200 K, some reactors fall outside of the temperature range which does not happen with 200 reactors. Another thing to note are the reactors at 300 K completely outside the temperature range, which represent the fuel and air inlet that we have imposed at this temperature, as a boundary conditions. From this analysis can deduce that the clustering that the Fluent code make can be considered acceptable, although as seen in the figures, the reactors that are created are all at a constant temperature and only varies the mixture fraction. A better clustering would be obtained if the clustering variables were not only the temperature, but also on the mixture fraction.

In the following pages are shown the profiles of aerosols present in higher quantities which are: KCl, $(KCl)_2$ and K_2SO_4; the profiles were plotted by vary the number of reactors on a fixed line for all three cases. In addition, all the species fields are displayed on the interface plane of the furnace, for the case with 200 reactors.

4.2.2 KCl field

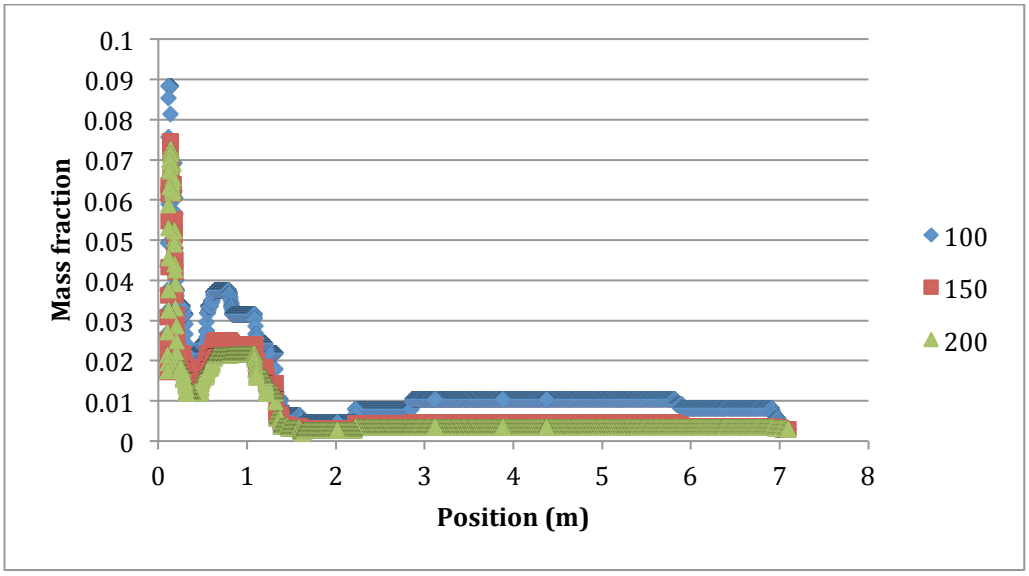

Fig. 4.11. KCl comparison between various reactor networks

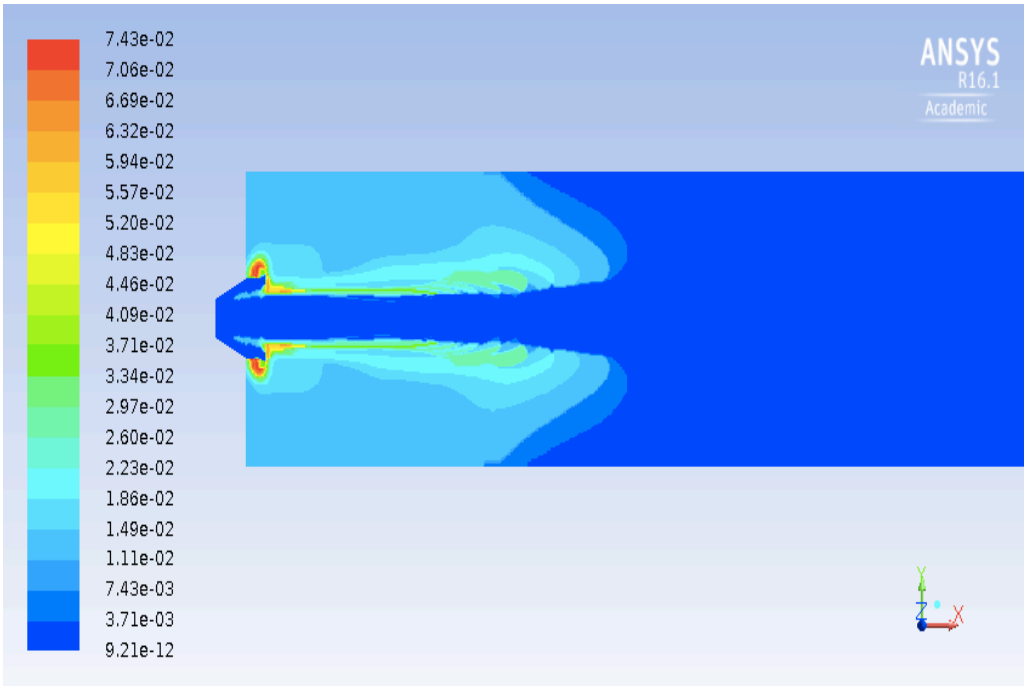

Fig. 4.12. Field of mass fraction of KCl

4.2.3 $(KCl)_2$ field

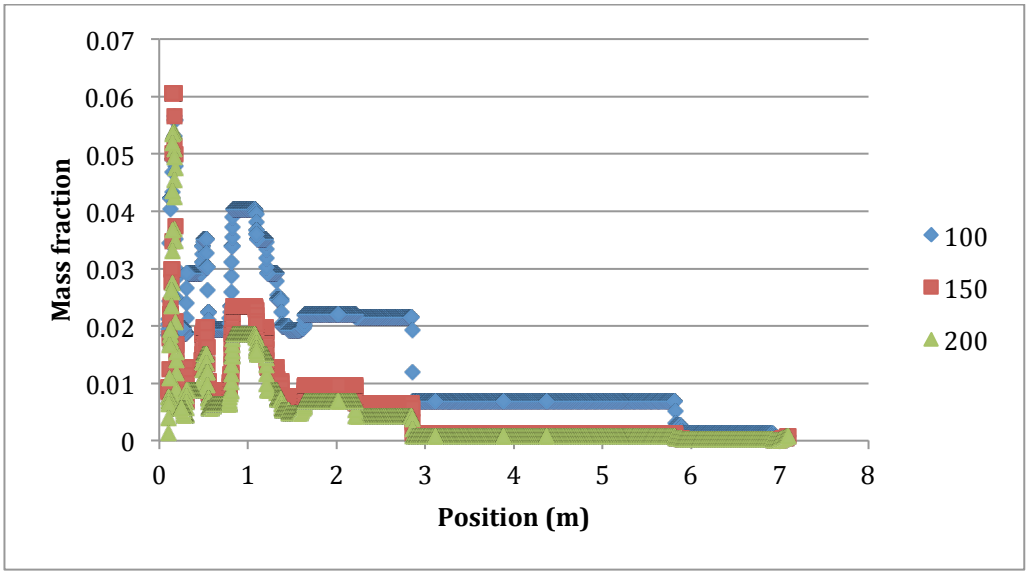

Fig. 4.13. $(KCl)_2$ comparison between various reactor networks

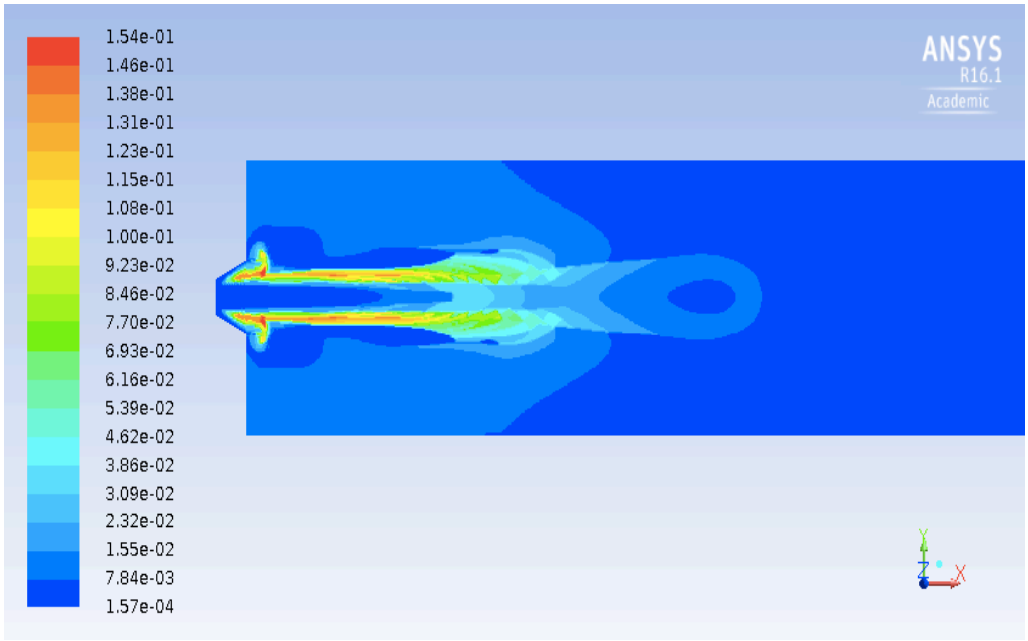

Fig. 4.14. Field of mass fraction of $(KCl)_2$

4.2.4 K_2SO_4 field

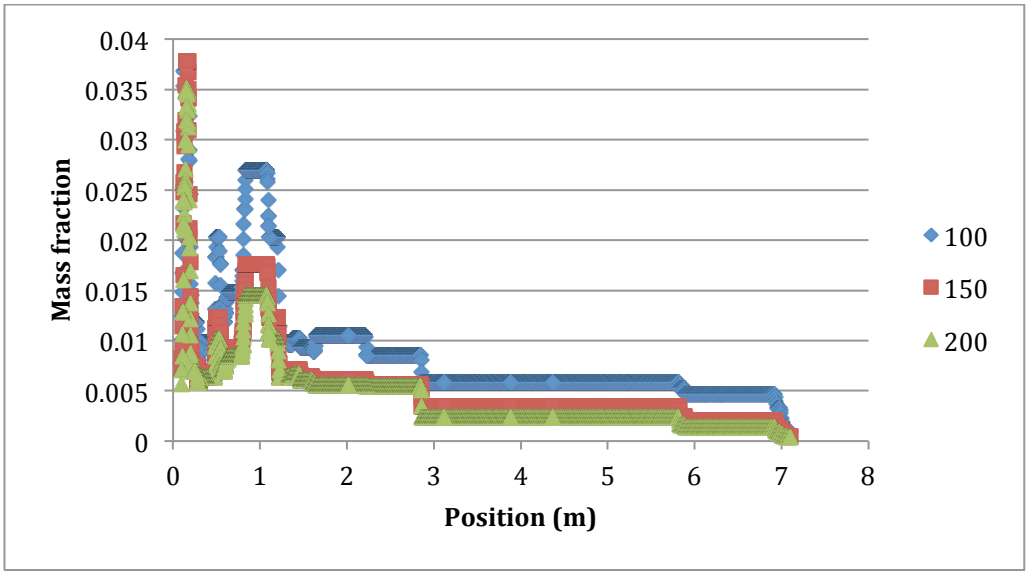

Fig. 4.15. K_2SO_4 comparison between various reactor networks

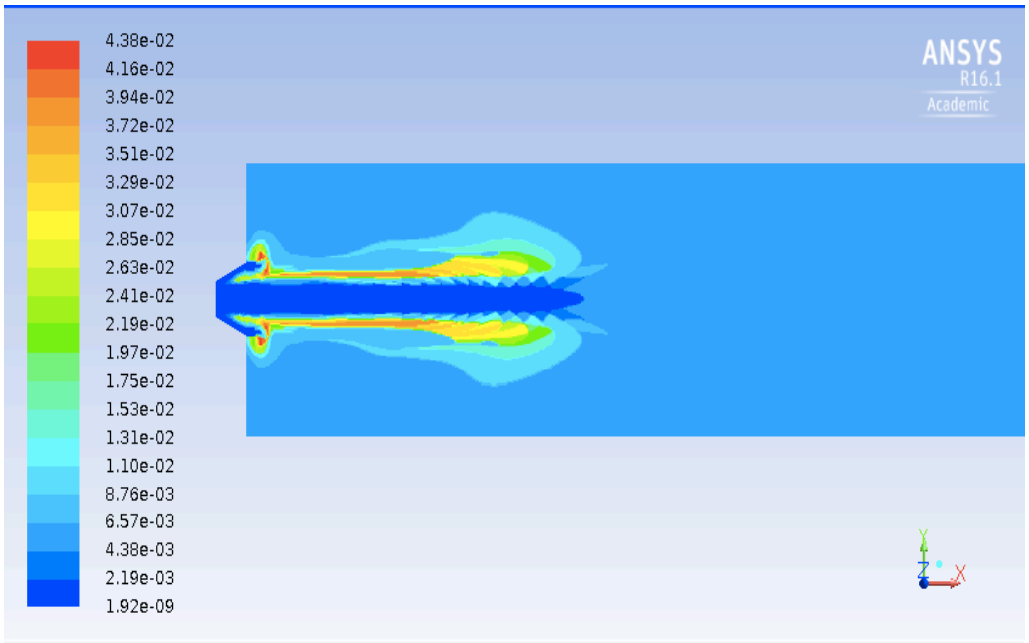

Fig. 4.16. Field of mass fraction of K_2SO_4

4.3 Final considerations

From the results obtained it can be deduced that varying the number of reactors can be noticed a different concentration, especially in the case with 100 reactors compared to the other two cases. Among the case with 150 reactors and with 200 reactors, even if some differences are present, the two profiles can be considered consistent with each other, and can neglect this small difference. As regards the KCl, from the figure 4.9 can see a peak concentration at the entrance in the furnace, this effect can be justified by the fact that the KCl is already present in the devolatilizing reaction, then the KCl contributions are summed. The $(KCl)_2$ and K_2SO_4 from figures 4.11 and 4.13 is seen that they have the same trend, although for the $(KCl)_2$ at higher concentrations. Even for the $(KCl)_2$ and K_2SO_4 is present a peak concentration at the entrance of the furnace, where the temperature is higher, even if the concentration is less than the KCl. It is observed that the KCl has low concentration after just a meter of the furnace, while for the other two compounds is seen that the concentration decreases at around three meters, that represent the lenght of the flame. This make us understand that the KCl is reacting and tends to become K_2SO_4. Using the equation of ideal gases is possible to calculate an estimate of the concentration of each species, using the following equations:

$$conc_i = \frac{P_{TOT} * Y_i}{RT} * PM_{TOT}$$

where *i* is the species and Y_i is the mass fraction of ith species.

The results found are around 400 mg/m^3 according to the limited data that can be found in the literature which give an estimate of 100 mg/m^3 as total sum of all aersols. At the outlet of the furnace, such as the inlet of the convective section, from the fields of the selected species can be seen that for the KCl and the $(KCl)_2$ the mass fractions are very low, while for the K_2SO_4 mass fractions are higher, this confirms perfectly the Glaborg mechanism that describes the transformation from SO_2 as the initial species and with a series of reactions converts into K_2SO_4. All these theoretical data found from the Reactor Network Analysis should be confirmed by experimental data for validation of the model that has not yet occured. The experimental campaign for the pilot system KVSA is scheduled for August 2016, so it will be possible in the future have a validation for the model.

Chapter 5

Analysis of vapour to solid mechanism of aerosol formation and deposition

5.1 Introduction

It is well known that ash deposition and pollutant (HCl, aerosols, mercury, etc.) formation are significantly influenced by the content of chlorine and alkali metals in the feeding fuel or fuel blend. These are indeed the elements experiencing more relevant variations in feed composition when coal is blended with RDF. The alkali species present in pulverised coal are known to be implicated in the initiation and build-up of deposits on surfaces. During combustion, a portion of alkali species is released to the vapor phase, where are usually present in the form of chlorides and sulphates. Part of the vaporised alkali are adsorbed on fly ash clays, while the remaining alkali vapours condense in the cooler convective regions of the furnace, or coagulate to form submicron aerosol and are a major cause of fouling. Direct condensation of alkali species on cooled tube surfaces may affect deposition by generating a sticky layer on the tube surface, thereby increasing the sticking efficiency of impacting ash particles and the thermal resistance. Adsorption on glassy silicate or aluminosilicate fly ash particles may also affect deposition. On one hand irreversible capture of alkali vapours by fly ash minerals can mitigate the fouling tendency by fume deposition, on the other hand the slag tendency can increase because alkali enriched fly ash present lower melting temperatures and higher sticking efficiencies. In order to evaluate solutions to these problems, it is necessary to increase the general knowledge of the fate of alkali elements and their interactions in the furnace environment. It is important to include this knowledge in numerical codes able to predict the behaviour of different types of fuels, burned singularly or in co-combustion, regarding air emissions and heat exchange tube fouling and corrosion problems.

In this chapter, a method formulated by coupling different modelling tools is developed and applied to predict the concentration of alkali chlorine vapours in the flue gas and the deposition inside the combustion chamber and the convective units. The thermochemical fields calculated with Fluent and the Reactor Network Analysis were the input data for the tools:

- NGDE, simulation of the processes of formation and growth of aerosol;
- Prediction of aerosol deposition on the convective section.

5.2 Processes of formation and growth of aerosol NGDE

Aerosol formation is dependent on both the thermodynamic equilibrium that the mechanisms of transport; in these therms, the aerosol system is described by the GDE (General Dynamics Equation). NGDE is a software, developed at the Department of Mechanical Engineering and Chemistry in Univesity of Minnesota by A. Prakash, et al, using a numerical algorithm for the resolution of GDE:

$$\frac{dN_k}{dt} = \left.\frac{dN_k}{dt}\right|_{coag} + \left.\frac{dN_k}{dt}\right|_{nucleat} + \left.\frac{dN_k}{dt}\right|_{cond}$$

The GDE is resolved for the nucleation phenomena, coagulation and growth superficial (condensation), neglecting other processes such as: fragmentation, evaporation, thermophoresis, diffusion to the surfaces and inertial impact. The diameter of aerosol particles between 1 nm and 10 μm are placed in 40 "nodes" in order to discretized according to the diameter. It is reports the equations for the resolution of NGDE for the nucleation, coagulation and growth surface.

- Nucleation

$$J_k = n_s^2 S \upsilon_1 \left(\frac{2\sigma}{\pi m_1}\right)^{0.5} exp\left(\theta - \frac{4\theta^3}{27log^2 S}\right)$$

$$\left.\frac{dN_k}{dt}\right|_{nucl} = J_k(t)\zeta_k$$

J_k = velocity of nucleation ($m^3\ s^{-1}$);
N_k = number of particles on the node k;
n_s = monomers concentration at saturation ($\#/m^3$), ns= Ps/(kb*T);
Ps- Pressure of saturation, kb- Boltzmann's costant, T- Temperature;
S= ratio of saturation, S= p/Ps, p- partial pressure of vapuor;
υ_1 = volume of monomer (m^3 / m^3 of aerosol);
σ = surface tension (Nm^{-1});
m_1 = mass of monomer (kg);
θ = suface tension adimensional;
θ = (s_1*σ)/(kb*T), s_1 – surface of monomer.

- Coagulation

$$\beta(vi, vj) = \left(\frac{3}{4\pi}\right)^{1/6} \left(\frac{6kT}{\rho_P}\right)^{1/2} \left(\frac{1}{v_i} + \frac{1}{v_j}\right)^{1/2} (v_i^{\frac{1}{3}} + v_j^{\frac{1}{3}})^2$$

$$\left.\frac{dN_k}{dt}\right|_{coag} = \frac{1}{2} \sum_{\substack{i=2 \\ j=2}} \chi_{i\,jk} \beta_{i\,j} N_i N_j - N_k \sum \beta_{i\,k} N_i$$

$\beta(vi, vj)$ = collision frequency;
vi e vj = particles volumes (m^3);
ρ_P = particles density (kg m^{-3});
k = Boltzmann's constant (J K^{-1});
$\chi_{i\,jk}$ = operator of division on the nodes.

- Growth superficial

$$\left.\frac{dN_k}{dt}\right|_{cond} = \begin{cases} \frac{\nu_1}{\nu_k - \nu_{k-1}} \beta_{1,k-1}(N_1 - N^S{}_{1,k-1}) N_{k-1} & if\ N_1 > N^S{}_{1,k-1} \\ -\frac{\nu_1}{\nu_{k+1} - \nu_k} \beta_{1,k+1}(N_1 - N^S{}_{1,k+1}) N_{k+1} & if\ N_1 < N^S{}_{1,k+1} \\ -\frac{\nu_1}{\nu_{k+1} - \nu_k} \beta_{1,k}(N_1 - N^S{}_{1,k}) N_k & if\ N_1 > N^S{}_{1,k} \\ \frac{\nu_1}{\nu_k - \nu_{k-1}} \beta_{1,k}(N_1 - N^S{}_{1,k}) N_k & if\ N_1 < N^S{}_{1,k} \end{cases}$$

β_{ik} = function of the collision frequency;
$N^S{}_{1,k}$ = saturation concentration of the monomers in the particle size of "k" ($\#/m^3$).

With the term nucleation is meant a homogeneous condensation process that leads to formation of new particles, which can later grow superficially, working also as condensation nucleus for other volatiles, or collide with each other and coagulate. The nucleation of new particles may compete with the surface growth process in which usually prevails, however, in the case where the number of condensation nucleus is insufficient or the supersaturation pressure is high enough in any case one can obtain the formation of new particles. Coagulation is a slower process which occursafter the nucleation and growth superficial; NGDE calculates the coagulation velocity assuming that the particles collide exclusively as a result of Brownian motion neglecting any contribution of the turbulence.

5.2.1 NGDE code

The NGDE is an executable file that one should use on a windows machine, written in C language. This C code is used to solve for nucleation, coagulation and surface growth problems. It can be used for any material whose properties are known. There are four different sections in this code:

- Coagulation;
- Nucleation (classical) + coagulation;
- Surface growth;
- Unified GDE with all the three phenomena combined.

The above phenomena constitute four different sections of the code. Each of the four sections are independent of each other. They have especially been written in such manner so that, one can identify the contribution of each phenomena to the GDE. Also, if one requires to use nucleation, coagulation or surface growth alone, it can be easily done. The solution algorithm involves a new approach to solve the Aerosol GDE, where the particle volume space is divided into nodes of zero width. Using nodes allows us to cover the entire size range of aerosol (1 nm to 10 micrometer) using just 40 nodes. The input file "main.inp" should contain all the property data. If the user wants to run the code for a specific coagulation or a surface growth problem, the corresponding input files "coag.inp" or "grow.inp" must be modified accordingly. The input data are surface tension, saturation pressure, molecular weight and density for each component. Some changes were made in the code that would write the granulometric distribution results every 400000 iterations.

5.2.1 Application to aerosol

To test the condensation model and growth of aerosol particles, were found the input data of NGDE (Appendix 6) for inorganic chemical species that contribute most the formation inorganic aerosols from burning coal and/or biomass: K_2SO_4, KCl and $(KCl)_2$. The surface tension data for solid species were found in literature in form: $\sigma = a - bT$.

$$\sigma_{KCl,(KCl)_2} = \begin{cases} 298.7 - 0.1376 * T \\ T < 1044\ K \\ \\ 241.7 - 0.1243 * T \\ T \geq 1044\ K \end{cases} \qquad \sigma_{K_2SO_4} = \begin{cases} 655.7 - 0.2942 * T \\ T < 1342\ K \\ \\ 212 - 0.065 * (T - 273.15) \\ T \geq 1342\ K \end{cases}$$

The data reported for the surface tensions are expressed in dyne/cm, as requires the input file of NGDE. The vapor pressure values, in the form Ps = exp (a – b/T), were taken from literature.

$$P_s(KCl) = 19.59699 - 27523.711 * T;$$

$$P_s((KCl)_2) = 19.53386 - 27453.2 * T;$$

$$P_s(K_2SO_4) = 11.00314 - 23716.63457 * T;$$

The matrix of tests carried out with the related input data, initial temperature and velocity of cooling, is reported in Table 5.1. The initial temperature was set at 953 K for the K_2SO_4 and 880 K for the KCl and the $(KCl)_2$. It was performed for the K_2SO_4 with T_i = 1000 K to evaluate the effect of the initial temperature in produced amount of aerosol. For these first tests, such as cooling rate, it was set an average velocity taken from other work, but modify appropriatly the NGDE will later be possible to change the cooling profile.

Aerosol type	**T_i (K)**	**T_{rate} (K/s)**
K_2SO_4 nucl, coag, growth	953	253
K_2SO_4 nucl, coag, growth	1000	253
KCl nucl, coag, growth	880	253
$(KCl)_2$ nucl coag, growth	880	253

Table 5.1. Conditions of the simulation made with NGDE

5.2.1.1 Homogeneous condensation of K_2SO_4 aerosols

A vapour of K_2SO_4 was cooled from an initial temperature of 953 K with a cooling ratio of 253 K/s. The particle size distribution of the massive particles obtained at the temperature of 300 K has been normalized respect to maxium. The result is a distribution characterized by a peak at 0.05 μm. The result obtained is reported in Figure 5.1.

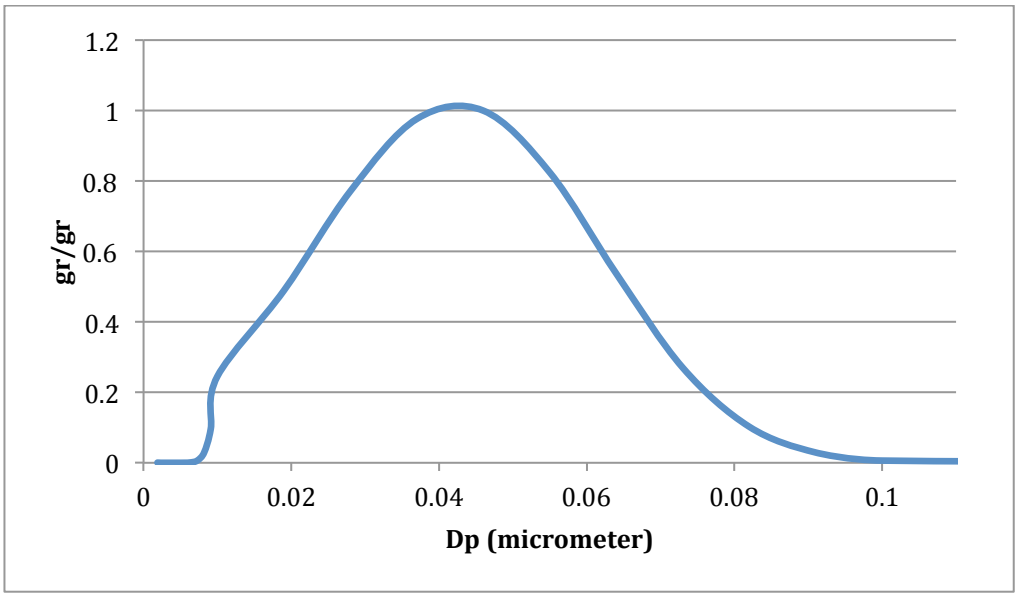

Fig. 5.1. Result K_2SO_4 with cooling rate of 953 K

To investigate the effect of initial temperature on the velocity of nucleation and on mass of aerosols produced, another test was made by cooling a vapour of K_2SO_4 from the initial temperature of 1000 K. From the results obtained, it possible deduce that starting from a higher temperature gas phase the particles begin to form at higher temperatures and, after the nucleation, is more active the growth superficial process that determines the production of a volume increased aerosol and a distribution shifted to larger diameters. Increasing the intial temperature the velocity of nucleation increases and the mass of aerosol is lower, as shown in Table 5.2.

$T_{initial}$ (K)	Total mass (g/m^3) a T= 300 K
953	0.0055
1000	0.0022

Table 5.2. Total mass of K_2SO_4 aerosol

In the graph of Figure 5.2 comparing the distribution calculated for K_2SO_4 at different temperatures. As already said previously and as is shown in Figure 5.2 that starting from a higher initial temperature produces a particle size distribution shifted towards larger diameters.

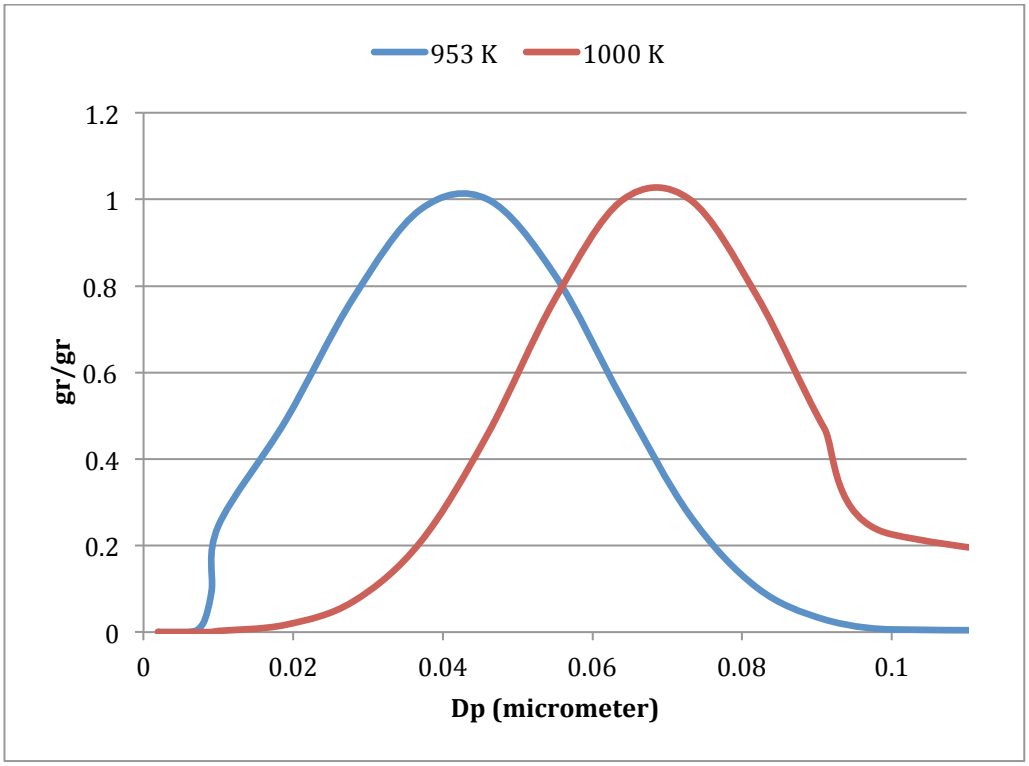

Fig. 5.2. Particle size distribution for K_2SO_4

5.2.1.2 Homogeneous condensation of KCl and (KCl)2 aerosols

Similar to the K_2SO_4 (T_{init} 880 K, T_{rate} 253 K/s) the formation was simulated by an aerosol of KCl and $(KCl)_2$. As it regards the vapour of KCl is not observed the formation of particles to temperatures taken into account (up to ~ 300 K).

In the case of $(KCl)_2$ is formed, instead, a distribution similar to that obtained for the K_2SO_4 but shifted to smaller diameters, as is shown in figure 5.3. From a quantitative point of view, the value of the mass is similar (0.0018 g/m^3) to that obtained for the K_2SO_4 (Table 5.2), the main contribution to the mass derives by particles of diameter between 0.01 and 0.06 microns.

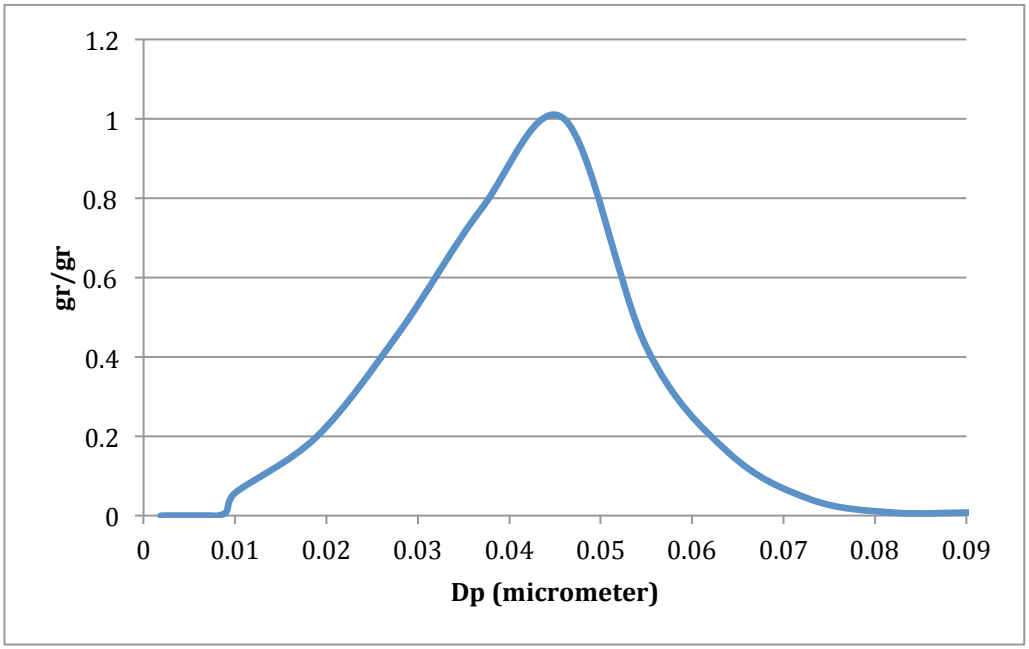

Fig. 5.3. $(KCl)_2$ particle size distribution

In the graph of Figure 5.4 comparing distribution calculated for K_2SO_4 and $(KCl)_2$, were is shown as said above.

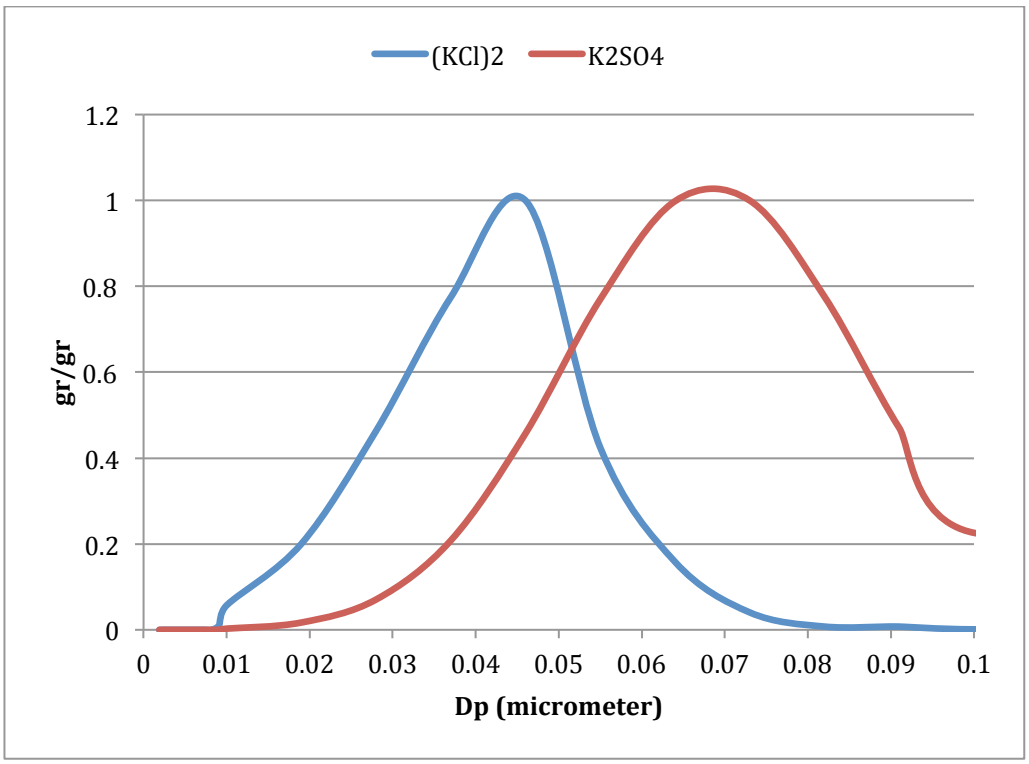

Fig. 5.4. Comparison between the particle distribution

5.2.2 Surface growth of an aerosol of $(KCl)_2$

From the results obtained, it can be deduced that the K_2SO_4 is the first chemical species to condense, in accordance with as reported in literature. Subsequently the newly particles can grow for further condensation of K_2SO_4 or also function as condensation nucleus for other chemical species as KCl and $(KCl)_2$. Since the surface growth generally prevails over nucleation of new particles and the KCl and $(KCl)_2$ tend to condense on particles already formed of K_2SO_4 without therefore giving rise to the formation of new particles. To simulate this phenomenon can use the single NGDE surface growth module, starting from an initial number of homogeneous particles in terms of size and supposing be in the presence of an increasingly oversaturated vapor, it simulates the growth of the particles for surface condensation of vapour. Then setting an initial number of particles equal to that obtained by solving the full GDE for a vapour of K_2SO_4, it is possible to condense on these a vapour of KCl or $(KCl)_2$. Since the module of "single surface growth" of NGDE provides for the possibility of set as input a homogeneous population of particles but not a distribution in diameter is assigned to an average particle diameter calculated from the distribution particle size of K_2SO_4. In the graph of Figure 5.5 shows a comparison between the distribution obtained by the module "single surface growth" for a vapour of $(KCl)_2$ over K_2SO_4 and the previously data for a pure aerosol of K_2SO_4 and $(KCl)_2$. In reality aerosols consits of particles of various nature deriving from a homogeneous condensation and a heterogeneous condesation of a chemical species on the particles of another chemical species. To obtain a theoretical destribution that is more representative of the real one, both in terms of form that a quantitative point of view, will therefore be necessary to interface between them different condensation phenomena that contribute in the production of aerosol particles in an actual combustion process.

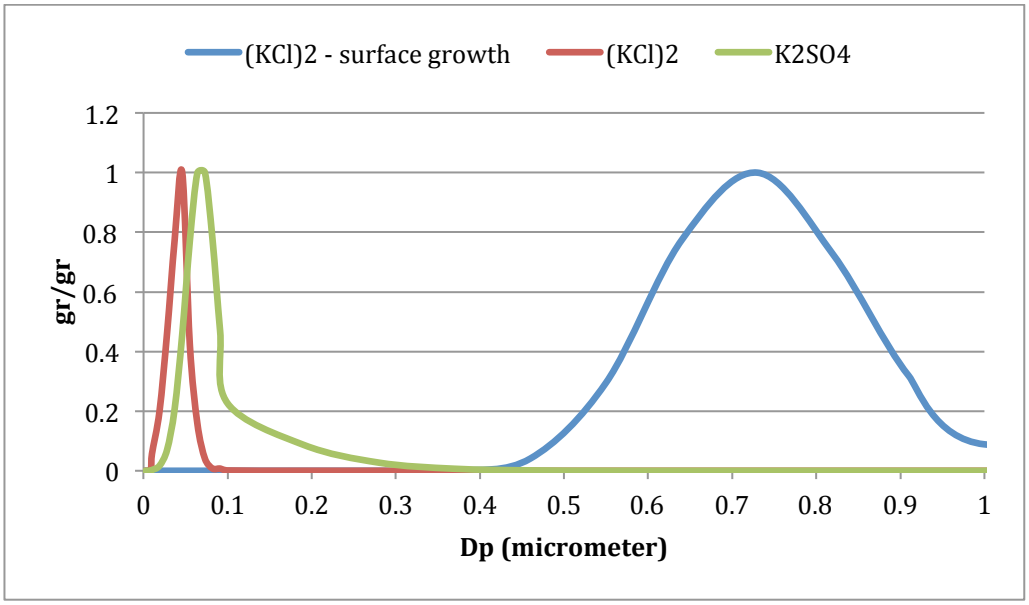

Fig. 5.5. Comaparison aerosol growth surface only with pure aerosols

5.2 Prediction of aerosol deposition on the convective section

The prediction of the deposition can be made by considering the properties of each alkaline species and the characteristics and conditions of the tube bank. The convective zone was reasonably restraint as the final zone of the combustion chamber. The deposition model described below is applied to all PF reactors starting from the conditions of the gas estimated with the previous Reactor Network Analysis. The aim is to predict the deposition of alkali compounds into the heat transfer surfaces in the three cases of different loads. Chemical reactions and mechanisms of condensation have been formulated for 3 species of alkali compounds, namely, KCl, $(KCl)_2$ and K_2SO_4. The concentration of each compound in the flue gas is assumed uniform in the section, as well as the temperature of the flue gas. The diffusion is simulated as the net transport of gas molecules and particles (aerosol, for instance) from an area with high concentration to an area at lower concentration. The concentration of condensing vapours and/or particles that are diffusing is depressed near an obstacle, like a tube of the heat-exchange units (Figure 5.6).

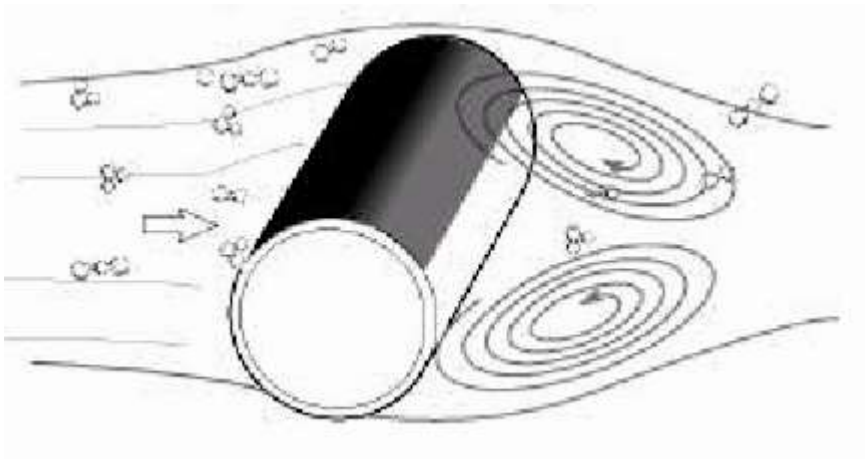

Fig. 5.6. Deposition on a heat exchange tube

The mass transfer rate for diffusion on the tube surface can be evaluated by using the following formula (Rosner 1986):

$$\dot{m}_d = \frac{D * Sh}{D_t}\, m$$

where D is the diffusion coefficient, Sh the Sherwood number, D_t the tube diameter and m the mass concentration of the super saturated vapour of the aerosol.

The Sherwood number is estimated by assuming that there is an analogy between mass and heat tranfer:

$$Sh = f(Re, Sc)$$

$$Nu = f(Re, \mathrm{Pr})$$

where the function *f* is the same for the Sherwood and Nusselt number. The Reynolds, Schimdt and Prandtl numbers are

$$Re = \frac{\rho_g V D_t}{\eta}$$

$$Sc = \frac{\eta}{\rho_g D}$$

$$Pr = \frac{c_p \mu}{k}$$

The Nusselt number can be obtained from the empirical correlation for a cylinder with axes perpendicular to the flow (Perry 1999):

$$Nu = a\, Re^b Pr^{1/3}$$

where a = 0.683 and b=0.466, for 40 < Re < 4000. By assuming this expression and considering the previous equations, the Sherwood number can be obtained:

$$Sh\ (Re, Sc) \sim 0.683\, Re^{0.466} Sc^{1/3} \qquad \text{for } 40 < \mathrm{Re} < 4000$$

The mass transfer rate for diffusion on the tube surface can be obtained by rearranging the previous equations:

$$\dot{m}_d \approx 0.683\, Re^{0.466} \frac{D^{\frac{2}{3}} \eta^{\frac{1}{3}}}{D_t\, \rho_g^{\frac{1}{3}}}\, m \qquad \text{for } 40 < \mathrm{Re} < 4000$$

The deposition model described above can quantify the deposition rate of alkali compounds in specific conditions of the convective pass and give an estimation of the most favourable factors to depostion. However some point should be remarked to be aware of the limitations of the approach:

- The model is in stationary conditions, so the effect of variations due to the deposition is not considered. Above all, the metal temperature is assumed indipendent of time, while the deposition will increase the thermal resistance and thus reduce the surface temperature;
- The deposition is considered uniform on the heat transfer surfaces, while it is known that preferred directions can be effectively recognized. This choice is indeed unavoidable due to the complex geometry of the convective pass, the required simplicity of the model approach and the strong assumptions made in adopting the model parameters.

The deposition rates predicted for the three cases of different loads are compared in Figure 5.7. The case of high load is simulated through the Reactor Network Analysis. In all three cases it was made to vary the temperature and as said before also the concentration.

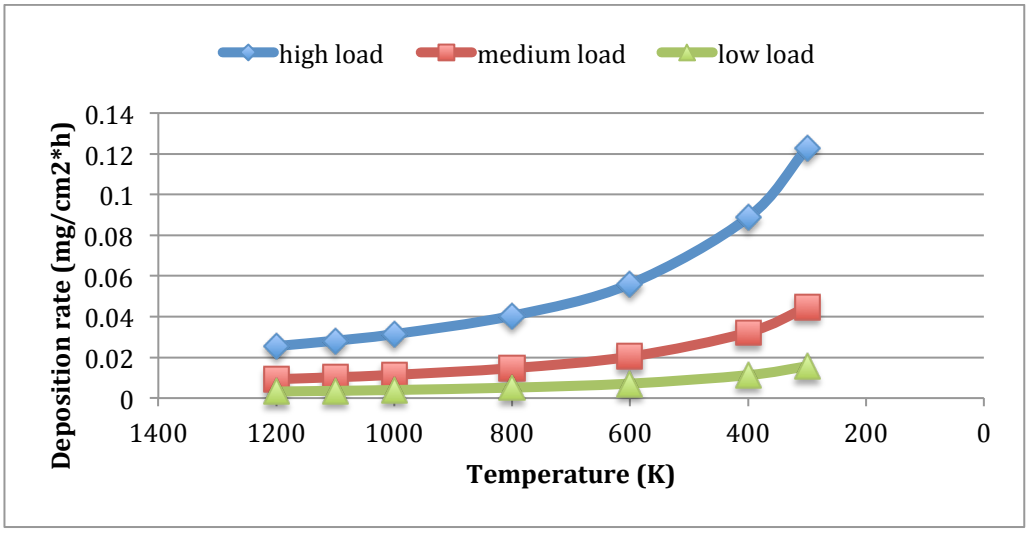

Fig. 5.7. Deposition rates of all alkali compounds

From the results in the figure show that the decrease of the concentration of alkaline compounds the temperature dependence decreases. The approach will need a deeper investigation, as the effective deposition surface is not the metal tube, the deposition on the tube is effectively non-uniform and the model doesn't inlcude any removal mechanism. The model can be used for studying instantaneous cases, and expected variations (due to different thermal resistances) should be taken into account.

Conclusions and future work

The main objective of the present work of graduation thesis was to be able to predict the aerosol in a biomass-fired power generation system through the Reactor Network Analysis model. The main precursors of aerosol from biomass systems are the potassium compounds, such as KCl, $(KCl)_2$ and K_2SO_4.

The first step of the work was devoted at analysis on experimental campaigns carried out in pilot-scale system on the formation of aerosols, in order to better understand factors influencing aerosol dimensional distribution and speciation. Subsequently a methodology for the prediction of aerosol formation in an entrained flow reactor was developed. The main idea was to provide a tool able to assist the experimental campaigns that are planned in the next future and will undertake the measurements of aerosol in case of biomass-fired. Hence the tool is expected to provide an estimation of particle concentration and size.

The starting point was a Computational Fluid Dynamics model of the burner and furnace. These required a strategy to reduce the computational cost: however the final grid for a quarter of the furnace consisted on 2.5 milion cells. Hence reacting runs, based on a two way Lagrangian coupling were carried out using global kinetics schemes. The resulting temperature and chemical species fields were used as input data to define interconnected pseudo-homogeneous regions that could be treated as Perfectly Strirred Reactors (PSR). Detailed kinetics scheme to predict aerosol forming compound in the gas phase could be solved using these reactors, with a number of reactors of approximately 100-200. The kinetic scheme included the Glaborg's mechanism for the aerosol, Hydrocarbons mechanism and the formation of NO_x, for a total of about 200 species and 3000 reactions. The analysis of the RNA clustering showed that this is based only on temperature, it could be improved in the future on clustering also the mixture fraction.

To validate the model and have a comparison with the results obtained might be interesting to use other models of RNA, such as Tognotti – Falcitelli and Kinetic Post Processor (POLIMI). Another idea to be more confident with the results would be to simulate the furnace on 360°, although the computational cost will be huge, there would be a best estimate of the aerosol in all zones of the domain.

Finally an attempt was made to looking at model able to predict the vapour to solid transformation to emulate the formation of aerosol particles and deposition that occurs once measuring probed are inserted in the test facility. With simplified models has studied the formation of aerosols through the nucleation, coagulation and surface growth mechanism was analyzed and the deposition on the tubes of the heat exchangers present in the convective section, the same model can be considered for the deposition of the particulates on the sampling probes.

The calculation is simplified by assuming a pure aerosol, which is formed by one chemical species. The tool was found to be able to predict different particle sizes depending on the operating conditions. A greater understanding of the mechanism of formation (nucleation, coagulation and surface growth) is necessary, having regards to what has been described before in the model limitations, above all due to the lack of a heat balance, neglecting the heat due to phase changes.

As for the deposition model is an extremely simplified model where is not taken in account that the thermal resistance change due to the deposition on the tubes and also the deposition is considered uniform. These two assumptions can be considered much strong, therefore an improvement of the model is required to obtain useful results that can be used in the experimental campaing.

Unfortunately, the results obtained are purely theoretical, since the lack of experimental data for the pilot system KVSA; an experimental campaigns and more detailed information are needed for a comparison with the results in terms of temperature and concentrations of the species present in larger quantities. However experimental campaigns are plannes in the next months.

Appendix A

Grid independency

For the indepence have carried out tests on three grids with different number of nodes then assesses which, among those developed, provides a reliable result with lower computational cost. As mentioned earlier, the geometry has been divided into the burner and furnace. For both was built a structured grid, to be more confident with the results obtained. For the burner and the furnace were taken of the lines on the domain and were compared for the different grids, the X velocity, Y velocity and Z velocity.

- **BURNER**

Case	Numbers of cells	Numbers of nodes
Grid 1	28728	40320
Grid 2	52800	69020
Grid 3	62592	81560

Tab. A.1. Grid parameters for the burner

- **FURNACE**

Case	Numbers of cells	Numbers of nodes
Grid 1	1027835	1142514
Grid 2	2458528	2634834
Grid 3	3827460	4048015

Tab. A.2. Grid parameters for the furnace

➢ **BURNER**

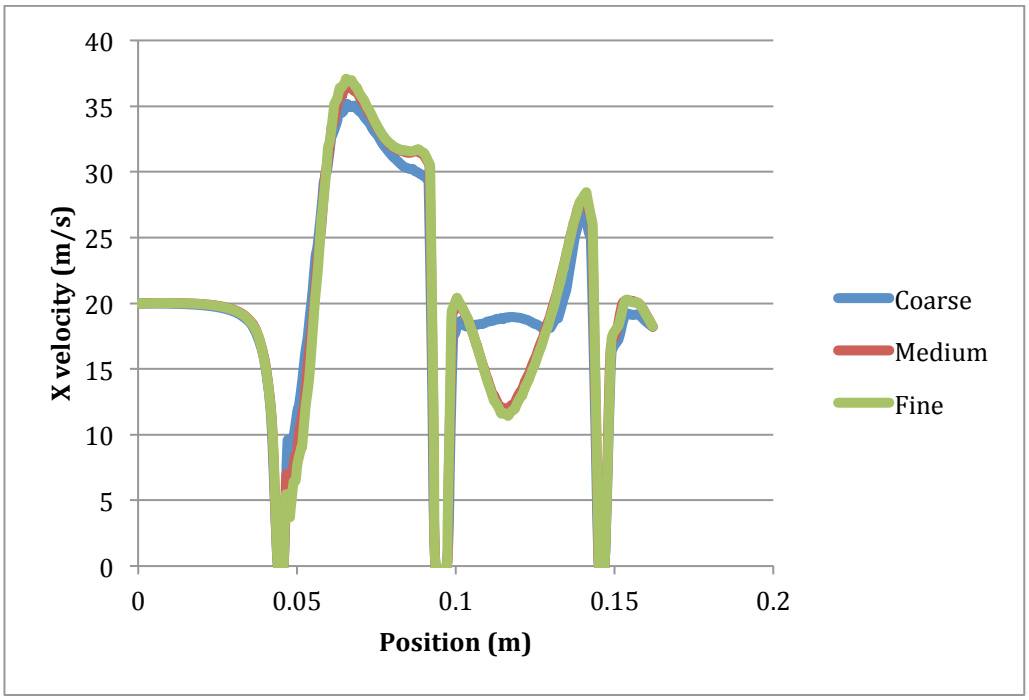

Fig. A.1. X velocity burner

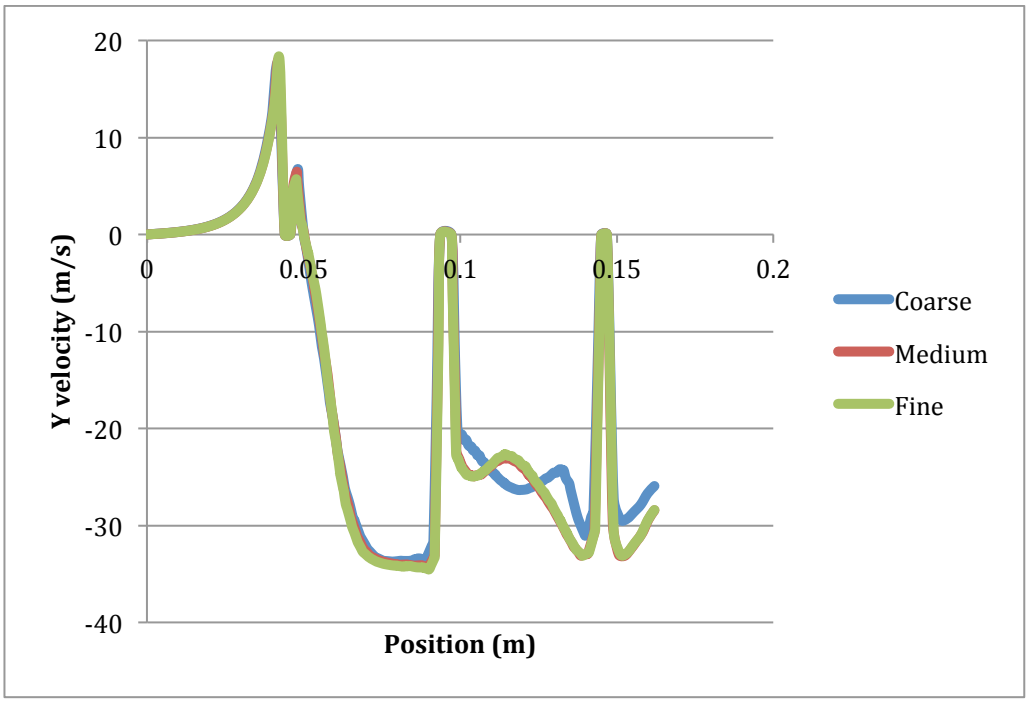

Fig. A. 2. Y velocity burner

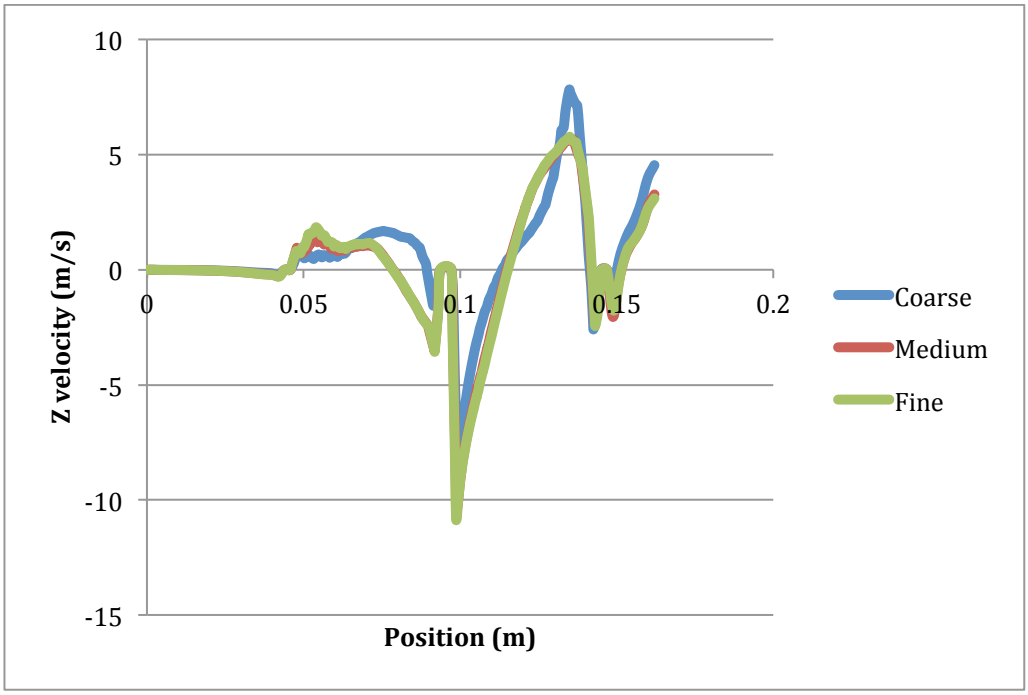

Fig. A. 3. Z velocity burner

- **FURNACE**

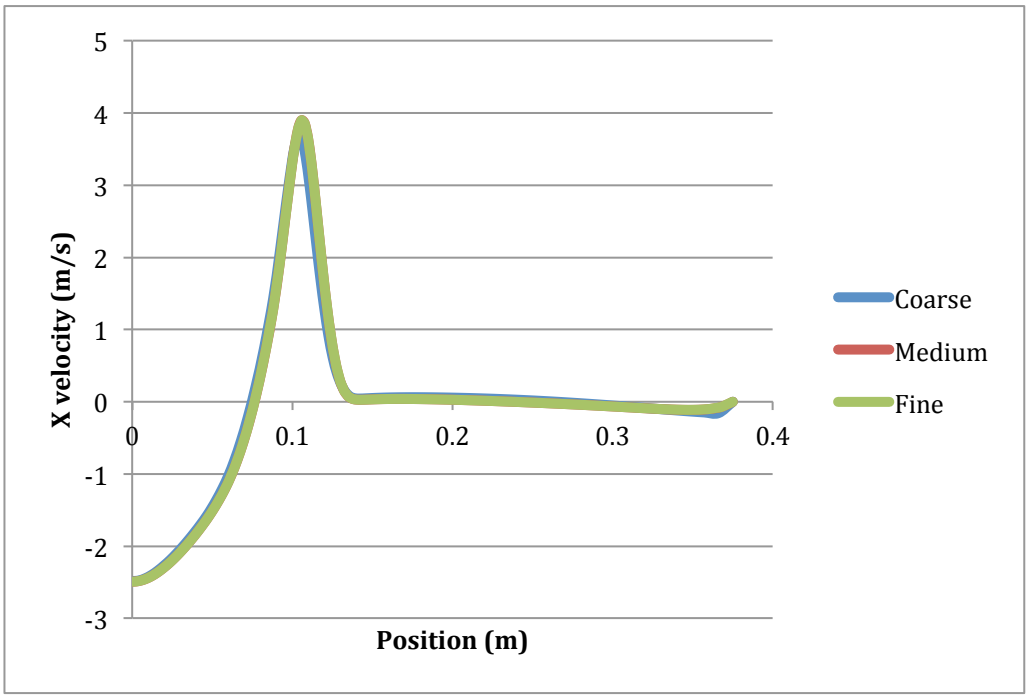

Fig. A. 4. X velocity furnace

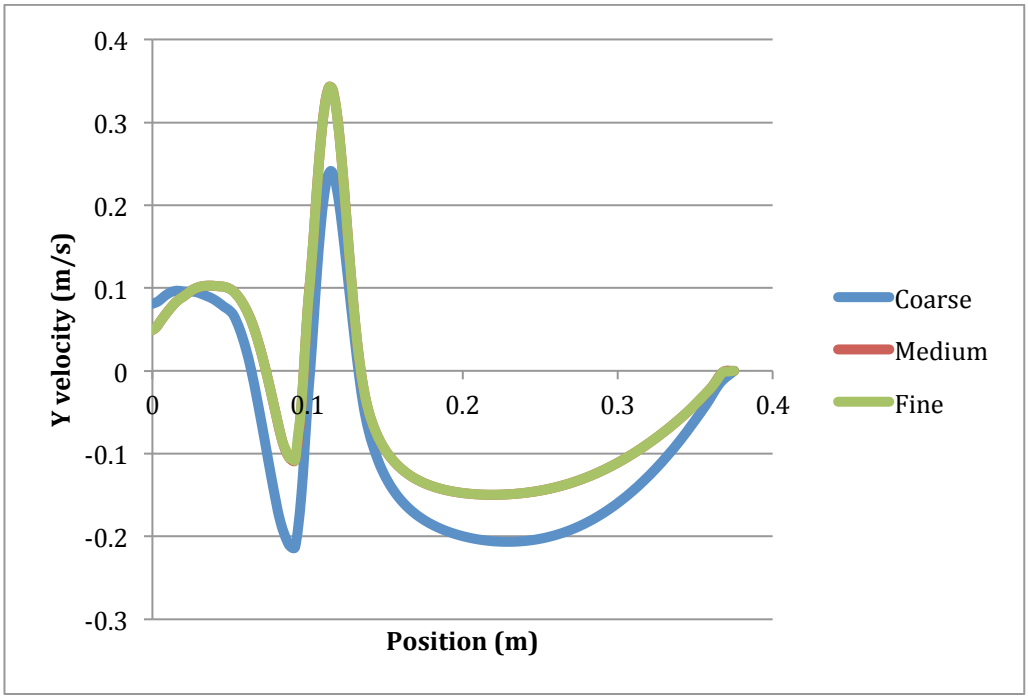

Fig. A. 5. Y velocity furnace

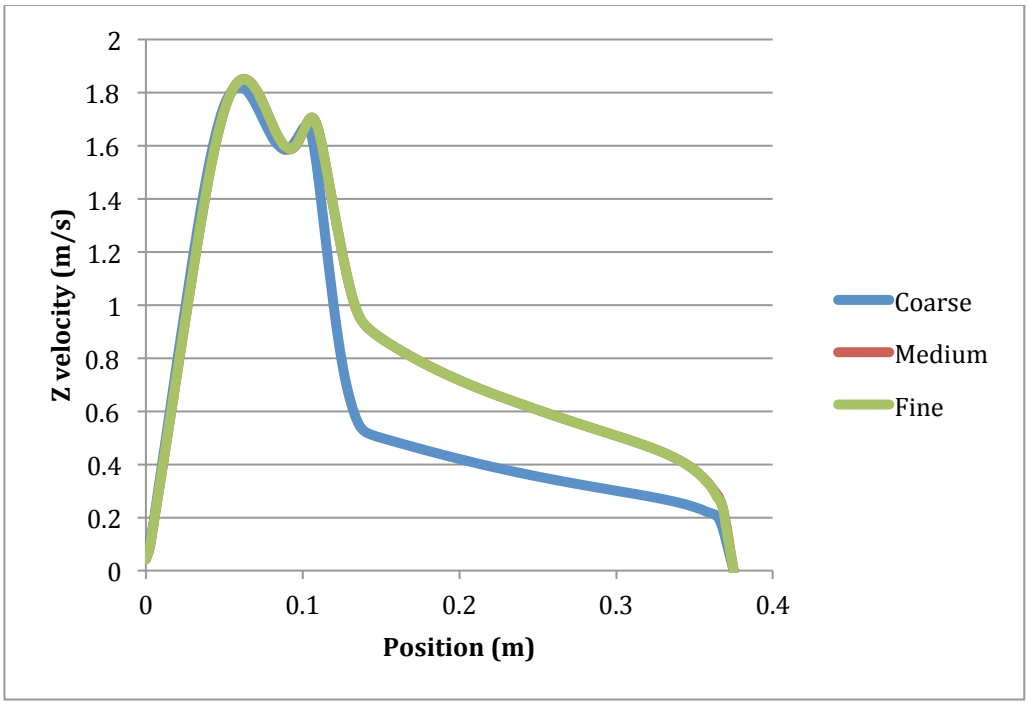

Fig. A. 6. Z velocity furnace

The graphs can show how the results obtained for the medium and fine grid are very similar to each other. In order to obtain an optimal result for the lowest computational cost, it is chosen to work in both cases with the medium grid.

Appendix B

Calculating composition species volatile

The composition of the volatile species, produced in the phase of devolatilizing, was obtained from the composition of the biomass supplied by the proximate and ultimate analysis reported in Table B.1.

Proximate Analysis	**Mass fraction (%dry)**
Volatiles	86.7
Fixed Carbon	7.3
Ash	5.9
Ultimate Analysis	**Mass fraction (%w/w, daf)**
Carbon	46.2
Hydrogen	5.9
Nitrogen	1.5
Sulfur	0.04
Oxygen	45.34
Chlorine	0.17
Potassium	0.85

Table B.1. Proximate and ultimate analysis

It has made the hypothesis of considering 100 gr. of volatile and has calculated the mass of H_2O, ash and volatile "dry ash free", which is considered already without ash and moiusture. The remaining part of fuel is representes by char, which is believed exclusively constituted by the carbon. The amount of C that does not constitute the char and the fraction of H, O, N, S, Cl and K are detected from the elementary analysis go to form the volatile species described by the empirical formula, $C_x H_y O_z S_j K_k N_w Cl_q$. They were calculated mass fractions of the individual elements by multiplying the dry ash free for the concentration given by proximate analysis, and for the carbon is subtracted char. The volatile species VM is modeled as a pure

substance, with thermodynamic properties equal to those of nitrogen and molecular weight equal to PM_{VM} = 30 kg/kmol; the mass fractions obtained are indicated in Table B.2.

Mass fraction (%)	
f_c	41.6
f_H	6.47
f_N	1.59
f_S	0.04
f_{Cl}	0.18
f_{O}	49.2
f_K	0.92

Table B.2. Mass fraction of the component of the volatile

To derive the formula of the volatile species in the form $C_xH_yO_zS_jK_kN_wCl_q$ must derive the mole fractions for each element:

$$x = \frac{n_C}{n_{tot}} = \frac{f_C}{PM_C}\, PM_{VM}; y = \frac{f_H}{PM_H}\, PM_{VM}; z = \frac{f_O}{PM_O}\, PM_{VM}; j = \frac{f_S}{PM_S}\, PM_{VM};$$

$$k = \frac{f_K}{PM_K}\, PM_{VM}; w = \frac{f_N}{PM_N} PM_{VM}; q = \frac{f_{Cl}}{PM_{Cl}}$$

From which is obtained:

$$\boldsymbol{VM = C_{1.04}H_{1.92}O_{0.92}S_{0.0004}K_{0.007}N_{0.034}Cl_{0.0015}}$$

Appendix C

RNA models

Tognotti – Falcitelli's approach

The full RNA provides four distinct phases (see Figure C.1):

a) The generation of data files needed to run the code PRONET from the output data of CFD Fluent through the use of UDF (User Defined Function) launched from the Fluent graphics;
b) The generation of the reactors network through the PRONET code;
c) The kinetic calculation performed with DESIBCO code;
d) The post processing of results through RNA2ASCII program.

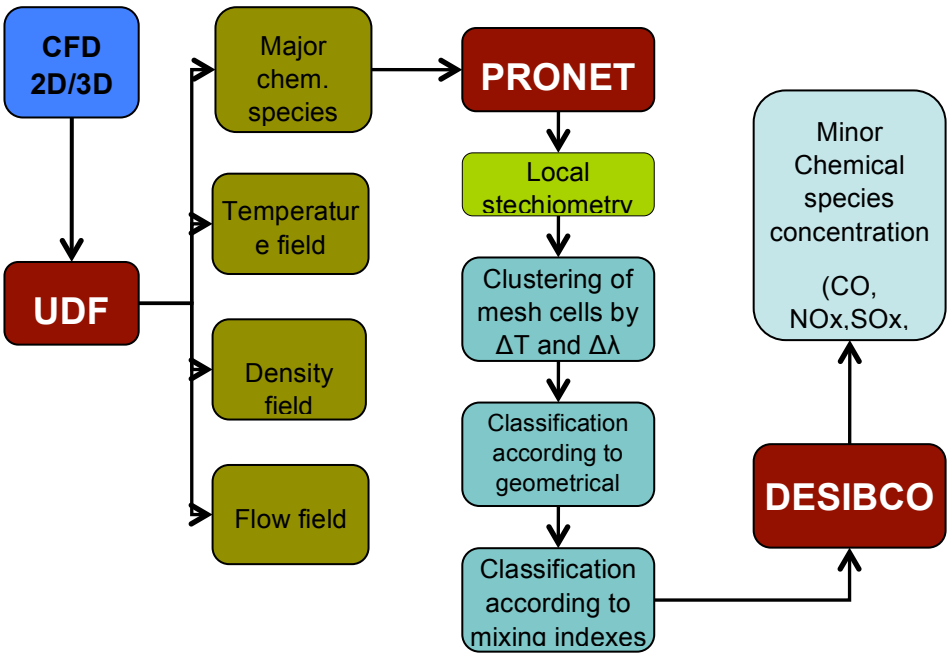

Fig. C.1. Logical flow of data and the chain operation for RNA codes

C.1 First step: UDF

The UDF is a program written in C language using the define macros provided by Fluent. It is compiled and run through the graphical interface once the CFD simulation performed. The task of this UDF is to recover the Fluent output that will be used to PRONET code (program that is used in the second phase). To bring coherence to all the programs that make up the RNA code, the user should choose a < name_case> that will identify the cases studied. This name will serve for identification of files and folder. After launching the UDF, must verify that the following files are generated and put them in a folder "CARNA/Job/<name_case>/Data":

- <name_case>.adi: contains for each face of each cell the numbers of the 2 cells that are adjacent;
- <name_case>. alles: mass fraction of all species in each cell;
- <name_case>.ch4, <name_case>.o2, <name_case>.co2, <name_case>.co, <name_case>.h2o, <name_case>.h2, <name_case>.oh, <name_case>.o, <name_case>.h, <name_case>. n2: for each species it contains the mass fraction at center of each species;
- <name_case>.flux : flows through all cells;
- <name_case>.geom : it contains the number of cells, following the face number and both coordinates of the center of the cell and of the faces;
- <name_case>.input_f2 : contains the value of the number of incoming or outgoing faces of domain;
- <name_case>.Numb_Of_Cells: contains the value of the number of cells that make up the grid;
- <name_case>.period : in the case of a geometry with periodicity conditions;
- <name_case>.ro : density at the center of each cells [kg/m3];
- <name_case>.specie : flow through the faces of each cell of the domain boundary;
- <name_case>.temp : temperature value [K] at the center of each grid cell;
- <name_case>.vol : volume of each cell [m3].

At this point, can proceed with the second phase, such as the PRONET code, to generate the network of reactors.

C.2 Second step: PRONET

When PRONET is launched, performs the following tasks (the user is no longer "active" until the end of calculation):

a) Read the input file (.inp);
b) Call the subroutine Stechio: this subroutine calculates, from the files of concentrations of the main chemical species, the stoichiometry in the center of each cell domain. These stoichiometries will be written in the file.ste;
c) Call the subroutine Clas_origin: in this subroutine it is proceed an inital classification of cells according to criteria of temperature and stoichiometry, that is, the cells are grouped into classes of which the temperature and stoichiometry belong to the same range; being imposed by the user, a maxium number of reactors (in the input file), is added a restriction as regards the number of cells present in each class, which must not exceed: num_max_cell. This value is calculated in this way:

$$num\_\max\ \_cell = \alpha \frac{N\_of\_cell}{NREA}$$

where α is a user selected parameter, N_of_cell the number of cells of the entire domain and NREA the number of reactors (α is read in the input file; N_of_cell is read in the file <name_case>.Numb_of_cells generated by UDF). The cells are grouped into classes defined by temperature ranges and stoichiometry as follows:

- For the temperature, we adopt a uniform spacing ΔT, calculated according to the number num_max_cell :

$$\Delta T = \frac{T_{max} - T_{min}}{nxx} \ \ where\ nxx = Int\left(1 + \sqrt{\frac{N\_of\_cell}{num\_\max\ \_cell}}\right)$$

- For the stoichiometry, the intervals are defined according to the relationships:

$$\begin{cases} \lambda_n = \lambda_{feeds} + n\Delta\lambda_s & for\ n\ \epsilon\ [\dots,-2,-1,0] \quad (\lambda_n \leq \lambda_{feeds}) \\ \lambda_n = \lambda_{feeds}\dfrac{1}{1 - n\Delta\lambda_d} & for\ n\ \epsilon\ [0,1,2,\dots] \quad (\lambda_n \geq \lambda_{feeds}) \end{cases}$$

$$\lambda_{feeds} = \frac{total\ air\ feed\ (\frac{kg}{s})}{air\ stoichiometric\ to\ the\ total\ fuel\ (\frac{kg}{s})}$$

$\Delta\lambda_s$ and $\Delta\lambda_d$ represent the range at left and right, respect to λ_{feeds} and are

calculated in function of num_max_cell.

In this way, the domain of stoichiometry is divided into two areas seperated by the stoichiometry value λ_{feeds} of the case study. For stoichiometries inferior to λ_{feeds}, it takes a subdivision of uniform intervals, while for higher values, it applies a scan proportional to the reciprocal of $\Delta\lambda_d$ with the aim of obtain the same degree of detail of the entire domain. A first classification is performed: if the number of cells in each class is less of num_max_class, we switch to another classification according to the connected volumes, otherwise, for each class make a new classification.

- If the class is in under stoichiometric area, it will be made a spacing uniform for both the temperature and stoichiometry.

- If the class is in up stoichiometric area, it will adopt a uniform spacing for the temperature, while for the stoichiometry, again, it will adopt a scan proportional to the reciprocal of $\Delta\lambda_d$.

This calculation is repeated until obtaining a classification where all classes contain a number of cells minor then num_max_celle .

d) Call the subroutine Connex: with this subroutine, any previously obtained class is in his turn divided into new classes according to a geometric criterion, that is, the adjacent cells are grouped, so that each new class represent a connex volume. At this point, the number of classes may be high. If this number of cells remains less than the number NREA imposed by the user, the classification is over. In case instead, it continues with a further classification by Reclas_glob subroutine.

e) Call the subroutine Calc_indmix that calculates a index of non – mixing:
It is defined an index of non – mixing Z_{TOT}

$$Z_{TOT} = \frac{1}{N}\sum_{i=1}^{N} Z_i$$

N is the number of the species present in considered zone and Z_i is the binary non–mixing index of the ith species, defined as:

$$Z_i = \frac{\overline{Y_i^2} - \overline{Y_i}^2}{\overline{Y_i}(1 - \overline{Y_i})}$$

where

$$\overline{Y_i} = \frac{\sum_j \rho_j V_j Y_{i,j}}{\sum_j \rho_j V_j} \qquad \overline{Y_i^2} = \frac{\sum_j \rho_j V_j Y^2{}_{i,j}}{\sum_j \rho_j V_j}$$

where ρ_j, V_j and $Y_{i,j}$ are the density, the volume and the mass fraction of the i-th species, relative to the j-th cell; the summation on index j includes all cells that belong to that zone. The index of not – mixing well defined expresses the state of mixing of a binary mixture: in the two limiting cases is 0 if the compounds have been perfectly mixed, and 1 if they are completely segregated, independently of the mixture. The state of mixing of a zone expressed by Z_{TOT} is the arithmetic average of the index of non – mixing calculated for each species. Once calculated this index of non – mixing for each species and for each class, we proceed to the last reclassification.

f) For this, is used the subroutine Reclas_Glob: the cells that belong to the classes in which the number is greater than NREA are redistributed. For each of these cells, called cells not classified, the subroutine are looking for classified cells that are adjacent with the subroutine celle_adiacenti. For each adjacent cell found, it looks at the number of class to which it belongs. Then calculates the variations of mixing index global would be if you put the cell in not classified class. For makes this, it used the subroutine Class_indmix_2. It considers the case in which the variation of the index is lower. Once assigned to the cell, it refresh the non – mixing index by the modified class and run it again the evaluation of the possible iterating assignments until all of the cells to be reclassified.

g) Call the subroutine Calc_Medstec: calculates the stoichiomety fields of reactors previously obtained.

h) Call the subroutine Calc_Temp_Reactors: calculates the temperature in each reactors according to the following relationship:

$$Temp_{reactor(i)}\%mean = \frac{\sum_k (cell(j)\%temp * cell(j)\%vol)}{Total\ volume\ of\ the\ reactor\ i}$$

$$Temp_{reactor(i)}\%sd =$$

$$= \left(\frac{\sum_k ((cell(j)\%temp)^2 * cell(j)\%vol)}{Total\ volume\ of\ reactor\ i} - (Temp_{reactror(i)}\%mean)^2 \right)^{1/2}$$

where k are the cells j that not belong to reactor i. The temperature in the reactor are calculated by the following relationship:

$$Temp_{reactor(i)} = Temp_{reactor(i)}\%mean + \left(Temp_{reactor(i)}\%sd * SD\right) + 0.15$$

where SD is a coefficient present in the input file.

i) The files that are written give values of stoichiometry, volume, etc. of each cell with an order that follows the classification of cells in Fluent.

j) Call the subroutine SCAMAS: this subroutine generates the input files needed for the DESIBCO code (third phase).

- Call the subroutine LEGGE. The task of this subroutine is to attribute to each cell of the domain, the number of the reactor to which it belongs. In addition, read the value of the flows in and out of the computational domain;
- Calculated via the CFD of mass flow rate, the exchange of material between all reactors and the feeding currents, summing the contributions of all the cells of boundary between the zones. In this way are considered all mass exchanges between reactors, including recycle;
- Writes the input files for DESIBCO program that performs the calculation on individual reactors:
    - DS#.RIC where # is the number of the reactor: in this file are set to each reactor, the currents coming from the other reactors, with information on the temperature, the flow rates and the chemical composition;
    - DS#.dat: contains the operating parameters of the reactor and any feeding current (air, fuel, recycling of fumes, etc.). They are also specifies the parameters of other ideals equipment (mixer and

splitter) used in the schematic of the exchanges of matter.

- DSName_case.RIC;
- Ricic4.inp

C.3 Third step: DESIBCO

To perform kinetic calculations, it throws the DESIBCO code (DEtailed SImulation Biphasic COmbustion). Before you begin, create a Name_case folder where you put the following files:

- The input file: Desibco_loop.inp;
- A file called Desibco.bat that contains the command string for launching the executable;
- A file called Mechanism.BIN that contains the kinetic and thermodynamic data for the mechanism of reactions;
- The four file that are generated from the PRONET code.

The DESIBCO code reads the operating parameters of the reactors, the dynamics of mass exchanges and chemical composition of the feeds from the input file and performs the calculation solving sequence each reactor network. The calculation proceeds by cycles: in a cycle are solved all reactors of the network, based on result updates the exchange currents and starts another cycle, repeating until convergence.

The number of cycles needed to reach convergence depends on the simulated event and the number of thereactors in the network. In output DESIBCO produces the following files:

- #loop: are the files that report for each reactor and for the overall system the composition of the system as well as the flow and temperature of the output current;
- DSName_case.TAU: each loop runs from the kinetic calculation module produced an input file (with a name equal to #loop) that specifies the current in output from each reactor and for the final flue gas stream composition and flow rate. At the end of the calculation, then, after solving all the loops required, the file written is DSName_case.TAU that lists the times of residence of reactors.

During execution also it is written a set of "service" files used by the program to speed up calculation: they are the files DS#.new and DSNome_caso.STR file. The type file DS#.new contains the composition, in terms of mass fraction, the current output from the reactor; it is used as a starting point of the solver for the next cycle. The file DSNome_caso.STR is incremented every time that a reactor is resolved, it allows the reboot of the calculation in the event of accidental interruption.

C.4 Fourth step: RNA2Ascii

In CARNA/Job/<Name_case>/Data folder, check the following files:

- The file of reactor r#.dat (generated by PRONET)

Add the following files:

- The last file #loop generated by DESIBCO;
- A file.bat that contains a command string for launcher the executable;
- An ASCII folder where will put the generated files, the species concentrations file;
- The input file for the RNA2ASII.inp.

Will be generated in CARNA Folder /Job/<Name_case>/Data/Ascii files called name_specie.dat represents the mass fractions of the relevant species in the input file.

Appendix D

Kinetic mechanism

The input file for the kinetic mechanism written in CHEMKIN format.

```
ELEMENTS
H O S NA K CL C N
SPECIES
SO2 O SO3 OH H HOSO2 O2 SO HO2 NA NAO NAOH NAO2 H2O2 H2O H2 CO CO2
NAOHNAOH CL NACL HCL CL2 CLO NACLNACL NASO2 NASO3 NA2SO4 NAHSO4
NASO3CL K KO KOH KO2 KOHKOH KCL KCLKCL KSO2 KSO3 KHSO4 K2SO4
KSO3CL N2
END
REACTIONS
SO2+O(+M)=SO3(+M) 3.7E+11 0.0 1690
LOW/ 2.4E+27 -3.6 5186/
TROE/ 0.442 316 7442/
N2/ 1.3/H2O/ 10.00/SO2/ 10.00/
SO2+OH=SO3+H 4.9E+02 2.69 23844
SO2+OH(+M)=HOSO2(+M) 7.2E+12 0.0 715
LOW/ 4.5E+25 -3.3 715/
TROE/ 0.7 1E-30 1E+30/
N2/ 1.5/H2O/ 10.00/SO2/ 10.00/
SO3+O=SO2+O2 1.3E+12 0.0 6100
SO3+SO=SO2+SO2 7.6E+03 2.37 2980
HOSO2+O2=SO3+HO2 7.8E+11 0.0 656
NA+O+M=NAO+M 1.5E+21 -1.5 0.0
NA+OH+M=NAOH+M 5.4E+21 -1.65 0.0
NA+HO2=NAOH+O 1E+14 0.0 0.0
NA+HO2=NAO+OH 3E+13 0.0 0.0
NA+O2(+M)=NAO2(+M) 3.6E+14 0.0 0.0
LOW/ 6.6E+21 -1.52 0.0/
NA+H2O2=NAOH+OH 2.5E+13 0.0 0.0
NA+H2O2=NAO+H2O 1.6E+13 0.0 0.0
NAO+H=NA+OH 2E+14 0.0 0.0
NAO+O=NA+O2 2.6E+14 0.0 0.0
NAO+OH=NAOH+O 2E+13 0.0 0.0
NAO+HO2=NAOH+O2 5E+13 0.0 0.0
NAO+HO2=NAO2+OH 5E+13 0.0 0.0
NAO+H2=NAOH+H 1.6E+13 0.0 0.0
NAO+H2=NA+H2O 3.1E+12 0.0 0.0
NAO+H2O=NAOH+OH 1.3E+14 0.0 0.0
NAO+CO=NA+CO2 1.3E+14 0.0 0.0
NAOH+H=NA+H2O 5E+13 0.0 0.0
```

NAOH+NAOH=NAOHNAOH 8E+13 0.0 0.0
NAO2+H=NA+HO2 2E+14 0.0 0.0
NAO2+H=NAO+OH 5E+13 0.0 0.0
NAO2+H=NAOH+O 1E+14 0.0 0.0
NAO2+O=NAO+O2 1.3E+13 0.0 0.0
NAO2+OH=NAOH+O2 2E+13 0.0 0.0
NAO2+CO=NAO+CO2 1E+14 0.0 0.0
NA+CL+M=NACL+M 1.1E+20 -1.00 0.0
NA+HCL=NACL+H 1.3E+15 0.0 9995
NA+CL2=NACL+CL 4.4E+14 0.0 0.0
NA+CLO=NACL+O 1E+14 0.0 0.0
NAO+HCL=NACL+OH 1.7E+14 0.0 0.0
NAOH+HCL=NACL+H2O 1.7E+14 0.0 0.0
NAO2+CL=NACL+O2 1E+14 0.0 0.0
NAO2+HCL=NACL+HO2 1.4E+14 0.0 0.0
NACL+NACL=NACLNACL 8E+13 0.0 0.0
NA+SO2(+M)=NASO2(+M) 1.2E+14 0.0 0.0
LOW/ 2E+23 -1.5 0.0/
NA+SO3(+M)=NASO3(+M) 1.2E+14 0.0 0.0
LOW/ 1.4E+35 -5.2 0.0/
NA+SO3=NAO+SO2 1E+14 0.0 20009
NAO+SO2(+M)=NASO3(+M) 1E+14 0.0 0.0
LOW/ 2E+23 -1.5 0.0/
NAOH+SO3(+M)=NAHSO4(+M) 1E+14 0.0 0.0
LOW/ 2.6E+42 -7.6 0.0/
NASO2+O=NAO+SO2 1.3E+13 0.0 0.0
NASO2+OH=NAOH+SO2 2E+13 0.0 0.0
NASO2+NAO2=NA2SO4 1E+14 0.0 0.0
NASO3+O=NAO+SO3 1.3E+13 0.0 0.0
NASO3+OH=NAOH+SO3 2E+13 0.0 0.0
NASO3+NAO=NA2SO4 1E+14 0.0 0.0
NAHSO4+NAOH=NA2SO4+H2O 1E+14 0.0 0.0
NAHSO4+NACL=NA2SO4+HCL 1E+14 0.0 0.0
NACL+SO3(+M)=NASO3CL(+M) 1E+14 0.0 0.0
LOW/ 1.9E+41 -7.8 0.0/
NASO3CL+OH=NAHSO4+CL 1E+14 0.0 0.0
NASO3CL+H2O=NAHSO4+HCL 1E+14 0.0 0.0
NASO3CL+NAOH=NA2SO4+HCL 1E+14 0.0 0.0
K+O+M=KO+M 1.5E+21 -1.50 0.0
K+OH+M=KOH+M 5.4E+21 -1.55 0.0
K+HO2=KOH+O 1E+14 0.0 0.0
K+HO2=KO+OH 3E+13 0.0 0.0
K+O2(+M)=KO2(+M) 3.6E+14 0.0 0.0
LOW/ 5.4E+21 -1.32 0.0/
K+H2O2=KOH+OH 2.5E+13 0.0 0.0
K+H2O2=KO+H2O 1.6E+13 0.0 0.0
KO+H=K+OH 2E+14 0.0 0.0
KO+O=K+O2 2.2E+14 0.0 0.0
KO+OH=KOH+O 2E+13 0.0 0.0
KO+HO2=KOH+O2 5E+13 0.0 0.0
KO+H2=KOH+H 1.6E+13 0.0 0.0
KO+H2=K+H2O 3.1E+12 0.0 0.0

```
KO+H2O=KOH+OH  1.3E+14  0.0  0.0
KO+CO=K+CO2  1E+14  0.0  0.0
KOH+H=K+H2O  5E+13  0.0  0.0
KOH+KOH=KOHKOH  8E+13  0.0  0.0
KO2+H=K+HO2  2E+14  0.0  0.0
KO2+H=KO+OH  5E+13  0.0  0.0
KO2+H=KOH+O  1E+14  0.0  0.0
KO2+O=KO+O2  1.3E+13  0.0  0.0
KO2+OH=KOH+O2  2E+13  0.0  0.0
KO2+CO=KO+CO2  1E+14  0.0  0.0
K+CL+M=KCL+M  1.8E+20  -1.00  0.0
K+HCL=KCL+H  9.1E+12  0.0  1180
K+CL2=KCL+CL  4.4E+14  0.0  0.0
K+CLO=KCL+O  1E+14  0.0  0.0
KO+HCL=KCL+OH  1.7E+14  0.0  0.0
KOH+HCL=KCL+H2O  1.7E+14  0.0 0.0
KO2+CL=KCL+O2  1E+14  0.0  0.0
KO2+HCL=KCL+HO2  1.4E+14  0.0  0.0
KCL+KCL=KCLKCL  8E+13  0.0  0.0
K+SO2(+M)=KSO2(+M)  3.7E+14  0.0  0.0
LOW/ 5.2E+23  -1.5  0.0/
K+SO3(+M)=KSO3(+M)  3.7E+14  0.0  0.0
LOW/ 4.7E+34  -4.9  0.0/
K+SO3=KO+SO2  1E+14  0.0  15578
KO+SO2(+M)=KSO3(+M)  3.7E+14  0.0  0.0
LOW/ 5.2E+23  -1.5  0.0/
KOH+SO3(+M)=KHSO4(+M)  1E+14  0.0  0.0
LOW/ 2.6E+42  -7.6  0.0/
KSO2+O=KO+SO2  1.3E+13  0.0  0.0
KSO2+OH=KOH+SO2  2E+13  0.0  0.0
KSO2+KO2=K2SO4  1E+14  0.0  0.0
KSO3+O=KO+SO3  1.3E+13  0.0  0.0
KSO3+OH=KOH+SO3  2E+13  0.0  0.0
KSO3+KO=K2SO4  1E+14  0.0  0.0
KHSO4+KOH=K2SO4+H2O  1E+14  0.0  0.0
KHSO4+KCL=K2SO4+HCL  1E+14  0.0  0.0
KCL+SO3(+M)=KSO3CL(+M)  1E+14  0.0  0.0
LOW/ 1.9E+41  -7.8  0.0/
KSO3CL+OH=KHSO4+CL  1E+14  0.0  0.0
KSO3CL+H2O=KHSO4+HCL  1E+14  0.0  0.0
KSO3CL+KOH=K2SO4+HCL  1E+14  0.0  0.0
END
```

Appendix E

Thermodynamic data

The thermodynamic data must be implemented in accordance with the NASA format. Especially the thermodynamic data for inorganic species are difficult to find in the usual sources of thermodynamic data, such as GRI Mech 3.0, Creck modeling (POLIMI), etc. In the following is shown the thermodynamic data only for the species that take part in the Glaborg's mechanism.

HOSO2 BOZ/R H 1O 3S 1 0G 300.000 1500.000 1500.00 0 1
0.24358474E+01 0.29991941E-01-0.40650871E-04 0.26047603E-07-0.62778546E-11 2
-0.48803251E+05 0.14364072E+02 0.24358474E+01 0.29991941E-01-0.40650871E-04 3
0.26047603E-07-0.62778546E-11-0.48803251E+05 0.14364072E+02 4
NA 120186NA 1 G 0300.00 2000.00 1000.00 1
2.50045944E+00 0.00000000E+00 0.00000000E+00 0.00000000E+00 0.00000000E+00 2
1.21608049E+04 4.24153840E+00 2.50045944E+00 0.00000000E+00 0.00000000E+00 3
0.00000000E+00 0.00000000E+00 1.21608049E+04 4.24153840E+00 4
NACL CL 1NA 1 G 0300.00 2000.00 1000.00 1
4.39000000E+00 2.15000000E-04-6.20000000E-08 1.27000000E-11-9.43000000E-16 2
-2.32000000E+04 2.49000000E+00 3.95000000E+00 1.51000000E-03-9.82000000E-07 3
-2.81000000E-10 3.54000000E-13-2.31000000E+04 4.70000000E+00 4
NACLNACL CL 2NA 2 G 0300.00 2000.00 1000.00 1
9.61932000E+00 7.13000000E-04-5.55000000E-07 2.02000000E-10-2.84000000E-14 2
-7.10000000E+04-1.59000000E+01 7.55092000E+00 1.13400000E-02-2.12677000E-05 3
1.81709000E-08-5.84479000E-12-7.06891324E+04-6.46325258E+00 4
NAHSO4 O 4NA 1S 1H 1G 0300.00 2000.00 1000.00 1
1.06477900E+01 1.18400000E-02-7.05000000E-06 1.57000000E-09 9.77000000E-17 2
-1.13000000E+05-2.32000000E+01 1.16762000E+00 5.45500000E-02-8.11003000E-05 3
5.98391000E-08-1.74599000E-11-1.11113208E+05 2.09161310E+01 4
NAO 40992 O 1NA 1 G 0300.00 2000.00 1000.00 1
0.04349803E+02 2.84996000E-04-8.61599000E-08 1.75400000E-11-1.30168000E-15 2
8.73169400E+03 2.61833900E+00 3.76572700E+00 1.98003000E-03-1.25630000E-06 3

-3.90980000E-10 4.66404000E-13 8.86688900E+03 5.56227300E+00 4

NAOH O 1NA 1H 1 G 0300.00 2000.00 1000.00 1
5.53000000E+00 1.42000000E-03-4.44000000E-07 6.64000000E-11-3.87000000E-15 2
-2.55000000E+04-4.37000000E+00 4.72789500E+00 5.00126200E-03-4.53439000E-06 3
7.05124000E-10 6.67112000E-13-2.53794600E+04-0.76496780E+00 4
NAOHNAOH O 2NA 2H 2 G 0300.00 2000.00 1000.00 1
1.19076700E+01 3.15000000E-03-1.31000000E-06 2.90000000E-10 3.38000000E-16 2
-7.87000000E+04-3.15000000E+01 3.64353000E+00 4.75300000E-02-9.01035000E-05 3
7.85248000E-08-2.55796000E-11-7.75982956E+04 5.69950184E+00 4
NAO2 O 2NA 1 G 0300.00 2000.00 1000.00 1
5.51890000E+00 2.45000000E-03-1.53000000E-06 3.40000000E-10 3.55000000E-17 2
-7.27000000E+03-1.14000000E+00 3.45877000E+00 1.16200000E-02-1.72532000E-05 3
1.25770000E-08-3.63295000E-12-6.95039548E+03 8.46645355E+00 4
NASO2 O 2NA 1S 1 G 0300.00 2000.00 1000.00 1
7.52066000E+00 4.10000000E-03-2.56013000E-06 5.69867000E-10-2.92255000E-16 2
-4.83122572E+04-8.45267975E+00 3.14784000E+00 2.37500000E-02-3.65502000E-05 3
2.72923000E-08-8.01329000E-12-4.76307411E+04 1.18932857E+01 4
NASO3 O 3NA 1S 1 G 0300.00 2000.00 1000.00 1
8.68507000E+00 7.18000000E-03-4.50508000E-06 9.99885000E-10 4.43275000E-16 2
-6.76153997E+04-1.30951498E+01 2.02833000E+00 3.71700000E-02-5.61900000E-05 3
4.12949000E-08-1.19401000E-11-6.65811888E+04 1.78550382E+01 4
NASO3CL O 3NA 1S 1CL 1G 0300.00 2000.00 1000.00 1
1.07694290E+01 8.56000000E-03-5.33000000E-06 1.18000000E-09 2.53000000E-16 2
-9.28732688E+04-2.19150912E+01 3.43508000E+00 4.11300000E-02-6.09631000E-05 3
4.43474000E-08-1.27780000E-11-9.17248158E+04 1.22269404E+01 4
NA2SO4 O 4NA 2S 1 G 0300.00 2000.00 1000.00 1
1.51000000E+01 4.51000000E-03-2.01000000E-06 3.96000000E-10-2.87000000E-14 2
-1.30000000E+05-4.68000000E+01 5.75000000E+00 2.96000000E-02-2.04000000E-05 3
-1.07000000E-09 3.96000000E-12-1.27000000E+05 1.02000000E+00 4
K 120186K 1 G 0300.00 2000.00 1000.00 1
2.50045944E+00 0.00000000E+00 0.00000000E+00 0.00000000E+00 0.00000000E+00 2
9.95969830E+03 5.03538011E+00 2.50045944E+00 0.00000000E+00 0.00000000E+00 3
0.00000000E+00 0.00000000E+00 9.95969830E+04 5.03538011E+00 4
KCL CL 1K 1 G 0300.00 2000.00 1000.00 1

4.43000000E+00 1.73000000E-04-3.87000000E-08 7.94000000E-12-5.93000000E-16 2
-2.72000000E+04 3.40000000E+00 4.15000000E+00 1.04000000E-03-7.03000000E-07 3
-1.20000000E-10 2.11000000E-13-2.71000000E+04 4.83000000E+00 4
KCLKCL CL 2K 2 G 0300.00 2000.00 1000.00 1
9.79587000E+00 3.95000000E-04-3.16000000E-07 1.18000000E-10-1.68000000E-14 2
-7.72000000E+04-1.35000000E+01 8.65608000E+00 6.34000000E-03-1.20249000E-05 3
1.03545000E-08-3.34977000E-12-7.70581260E+04-8.30814644E+00 4
KHSO4 O 4K 1S 1H 1G 0300.00 2000.00 1000.00 1
1.03145400E+01 1.26000000E-02-7.61000000E-06 1.69000000E-09-7.25000000E-16 2
-1.17000000E+05-2.00000000E+01 2.16906000E+00 4.89100000E-02-6.86688000E-05 3
4.76840000E-08-1.30789000E-11-1.15987957E+05 1.79276447E+01 4
KO 40992 O 1K 1 G 0300.00 2000.00 1000.00 1
4.40000000E+00 2.39000000E-04-5.88000000E-08 1.21000000E-11-9.01000000E-16 2
7.22000000E+03 3.43000000E+00 3.99000000E+00 1.47000000E-03-9.48000000E-07 3
-2.42000000E-10 3.26000000E-13 7.31000000E+03 5.52000000E+00 4
KOH O 1K 1H 1 G 0300.00 2000.00 1000.00 1
6.58397000E+00-1.30000000E-03 2.16358000E-06-1.02000000E-09 1.64000000E-13 2
-2.94653465E+04-8.54695580E+00 3.50118000E+00 1.39100000E-02-2.67378000E-05 3
2.37079000E-08-7.79416000E-12-2.90121035E+04 5.56421343E+00 4
KOHKOH O 2K 2H 2 G 0300.00 2000.00 1000.00 1
1.25375400E+01 2.22000000E-03-7.77000000E-07 1.78000000E-10-1.70000000E-15 2
-8.09000000E+04-3.08000000E+01 7.79516000E+00 2.91600000E-02-5.60277000E-05 3
4.92386000E-08-1.60221000E-11-8.03119031E+04-9.77076321E+00 4
KO2 O 2K 1 G 0300.00 2000.00 1000.00 1
5.58360000E+00 2.33000000E-03-1.45068000E-06 3.22571000E-10-5.28409000E-17 2
-9.81000000E+03-0.12408342E+00 3.98796000E+00 9.16000000E-03-1.27384000E-05 3
8.84546000E-09-2.47133000E-12-9.55774023E+03 7.36197430E+00 4
KSO2 O 2K 1S 1 G 0300.00 2000.00 1000.00 1
7.63052000E+00 3.92000000E-03-2.45000000E-06 5.45000000E-10 4.00000000E-17 2
-5.05000000E+04-7.54000000E+00 3.80783000E+00 2.09500000E-02-3.17157000E-05 3
2.34331000E-08-6.83749000E-12-4.98676218E+04 1.02761844E+01 4
KSO3 O 3K 1S 1 G 0300.00 2000.00 1000.00 1
8.64109000E+00 7.31000000E-03-4.60000000E-06 1.02000000E-09-8.12000000E-16 2
-7.07000000E+04-1.15000000E+01 2.62681000E+00 3.43600000E-02-5.08823000E-05 3
3.66819000E-08-1.04124000E-11-6.97523799E+04 1.65039891E+01 4

KSO3CL O 3K 1S 1CL 1G 0300.00 2000.00 1000.00 1
1.10301800E+01 8.03000000E-03-4.97607000E-06 1.10637000E-09-1.44826000E-16 2
-9.84538848E+04-2.15769265E+01 4.81342000E+00 3.50700000E-02-5.06592999E-05 3
3.65317000E-08-1.05704000E-11-9.74638146E+04 7.51938459E+00 4
K2SO4 O 4K 2S 1 G 0300.00 2000.00 1000.00 1
1.24896200E+01 1.15100000E-02-8.64804000E-06 3.06756000E-09-4.21608000E-13 2
-1.35859843E+05-2.86169360E+01 4.63832000E+00 4.03500000E-02-4.71493000E-05 3
2.46761000E-08-4.50735000E-12-1.34401764E+05 9.04530899E+00 4

When import the CHEMKIN file into Fluent, it is unable to import the molecular weights of the inorganic species, so all the correlations for calculations of the specific heat, entalphy and entropy are wrong because the NASA format provides the correlations in mole and then Fluent converted in kg. For the entalpy and entropy is easy because are constant. For the specific heat the correlations are in piecewise-polynomial. The piecewise-polynomial function is on temperature.

$$\text{For } T_{min,1} < T < T_{max,1} : \phi(T) = A_1 + A_2 T + A_3 T^2 + \cdots$$

$$\text{For } T_{min,2} < T < T_{max,2} : \phi(T) = B_1 + B_2 T + B_3 T^2 + \cdots$$

In the equations above, ϕ is the property.

The all the coefficients were calculated and entered manually in the Fluent code.

Appendix F

NGDE input

Input file for a K_2SO_4 aerosol:
Number of nodes: 41
Starting Temperature(Kelvin): 953
Cooling Rate(Kelvin/s):253
Pressure(Atm): 1
Molecular Weight(Kg/mol): 0.1742602
Density(Kg/m3): 2660
Surface Tension in the form A-BT(dyne/cm): A=655.7 B=0.2942
Saturation Vapor Pressure of material in form Ps=exp(C-D/T)P: C=11.00314 D=23716.71102
Enter your choice - 1)Coagulation,2)nucleation+coagulation,3)nucleation + coagulation + surface growth,4)surface growth:3
Choice of collision frequency function:1)Free Molecular Regime,2)Fuchs form for free molecular and transition regime:2
Sutherland's constants for carrier gas in the form A*T^1.5/(B+T): A=1.966e-6 B=147.47
If you choose to run either "coagulation" or "surface growth" problem, you must modify the input files "coag.inp" or "grow.inp" as required.

Input file for a KCl aerosol:
Number of nodes: 41
Starting Temperature(Kelvin): 880
Cooling Rate(Kelvin/s):253
Pressure(Atm): 1
Molecular Weight(Kg/mol): 0.074551
Density(Kg/m3): 1980
Surface Tension in the form A-BT(dyne/cm): A=298.7 B=0.1367
Saturation Vapor Pressure of material in form Ps=exp(C-D/T)P: C=19.59699 D=27523.71102
Enter your choice - 1)Coagulation,2)nucleation+coagulation,3)nucleation + coagulation + surface growth,4)surface growth:3
Choice of collision frequency function:1)Free Molecular Regime,2)Fuchs form for free molecular and transition regime:2
Sutherland's constants for carrier gas in the form A*T^1.5/(B+T): A=1.966e-6 B=147.47
If you choose to run either "coagulation" or "surface growth" problem, you must modify the input files "coag.inp" or "grow.inp" as required.

References

[1] L. Biasci, G.Coraggio, M. Faleni, Report operativo Aerosol, ENEL 2011

[2] E. Castellani, M. Falcitelli, L. Tognotti, Simulazione e misura dell'aerosol inorganico dalla combustione di carbone e biomassa, CPR 2007

[3] M. Falcitelli, Supporto alla sperimentazione su scala pilota per la produzione e misura dell'aerosol inorganico dalla combustione mista di biomasse, carbone, CPR 2012

[4] M. Falcitelli, Supporto alla sperimentazione su scala pilota per la produzione e misura dell'aerosol inorganico dalla combustione mista di biomasse, carbone. Appemdice, CPR 2012

[5] DEKATI Ltd. (2011), ELPI User Manual ver. 1.12

[6] T. Faravelli, E. Ranzi, A. Frassoldati, T. Maffei, Modellazione della volatilizzazione e ossidazione di carbone del Sulcis, ENEA 2010

[7] M. Faleni, 500 kWth Furnace Characteristics and operaton, IFRF 2012

[8] G. Bonvicini, L. Biasci, G. Coraggio, M. Faleni, M. Landi, Coal – biomass blends combustion characterization in a 500 kW_t furnace, IFRF 2013

[9] L. Biasci, G. Coraggio, M. Faleni, M. Landi, V. Colucci, Caratterizzazione blends carbone – biomassa, IFRF 2012

[10] Collins Ndibe, Simon Grathwohl, Manoj Paneru, Jörg Maier, Günter Scheffknecht, Emissions reduction and deposits characteristics during cofiring of high shares of torrefied biomass in a 500 kW pulverized coal furnace, IFK 2015

[11] E. Ranzi, A. Cuoci, T. Faravelli, A. Frassoldati, G. Migliavacca, S. Pierucci, S. Sommariva, Chemical Kinetics of Biomass Pyrolysis, Energy and Fuels 2008

[12] Bonnie J. McBride, Sanford Gordon, Martin A. Reno, Coefficients for calculating thermodynamic and transport properties of individual species, NASA 2000

[13] P. Glaborg, P. Marshall, Mechanism and modeling of the formation of gaseous alkali sulfates, Combustion and flame 2004

[14] Sam Ghazi-Hesami, Cost effective emissions and minor species predictions via coupling of computational Fluid dynamics and chemical reactor network analysis, Concordia univesrity 2009

[15] L. Goldsworthy, Reduced kinetics scheme for oxides of nitrogen emissions from a slow-speed marine diesel engine, Australian maritime college 2002

[16] P. Kilpinen, P. Glaborg, M. Hupa, Reburning chemistry: a Kinetic modeling study, University of Denmark 1992

[17] L. Tognotti, M. Falcitelli, CFD + reactor network analysis: An integrated methodology for the modeling and optimisation of industrial systems for energy saving and pollution reduction, Applied Thermal Engineering 2002

[18] P. E. Amaral Debiagi, C. Pecchi, G. Gentile, A. Frassoldati, A. Cuoci, T. Faravelli, E. Ranzi, Extractives extend the applicability of multistep kinetic scheme of biomass pyrolysis, Energy fuels 2015

[19] E. Ranzi, A. Cuoci, T. Faravelli, A. Frassoldati, G. Migliavacca, S. Pierucci, S. Sommariva, Chemical kinetics of biomass pyrolysis, energy and fuels 2008

[20] M. Falcitelli, L. Tognotti, E. Castellani, A study of alkali aerosol formation in biomass-coal co-combustion with a mechanism approach, 10th conference on energy for a clean environment 2009

[21] M. Corsi, M. Falcitelli, C. La Marca, S. Malloggi, N. Rossi, L. Tognotti, Developments of an integrated kinetic based modeling approach to alkali-salt formation and deposition in PF boilers

[22] M. U. Garba, D. B. Ingham, L. Ma, R. T. J. Porter, M. Pourkashnian, H. Z. Tan, A. Williams, Prediction of potassium chloride sulfation and its effect on deposition in biomass fired boilers, Energy and fuels 2012

[23] A. Prakash, A. P. Bapat, M. R. Zachariah, A simple numerical algorithm and software for solution of nucleation, surface growth and coagulation problems, Aerosol science and technology 2003

[24] K. A. Christensen, H. Livbjerg, A field study of submicron particles from the combustion of straw, Aerosol science and technology 2007

[25] S. Jiménez, J. Ballester, A comparative study of different methods for the sampling of high temperature combustion aerosols, Aerosol science and Technology 2007

[26] M. Falcitelli, S. Pasini, N.Rossi, L. Tognotti, CFD + reactor network analysis: an integrated methodology for the modeling and optimisation of industrial systems for energy saving and pollution reduction, Applied thermal engineering 2002

[27] C. M. Campelli, A. Stagni, T. Faravelli, A. Cuoci, A. Barresi, Metodi numerici di calcolo parallelo per la soluzione di reti di reattori, POLIMI 2011

[28] E. Biagini, L. Tognotti, Fusina power plant – evaluation of alkali deposition in RDF/coal cofiring, CPR 2012

[29] C. Leroy, M. Falcitelli, L. Tognotti, Codice RNA: versione 1.0 per Fluent, Manuale di uso, CPR 2009

[30] S. Carbone, M. Falcitelli, L. Tognotti, Sviluppo dell'interfaccia tra il codice RNA e il codice CFD Fluent, CPR 2007

[31] C. Leroy, A. Modesti, M. Falcitelli, A. Parente, L. Tognotti, Sviluppo della versione di RNA per il post.processing degli output Fluent, CPR 2009

[32] M. Falcitelli, S. Pellegrini, Parallelizzazione del codice RNA su macchina a multiprocessore, CPR 2007

[33] http://www.grc.nasa.gov/WWW/CEAWeb/ceaThermoBuild.htm,Thermodynamic data avaible online

[34] R. J. Kee, F. M. Rupley, J. A. Miller, M. E. Coltrin, J. F. Grcar, E. Meeks, H. K. Moffat, A. E. Lutz, G. Dixon-Lewis, M. D. Smooke, J. Warnatz, G. H. Evans, R. S. Larson, R. E. Mitchell, L. R. Petzold, W. C. Reynolds, M. Caracotsios, W. E. Stewart, P. Glarborg, C. Wang, and O. Adigun, CHEMKIN Collection, Release 3.6, Reaction Design 2000

[35] http://gpt.unizar.es/sites/default/files/sox.txt, Thermodynamic data for $HOSO_2$

[36] L. Sorrentino, Cattura della CO_2 nella produzione elettrica: analisi sperimentale e modellistica di combustione con ossigeno, tesi di laurea 2008

[37] L. Giovannini, Validazione di modelli fluidodinamici di sistemi operanti in condizioni di ossicombustione

[38] M. Falcitelli, S. Pasini, L. Tognotti, An algorithm for extracting chemical reactor network models from CFD simulation of industrial combustion systems, ENEL 2002

[39] M. Falcitelli, C. Leroy, Methods of reactor network analysis for combustion chambers simulated with CFD codes, ENEL CPR 2011

[40] M. Landi, L. Tognotti, G. Coraggio, Impianti di ricerca per la combustione del carbone e componentistica per analisi in camera di combustione, IFRF

[41] M. Kanniche, Coupling CFD with chemical reactor network for advanced NO_x prediction in gas turbine, 2010

[42] M. Mancini, Analysis of mild combustion of natural gas with preheated air, Clausthal University of Technology 2006

[43] M. Falcitelli, N. Rossi, L. Tognotti, RNA modeling for the optimisation of industrial combustion devices, IFRF 2007

[44] G. Perry, Perry's chemical engineers handbook, 1999

[45] Fluent User Guide

[46] Fluent Theory Guide

[47] Ansys online support

Ringraziamenti

Desidero ringraziare innanzitutto il Prof. Leonardo Tognotti per avermi dato l'opportunità di svolgere il tirocinio di tesi, per la preziosa supervisione durante le varie fasi del lavoro e per avermi dato sempre i consigli giusti al momento giusto.

Un doveroso ringraziamento va alla Dott.ssa Chiara Galletti per non avermi mai fatto mancare la sua guida, il suo supporto in ogni step e la pazienza dedicatemi durante il mio lavoro di tesi, anche quando la situazione sembrava disperata. Un grazie per essere stata sempre disponibile a risolvere ogni più piccolo problema e per avermi trasmesso almeno una piccola parte della sua conoscenza. Grazie per avermi aperto gli occhi sull'affascinante mondo della ricerca e della Fluidodinamica Computazionale, sperando che sia solo l'inizio di un percorso insieme.

Grazie ad una persona senza la quale oggi non indosserei una corona d'alloro, Ludovica. Il primo giorno del nostro primo anno di università ci siamo incontrate e da quel giorno mai più separate. Grazie per tutti i buoni consigli di cui ho fatto tesoro, per avermi consolato nei momenti tristi, per aver gioito con me per tutti quelli felici e per aver condiviso ogni giorno insieme, anche se piene sempre d'impegni. Grazie Ludo.

Grazie alla mia amica di sempre Elisa, per essere stata sempre presente anche se a chilometri di distanza e con mille impegni al giorno. Grazie per trovare sempre il tempo per me, di raccontarci tutto come facevamo al tempo del liceo sul letto di casa mia. Grazie per non essere mai cambiata ed essere rimasta sempre la mia migliore amica. Grazie perchè sei capace di capirmi anche da una sola parola o da uno sguardo. Grazie per esserci oggi in un giorno così importante per me e so che anche nel futuro, insieme o separate, potrò sempre contare su di te.

Grazie al mio CDC, Centro Di Calcolo, dove tra una simulazione e l'altra ci sono stati anche momenti di svago che ho condiviso con chi come me si trovava a trascorrerci molte ore. A tutti voi, Stefania, Andrea e Niccolò va il mio grazie per aver reso più leggeri e piacevoli i lunghi giorni passati in laboratorio. Un grazie particolare va a Leonora, conosciuta pochi mesi fa, ma con cui ho affrontato gli ultimi mesi di percorso e con cui ho condiviso tutte le emozioni e soprattutto l'ansia che si prova prima del grande giorno.

Grazie alle mie coinquiline, confidenti e amiche, Jessica e Luisa, per tutti i bellissimi momenti passati insieme, per avermi sempre fatta sorridere anche nei momenti peggiori, per aver festeggiato insieme a me nei momenti più belli, per avermi dato sempre una forza incredibile ogni volta che pensavo di non farcela. Grazie per aver trascorso ogni giorno nella "nostra" casa, che resterà per sempre nostra, con felicità e amore che solo una famiglia può dare. So che se anche la vita dovesse dividerci ci saremmo sempre l'una per l'altra, perchè per me ormai siete come delle sorelle.

Grazie alle mie “arancine”, Marina, Anna Maria e Federica, che mi hanno accompagnato durante tutto il mio percorso univesitario, dal primo anno fino ad oggi. Grazie per aver scelto di crescere insieme a me, grazie per essere state per me sempre un punto di riferimento, grazie per tutti i momenti belli e anche per quelli brutti, sono ricordi che non dimenticherò mai.

Grazie alla mia famiglia pisana, composta da tutti gli amici conosciuti qui a Pisa, grazie per tutti i momenti passati insieme, grazie per avermi fatta sentire sempre protetta anche solo con una parola, grazie per essere stati tutti miei fratelloni: Grazie Luigi, Bruno, Davide, Frà, Giacomo, Giuseppe, Dario, Flavio, Gianluca, Carmelo, Vincenzo, Saverio e Picconi.

Grazie a Riccardo, per riempire ogni giorno la mia vita di felicità, per essermi sempre stato accanto e per avermi sempre supportata in ogni mia decisione. Grazie perchè quando credevo di non farcela tu hai sempre trovato le parole giuste, grazie per avermi dato sempre la forza di andare avanti e non mollare mai. Insieme siamo cresciuti e siamo diventati grandi, abbiamo vissuto giorni felici e alcuni giorni un pò meno, ma nonostante ciò abbiamo superato tutto e siamo arrivati insieme a questo giorno, senza di te non ce l’avrei mai fatta. Grazie amore.

Grazie a mia madre e mio padre, per avermi spronato, stimolato ed insegnato che l’unico strumento di forza nella vita è la cultura. Grazie alla mia mamma per avermi insegnato a mettere la passione in tutto ciò che si fa. Grazie al mio papà, per avermi sempre dato i consigli giusti, per avermi aiutato in tutte le scelte durante il mio percorso univesitario, per avermi insegnato che solamente con la costanza e lo studio tutti gli obiettivi prefissati possono essere raggiunti. Grazie papà per tutto quello che fai per me ogni giorno, anche solo con una parola, per aver sempre creduto in me e quando pensavo di non farcela grazie per avermi spinto a non mollare mai. Vi ringrazio per tutto quello che mi avete insegnato, senza di voi oggi non sarei la persona che sono diventata.

Ultima, ma non per importanza, la mia sorellona Anna. Anche se a 7000 km di distanza mi sei sempre stata vicina, grazie per essere stata una seconda mamma per me. Grazie per avermi mostrato che con il duro lavoro le soddisfazioni arrivano sempre, grazie per avermi regalato due gioie (quasi tre), Stephen e George, che anche se a distanza riempiono le mie giornate di amore e felicità. Grazie per esserci sempre stata, sei sempre stata il mio esempio di vita, spero un giorno di diventare almeno un pò come te, perchè sarebbe già abbastanza.

Il mio percorso universitario si conclude qui, ma un altro ben presto si aprirà. Volevo ringraziare tutte le persone che mi sono state vicine in questi lunghi sette anni, ogni ricordo è riposto nella mia memoria e non dimenticherò mai nessuno di voi.